Properties of Strongly Interacting Matter under Extreme Conditions

A THESIS

submitted for the award of Ph.D degree of

MOHANLAL SUKHADIA UNIVERSITY

in the

Faculty of Science

by

Sreekanth V.

Under the Supervision of

Hiranmaya Mishra

Associate Professor

Theoretical Physics Division

Physical Research Laboratory

Ahmedabad, India

DEPARTMENT OF PHYSICS

MOHANLAL SUKHADIA UNIVERSITY

UDAIPUR

Year of submission: 2011

DECLARATION

*I, **Mr. Sreekanth V.**, S/o Prof. P. K. Madhavan, resident of A-003, PRL Residences, Navrangpura, Ahmedabad 380009, hereby declare that the work incorporated in the present thesis entitled, **"Properties of Strongly Interacting Matter under Extreme Conditions"** is my own and original. This work (in part or in full) has not been submitted to any University for the award of a Degree or a Diploma.*

Date :

(Sreekanth V.)

CERTIFICATE

I feel great pleasure in certifying that the thesis entitled, "***Properties of Strongly Interacting Matter under Extreme Conditions***" embodies a record of the results of investigations carried out by Mr. Sreekanth V. under my guidance.

He has completed the following requirements as per Ph.D. regulations of the University.

(a) Course work as per the university rules.

(b) Residential requirements of the university.

(c) Presented his work in the departmental committee.

(d) Published minimum of two research papers in a referred research journal.

I am satisfied with the analysis of data, interpretation of results and conclusions drawn.

I recommend the submission of thesis.

Date :

Hiranmaya Mishra
Associate Professor
(Thesis Supervisor)

Countersigned by

Head of the Department

Acknowledgements

This thesis would not have been possible without help from many people. First of all, I owe my deep gratitude to my supervisor Dr. Hiranmaya Mishra for introducing me to the research work with care, help and motivation. Learning from him was a good experience and I particularly value his insight on the subject, strive for perfection and hard work. I thank him for allowing me to pursue my research under him. I enjoyed the full freedom he gave me regarding my work.

I am greatly indebted to Dr. Jitesh Bhatt for giving me time and teaching me many things in the subject with utmost care. His logical reasoning and intuitive arguments left an impression on me. It was a pleasure to work with both of them (HM & JB). I am greatly indebted to their efforts to teach me many aspects of the subject with lot of patience. I learned a great deal from them. This thesis takes its final form due to the wholehearted support I received from them throughout. Any shortcoming is solely due to the author.

It is an honor for me to thank Prof. Utpal Sarkar, who always motivated me and kept a keen interest in my progress; Prof. Saurabh Rindani, who helped me whenever I approached; Prof. Anjan Joshipura for discussions and Prof. Ashok Das for motivation and guidance. I would like to thank Prof. Subhendra Mohanty for checking my research progress during evaluations and many interesting interactions. Prof. P. K. Panigrahi is remembered here for rightfully guiding me in to the world of research at a very crucial juncture of my academic career. I would like to thank Prof. R. Amritkar, Prof. R. Ramesh, Dr. R. Rangarajan, Dr. Santhanam, Dr. D. Angom, Dr. N. Mahajan, Prof. J. Banerji, Dr. R. P. Singh and Prof. Subrahmanyan for many helpful discussions and suggestions.

Dr. T. K. Jha is being acknowledged here for the fruitful collaboration. It was a pleasure to work with him and his help during the early stages of my research is duly noted. I thank Dr. Kumar and Dr. Purnendu for discussions and advises.

I would like to show my gratitude to Profs. D. Blaschke, M. Nardi, T. Biró, M. Buballa, A. Rebhan, M. Lombardo for arranging visits to their institutes and interactions, from which I have benefited immensely. I would like to thank Prof. R. Bhalerao, Dr. P. Romatschke, Prof. K. Rajagopal and Prof. D. Rischke for *discussions and suggestions which helped me in my research.*

I am indebted to many of my colleagues for their support throughout my tenure at PRL. I thank my batch-mates Amzad, Anand, Arvind, Ashok, Bhaswar, Naveen, Pankaj, Priyam, Rabiyul, Rohit, Sandeep, Soumya, Suman, Vimal, Vineet and Vivek for their support. I thank Subimal, Suman and Soumya for all Linux related stuffs. I thank Rajneesh, Santhosh, Kushwahji, R.K. Das, Bhavik, Vishal, Ashiwini, Manan, Harinder, Ketan, Patra, Khan, Tapas, Moumita, Abhishek, Zeen, Chithra for their support. Discussions with Avdhesh and Ananya were interesting.

It is a pleasure to thank my friends, Mahesh, Dr. Yura Bystritskiy and Dr. Nirali Shah, whose care and support at different junctures helped me in many regards.

Acknowledged here is Dr. Arul Lakshminarayan (IIT Madras), for showing belief in me and allowing me to complete my M.Sc. project work under his guidance. His affection and care are duly noted.

Fondly remembered here is Radhakrishnettan, who introduced me to the world of physics and I thank him for everything that I owe in the subject. His way of teaching and making me understand the subject with its all subtle features through problem solving really made the difference. My B.Sc. teachers Prof. U. Nirmalakumari and (late) Prof. V. Vijayan are acknowledged for their teachings and special affection.

My B.Sc. friends have been very supportive all these years and the warmth of their love and support is noted here. I thank Geetha for her unconditional support and care.

Motivational discussions, helpful suggestions and guidance from Achhan and Venumama are highly noted here. I would also like to thank Kunjamman for all those wonderful discussions. My cousin, friend, Sreejith is being remembered here for the wonderful chemistry and interests we share. Our curiosity driven expeditions to know more about the world around us, helped me in my research career also.

I would like to thank my brothers, cousins and all other family members for their affection and support during all these years. Final words I reserve for my parents, and words are inadequate to express what I wish to say.

December 2011, PRL SKV

Dedicated to,

---

my parents

Prof. P. K. Madhavan & Smt. V. Sathi

pādaspàrśam smarāmyahàm

♣

List of publications

1. *On attributes of a rotating neutron star with a hyperon core*,
   T.K. Jha, H. Mishra and **V. Sreekanth**,
   Phys. Rev. C **77**, 045801 (2008).

2. *Bulk viscosity in hyperonic star and r-mode instability*,
   T.K. Jha, H. Mishra and **V. Sreekanth**,
   Phys. Rev. C **82**, 025803 (2010).

3. *Photon emission from out of equilibrium dissipative parton plasma*,
   Jitesh R. Bhatt and **V. Sreekanth**,
   Int. J. Mod. Phys. E 19, 299-306, (2010).

4. *Thermal photons in QGP and non-ideal effects*,
   Jitesh R. Bhatt, H. Mishra and **V. Sreekanth**,
   JHEP 1011, 106 (2010).

5. *Cavitation and thermal dilepton production in QGP*,
   Jitesh R. Bhatt, H. Mishra and **V. Sreekanth**,
   to appear in Nucl. Phys. A,
   arXiv:1101.5597 [hep-ph] (2011).

6. *Shear viscosity, cavitation and hydrodynamics at LHC*,
   Jitesh R. Bhatt, H. Mishra and **V. Sreekanth**,
   Phys. Lett. **B704**, 486-489 (2011).

   Other works (not included in thesis)

7. *Boson stars: Chemical potential and quark condensates*,
   Jitesh R. Bhatt and **V. Sreekanth**,
   arXiv:0910.1972 [hep-ph] (2009).

Abstract

This thesis deals with certain aspects of the effect of dissipation on the nuclear matter at extreme conditions like high temperature or/and high density. First, we study nuclear matter at high baryon density and low temperature, which can be found inside neutron stars. We consider a rotating neutron star with the presence of hyperons in its core. Hyperonic matter is described by an effective chiral sigma model within relativistic mean field approximation. We calculate the hyperonic bulk viscosity coefficient due to non-leptonic weak interactions. By estimating the damping timescales of the dissipative processes, we investigate its role in the suppression of gravitationally driven instabilities in the r-mode. We observe that r-mode instability remains very much significant for hyperon core temperature of around 10^8 K, resulting in a comparatively larger instability window. We find that such instability can reduce the angular velocity of the rapidly rotating star considerably upto $\sim 0.04\ \Omega_K$, with Ω_K as the Keplerian angular velocity.

Next we consider the hot and almost zero baryon density quark-gluon matter produced in relativistic heavy ion collision experiments like RHIC and LHC. Using the second order causal Israel-Stewart dissipative hydrodynamics we discuss the effect of both bulk and shear viscosities in the hydrodynamic expansion of the plasma for one dimensional boost-invariant (*Björken*) flow. Using the recent lattice QCD estimates for a temperature dependent bulk viscosity ζ/s, which has a peak near critical temperature T_c, and the minimal value of shear viscosity $\eta/s \approx 1/4\pi$, we show that during hydrodynamical evolution effective longitudinal pressure of the system can become negative at RHIC energies, thus triggering the phenomenon of *cavitation*. Further, we also found that at LHC energies such a high value of bulk viscosity cannot drive system to a cavitating phase. However, using various prescriptions for a temperature dependent η/s we found, at LHC energies, shear viscosity alone can cause cavitation. Cavitation happens at very early time of the evolution. We also demonstrate that the conformal terms used in equations of the relativistic dissipative hydrodynamic can influence the cavitation time. Further, we study the role of finite shear viscosity on the chemical equilibration of the thermalised plasma at RHIC and RHIC energies. We found that even the smallest

possible value of shear viscosity alone can make the system take more time to reach equilibrium stage.

Further, we investigate the effect of viscosity, both bulk and shear on the thermal particle production from QGP. We use one dimensional boost-invariant second order relativistic hydrodynamics to find proper time evolution of the temperature. First we consider thermal photon emission from the chemically non-equilibrated plasma. We find that photon production rates can enhance by several factors due to the minimal value of shear viscosity. We propose that this enhancement in photon spectrum can be used to measure the viscosity of the hot quark-gluon matter formed. Next we consider the effect of bulk viscosity and shear viscosity on thermal photon production from QGP. The effect of bulk viscosity and equilibrium equation of state are taken into account in a manner consistent with recent lattice QCD estimates. Ratio of the shear viscosity to entropy density is taken to be $\eta/s \sim 1/4\pi$. We study the resulting photon spectra in presence of the viscosities. We analyse the effect of novel phenomenon of bulk viscosity induced cavitation on the thermal photon production. We demonstrate that ignoring the cavitation phenomenon can lead to an erroneous estimation of the particle flux. Further, we calculate the corrections on the dilepton production rates due to modification in the distribution function, arising due to the presence of the bulk and shear viscosities. It is shown that when the system temperature evolves close to T_c the effect of the bulk viscosity on the dilepton emission rates can not be ignored. It is demonstrated that the bulk viscosity can suppress the thermal dilepton spectra where as the effect of the shear viscosity is to enhance it. We find that even though the finite bulk viscosity corrections and the onset of the cavitation reduce the production rates, the effect of the minimal $\eta/s = 1/4\pi$ can enhance the dilepton production rates significantly in the regime $p_T \geq$2 GeV.

Finally we would like to note that we have analyzed the role of viscosity of the nuclear matter under high temperature or/and high density. We have shown that the viscous dynamics can significantly influence the observed signal of the plasma from heavy ion collisions. Moreover, we have demonstrated that high values of $\eta/s >> 1/4\pi$ can lead to a novel phenomenon of shear viscosity driven cavitation.

Contents

List of Tables

List of Figures

Chapter 1

Introduction

Studies of nuclear matter at extreme conditions like high density and/or high temperature is of great interest and a topic of extensive research in recent times [1]. By extreme conditions we mean densities $\geq (2-3)\, n_0$, where n_0= 0.153 fm^{-3} = 2.7×10^{14} gm cm^{-3} is normal nuclear matter density and temperatures $T \geq 150$ MeV $\sim 10^{12}$ K. One knows from the standard model of particle physics, the force that binds quarks into composite particles called hadrons of size ~ 1 fm $= 10^{-13}$ cm, is the *strong force* and is described by the theory of quantum chromodynamics (QCD). The scale of this theory $\Lambda_{QCD} \sim 150$ MeV, gives the information regarding the strength of interaction in different energy regimes. Asymptotically free nature of this theory implies that the interaction between quarks and gluons becomes weak at high energies $Q \gg \Lambda_{QCD}$, whereas at low energies $Q \ll \Lambda_{QCD}$ interaction becomes stronger and leads to the confinement of color [2–4]. This may explain the non-observance of free quarks and gluons in nature. It is interesting to note that extreme conditions, like high density and or temperature, do exist in nature. It is expected that after the big-bang ($\sim 10^{-5}$ s), universe had gone through a phase where the temperature was comparable to that of QCD phase transition. It is also expected that high density quark matter is realised inside neutron stars. Apart from these natural occurrences, hot quark-gluon matter is believed to be formed in relativistic heavy ion collider experiments. Study of nuclear matter under extreme conditions is of fundamental importance since it will help us to test our understanding of the elusive QCD vacuum structure and its modification via

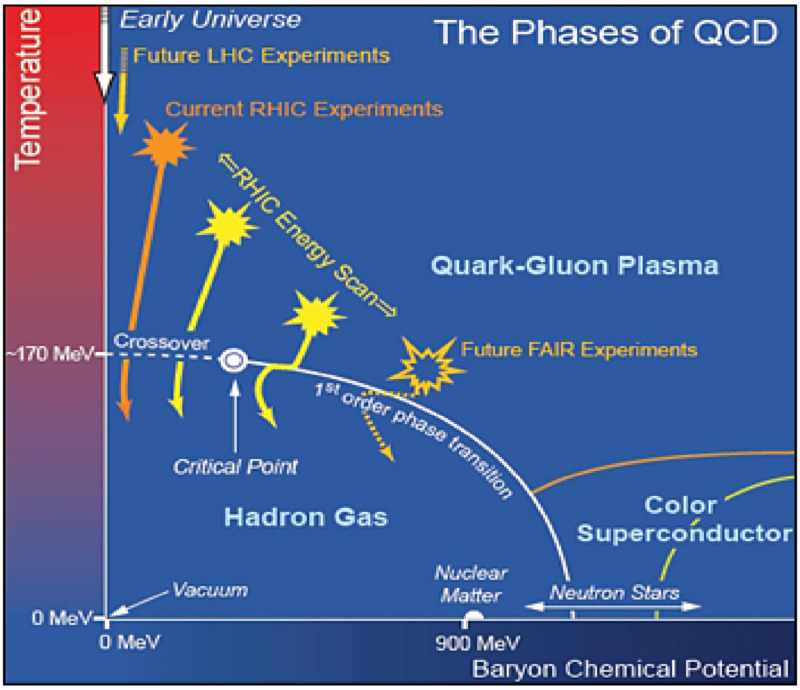

Figure 1.1: *Proposed phase diagram of QCD matter (picture taken from Ref. [5]).*

temperature and density. These will be useful in improving our understanding of the confinement, hadronic structure etc.

The wealth of information from theoretical as well as experimental studies on matter under extreme conditions are used to propose the phase diagram of QCD, represented in Fig. [1.1]. The diagram shows the various conjectured phases of QCD in baryon chemical potential and temperature (μ_B, T) plane. As shown by the figure, the baryon free high temperature regime is explored by the ongoing experiments like RHIC and LHC, while the regime with finite baryon chemical potential and temperature will be probed by the future experiments like FAIR[1].

What we can expect if we increase the temperature or density of the matter to very high values? At temperature (or density) above the critical temperature (or density), the hadronic degree of freedom is no longer valid. The quarks and gluons are now not confined in a hadronic volume, but they can move in to a bigger volume occupied by the nuclear matter. The exact nature of the phase transition is currently not fully understood, but at high temperature it is expected to be a

[1]RHIC: Relativistic Heavy Ion Collider (BNL, US), LHC: Large Hadron Collider (CERN, Geneva), FAIR: Facility for Antiproton and Ion Research (GSI, Germany)

crossover rather than a phase transition [6]. The critical temperature of QCD is under extensive study and it is believed to be in the range 150-200 MeV [7]. In the high density and low temperature regime, the deconfinement transition can lead to a highly degenerate quark-gluon matter. Such a scenario can be realized inside a neutron star. At ultra-high densities we expect to find the conjectured color-flavor-locked (CFL) phase of color-superconducting quark matter. Thus the phase diagram of QCD matter contains many exotic and mysterious regions posing challenging questions to be explored [8–14].

We would like to study certain aspects of extremely dense or hot matter regions of QCD phase diagram, which can be probed through some observations or experiments. The cold and dense matter inside neutron stars and hot baryon free ($\mu_B = 0$) QGP produced in heavy ion collider experiments (RHIC & LHC) are two such regions [13, 14].

1.1 Dense and cold nuclear matter inside neutron stars

Neutron stars are natural testing ground for studying extremely dense matter. The densities in the interior of such stars can reach up to several times the nuclear matter saturation density. At such high densities, with higher fermi momenta being available, high mass hadrons can be accommodated leading to a hyperonic core in the neutron star interior [13, 15–18]. There could also be the possibility that at such densities, when the nucleons are crushed, there could be quark matter [19, 20] which can result in a color superconducting core in the interior of the neutron star [11, 21–29]. In fact, there are different possibilities of the ground state of dense matter, which could be stable strange quark matter [30], and various possibilities of color superconducting matter [31–33]. The reason is that the true ground state of the dense matter system for densities relevant for the densities in the interior of neutron stars is still an open problem because of the inherent nonperturbative nature of strong interaction physics. Moreover, external conditions like electrical and color charge neutrality conditions for the bulk matter in the interior of the star can also lead to various different possible phases of quark matter [33–39]. This has given rise to various possibilities of compact stellar objects like neutron stars, strange stars, hyperonic stars or hybrid stars with a quark matter core and a crust of hadronic matter [18, 40].

Since description of dense nuclear matter is inherently non-perturbative, therefor, we need to rely upon certain approximation schemes to make progress. In field theory, one of the ways to tackle this problem is by means of *relativistic mean field theory* (RMFT) approximation [41–45]. In the next subsection, we discuss the Walecka model, a toy model to describe the nuclear matter within RMFT; since many realistic and successful nuclear matter models are extension of this basic model.

1.1.1 The Walecka model & RMFT

Walecka model is a simple model to describe the nuclear matter where the interaction among nucleons are mediated via scalar (ϕ) and vector (V^μ) particles (mesons) [45]. The choice of the model is motivated by the empirically observed large values of Lorentz scalar and vector contributions in the $N-N$ interaction. Secondly the dominant bulk properties of the matter can be described in this fashion. With this model it is also possible to reproduce the effective nucleon-nucleon potential; repulsion at short distance and attraction at large distance, with the aforesaid meson exchange in the limit of static heavy baryons.

The Lagrangian density of the system is given by

$$\begin{aligned}\mathscr{L} &= \bar{\psi}\left[i\gamma^\mu\partial_\mu - g_v\gamma^\mu V_\mu - (M - g_s\phi)\right]\psi \\ &\quad + \frac{1}{2}\left(\partial_\mu\phi\partial^\mu\phi - m_s^2\phi^2\right) - \frac{1}{4}F_{\mu\nu}F^{\mu\nu} + \frac{1}{2}m_v^2 V_\mu V^\mu,\end{aligned} \tag{1.1}$$

where $F_{\mu\nu} \equiv \partial_\mu V_\nu - \partial_\nu V_\mu$. The neutral ϕ meson is coupled to the scalar density of the baryons through $g_s\bar{\psi}\psi\phi$ and neutral vector meson is coupled to the conserved baryon current through $g_v\bar{\psi}\gamma^\mu\psi V_\mu$. One must note here that we don't consider spin or isospin dependent interactions as they tend average to be zero when we consider bulk properties of the system. When $m_v > m_s$ and $g_s > g_v$ the potential is repulsive in short distances due to the vector meson exchange and attractive at large distances due to scalar meson exchange. One can write out the equations of motion (Euler-Lagrangian) for the fields ϕ, V^μ and ψ now:

$$\begin{aligned} [\partial_\mu \partial^\mu + m_s^2]\,\phi &= g_s \bar{\psi}\psi, & (1.2)\\ \partial_\mu F^{\mu\nu} + m_v^2\, V^\nu &= g_v \bar{\psi}\gamma^\nu \psi, & (1.3)\\ [i\gamma^\mu \partial_\mu - g_v \gamma^\mu V_\mu - (M - g_s\phi)]\,\psi &= 0. & (1.4) \end{aligned}$$

However these non-linear equations are difficult to deal and their exact solutions are very complicated. Since we expect the couplings g_v and g_s are large, perturbative methods also fail.

We use the *relativistic mean field theory* (RMFT) to simplify the problem. In this non-perturbative technique we replace the meson field operators with their classical expectation values. RMFT is valid when the source terms are large. As the baryon density becomes large, the source terms involving the baryon field increase and hence the meson fields also become stronger. In such a situation it is reasonable to replace the quantum fields by classical fields. With $|\psi_0\rangle$ denoting the ground state of the nuclear matter, RMFT approximation can be written as,

$$\begin{aligned} \phi &\rightarrow \langle \psi_0|\phi|\psi_0\rangle = \phi_0, & (1.5)\\ V_\mu &\rightarrow \langle \psi_0|V_\mu|\psi_0\rangle = \delta_\mu^0 V_0. & (1.6) \end{aligned}$$

For a *uniform*, *static* system there is no preferred spatial direction and hence vector field can develop only a time component. Further, for such systems, the classical fields ϕ_0 and V_0 are *constants* independent of x^μ. These meson field equations within RMFT become

$$\begin{aligned} \phi_0 &= \frac{g_s}{m_s^2}\langle \psi_0|\bar{\psi}\psi|\psi_0\rangle = \frac{g_s}{m_s^2}\, n_{SB}, & (1.7)\\ V_0 &= \frac{g_v}{m_v^2}\langle \psi_0|\psi^\dagger\psi|\psi_0\rangle = \frac{g_v}{m_v^2}\, n_B; & (1.8) \end{aligned}$$

with the scalar density n_{SB} and baryonic density n_B. Now the equation for ψ field becomes

$$\left[i\gamma^\mu \partial_\mu - g_v \gamma^0 V_0 - M^*\right]\psi = 0, \tag{1.9}$$

where we have defined $M^* = M - g_s\phi_0$ as the *effective mass*. We look for the stationary state solutions of the form

$$\psi = U_r(\vec{k})\, e^{-ik\cdot x}, \tag{1.10}$$

where $k \cdot x = k^\mu x_\mu = Et - \vec{k} \cdot \vec{x}$ and $U_r(\vec{k})$ denotes the four-component Dirac spinor with r being its spin index. Now Dirac equation becomes,

$$\left[\not{\mathcal{K}} - M^*\right] U_r(\vec{k}) = 0 \tag{1.11}$$

with $\not{\mathcal{K}} = \gamma^\mu \mathcal{K}_\mu$ and $\mathcal{K}_\mu = k_\mu - g_v \delta^0_\mu V_0$. In order to find the eigenvalues, we multiply both sides of the above equation with $\not{\mathcal{K}} + M^*$ resulting in

$$\left[\not{\mathcal{K}}\not{\mathcal{K}} - M^{*2}\right] U_r(\vec{k}) = \left[\mathcal{K} \cdot \mathcal{K} - M^{*2}\right] U_r(\vec{k}) = 0, \tag{1.12}$$

where we used the relation $\gamma_\mu \gamma_\nu + \gamma_\nu \gamma_\mu = 2g_{\mu\nu}$. From the above equation we get

$$E^{(\pm)} = g_v V^0 \pm \sqrt{\vec{k}^2 + M^{*2}}, \tag{1.13}$$

with $+(-)$ denoting the positive (negative) energy solution of Dirac equation. We can expand the baryon field operator in terms of complete set of solutions to the Dirac equation with both positive and negative energy solutions,

$$\psi(x) = \sum_{\vec{k}\ r} \frac{1}{\sqrt{2V\mathcal{K}^0}} \left[a_{\vec{k}\ r} U_r(\vec{k})\, e^{-iE^+ t + i\vec{k}\cdot\vec{x}} + b^\dagger_{\vec{k}\ r} V_r(\vec{k})\, e^{-iE^- t - i\vec{k}\cdot\vec{x}}\right], \tag{1.14}$$

where $a_{\vec{k}\ r}$ is the annihilation operator for baryons and $b^\dagger_{\vec{k}\ r}$ is the creation operator for anti-baryons. However, since we are interested in cold nuclear matter inside neutron stars ($T \approx 0$), we do not consider antiparticles in the present problem. Further, we can get the normalisation conditions for the spinor as

$$\begin{aligned} \bar{U}_r(\vec{k}) U_s(\vec{k}) &= 2M^* \delta_{rs}, \\ U^\dagger_r(\vec{k}) U_s(\vec{k}) &= \frac{\sqrt{\vec{k}^2 + M^{*2}}}{M^*}\, \bar{U}_r(\vec{k}) U_s(\vec{k})\,. \end{aligned} \tag{1.15}$$

For uniform nuclear matter, ground state is obtained by filling the states with $\vec{k}$ and spin-isospin degeneracy factor γ (= 4 for symmetric nuclear matter) till Fermi momenta k_F. Now the baryon density is given by

$$n_B = \langle \psi^\dagger \psi \rangle = \frac{\gamma}{(2\pi)^3} \int_o^{k_F} d^3k = \frac{\gamma}{6\pi^2}\, k_F^3, \tag{1.16}$$

whereas the scalar density is obtained as

$$n_{SB} = \langle \bar{\psi}\psi \rangle = \frac{\gamma}{(2\pi)^3} \int_o^{k_F} \frac{M^*\, d^3k}{\sqrt{\vec{k}^2 + M^{*2}}}; \tag{1.17}$$

where (and henceforth), for brevity, we denote $\langle\psi_0|\mathcal{O}|\psi_0\rangle = \langle\mathcal{O}\rangle$. It is to be noted here that V_0 is obtained using the conserved baryon density n_B, i.e.; by Eq. (1.8). Whereas, ϕ_0 is a dynamic quantity that needs to be evaluated self consistently from Eqs. (1.7 & 1.17) for a given k_F.

In order to get the thermodynamic quantities one need to construct the energy-momentum tensor $T_{\mu\nu}$ from the Lagrangian (within RMFT here),

$$\begin{aligned} T^{\mu\nu} &= -g^{\mu\nu}\,\mathscr{L} + \frac{\partial\psi}{\partial x_\nu}\frac{\partial\mathscr{L}}{\partial\partial\psi/\partial x^\mu} && (1.18)\\ \Rightarrow T^{\mu\nu}_{RMFT} &= i\bar{\psi}\gamma^\mu\partial^\nu\psi - \left(\frac{1}{2}m_v^2V_0^2 - \frac{1}{2}m_s^2\phi_0^2\right)g^{\mu\nu}. && (1.19)\end{aligned}$$

For a uniform system, the *observed* energy-momentum tensor is given by [46]

$$\langle T_{\mu\nu}\rangle = (\varepsilon + P)u_\mu u_\nu - Pg_{\mu\nu}, \tag{1.20}$$

where ε and P are the energy density and pressure of the system respectively. The 4-velocities u^μ are related by the relation $u^\mu u_\mu = 1$. And for a fluid at rest: $u^\mu = (0, \vec{1})$, we have

$$\varepsilon = \langle T_{00}\rangle\,, \qquad P = \frac{1}{3}\langle T_{ii}\rangle\,. \tag{1.21}$$

Therefor, we get

$$\begin{aligned} \varepsilon &= \frac{g_v^2}{2m_v^2}n_B^2 + \frac{m_s^2}{2g_s^2}(M-M^*)^2 + \frac{\gamma}{(2\pi)^3}\int_o^{k_F}\sqrt{\vec{k}^2 + M^{*2}}\,d^3k && (1.22)\\ P &= \frac{g_v^2}{2m_v^2}n_B^2 - \frac{m_s^2}{2g_s^2}(M-M^*)^2 + \frac{1}{3}\frac{\gamma}{(2\pi)^3}\int_o^{k_F}\frac{\vec{k}^2\,d^3k}{\sqrt{\vec{k}^2 + M^{*2}}}. && (1.23)\end{aligned}$$

For a given k_F, we get n_B from Eq. (1.16) and ϕ_0 by self-consistently solving Eqs. (1.7 & 1.17); which eventually gives M^*. Now we obtain $\varepsilon(k_F)$ and $P(k_F)$ from the above Eqs. (1.22 & 1.23) and these two equations represent the nuclear matter equation of state (EoS) (at zero temperature) in parametric form.

Now let us analyse the predictions for the bulk properties of symmetric nuclear matter by this model. Now by tuning the coupling constants $C_s^2 = g_s^2\left(\frac{M^2}{m_s^2}\right)$ and $C_v^2 = g_v^2\left(\frac{M^2}{m_v^2}\right)$, we get the symmetric nuclear matter at saturation density $n_0 =$ 0.153 fm^{-3} with an equilibrium fermi wave number $k_F^0 = 1.31$ fm^{-1} and an energy per nucleon $(\varepsilon/n_B - M) = -16.3$ MeV. However, compressibility of the nuclear matter, given by

$$K = k_F^2\,\frac{d^2(\varepsilon/n_B)}{dk_F^2}, \tag{1.24}$$

turns out to be ~ 550 MeV in this approximation, which is rather high (around two times) compared to the experimental values. Further, effective mass at saturation $M^*/M \approx 0.5$ is also not in agreement with the observed value $M^*/M \approx 0.7...0.8$. One tries to modify this model by including non-linear terms in the meson fields, so as to have a better agreement with experimental results for saturation properties of the nuclear matter.

Phenomenologically, parallel to Walecka model (also known as $\sigma - \omega$ model), the chiral effective models for hadronic matter have been developed and are applied to nuclear matter [13]. A chiral $\sigma - \omega$ model along with dilatons in the context of phase transition has been developed in Ref. [47] and further generalised to describe strange hadronic matter [48–50]. Another approach that was also considered is the parity doublet model [51]. Also, attributes of rotating hyperonic star within a chiral σ model has been studied in Refs. [52–54]. Further, a chiral σ hadronic model, with a dynamical generation of the vector meson mass, along with non-linear terms in the scalar field interactions to reproduce nuclear saturation properties at reasonable incompressibility, was also considered [55, 56]. This model was then generalised to include the lowest lying octet of baryons [57].

Once we get the EoS of the neutron star matter under consideration, by means of stellar structure equations obtained using general relativistic considerations; static or rotating stellar equilibriums can be studied [58–60]. As mentioned before, theoretically many states of dense cold matter can be realised inside a neutron star. However, it is very challenging to distinguish various compact stellar objects observationally, and sort out the ambiguity regarding its constituent particles.

1.1.2 r-mode instability

One of the various signatures suggested to distinguish different compact stars has been the r-mode instability [61–65]. A rotating star is subjected to various kinds of pulsating modes, which are classified in terms of their restoring forces. r-modes are one kind of such (axial) modes caused by the velocity perturbations, where the restoring force is Coriolis force [67, 68]. The r-mode frequency ω in the co-rotating frame, to first order in the rotation frequency Ω of the star is given by [69]

$$\omega = \frac{2m\Omega}{l(l+1)} + \mathcal{O}(\Omega^3) \tag{1.25}$$

The r-modes correspond to $l = m$ [67]. It was discovered recently that these modes are unstable due to emission of gravitational radiation [61]. The gravitational radiation couples with r-mode oscillations and make the star radiate its rotational energy due to the Chandrasekhar-Friedman-Schutz mechanism [70, 71], thus effectively reducing the angular momentum of the star. What makes r-mode important in a star compared to other modes, is that, it is unstable for *all* rotational velocities [61]. This process, if unsuppressed due to viscous effects, saturates eventually due to non-linear effects, which transfer r-mode energy to other modes which are not coupled with gravitational radiation [72]. But by this time star would emit sufficient gravitational radiation which can be detected using experiments like Advanced Laser Interferometer Gravitational Wave Observatory (LIGO) [64]. Thus a newly born neutron star will be subjected to r-mode instability and can get its angular momentum lowered, due to gravitational radiation. This may be the reason for the observational indication that most of the stars detected (millisecond pulsars) have a very low rotational frequency although theoretically a star can support much higher rotational frequency. Most of these stars lie in the low-mass X-ray binary systems (LMXBs) [73]. Further, the gravitational radiation emitted from such stars can be detected using LIGO.

The growth of r-mode may get damped if the viscosity of the stellar matter is large enough. Thus study of r-mode gives an opportunity to probe the viscosity of the stellar matter at high densities inside a neutron star. One can study how effectively viscosity can damp the unstable modes, before these modes reduce the stellar angular momentum considerably [63].

While shear viscosity prevents differential rotation in a star, bulk viscosity dampens the density fluctuations in the star. At relatively low temperatures, the primary dissipation mechanism arises from momentum transport due to particle scattering which produces shear viscosity. In a normal fluid star nn scattering gives the primary contribution to shear viscosity [74, 75]. At higher temperatures (above few times $10^9 K$), bulk viscosity- which dampens the density fluctuation of the star; turns out to be the dominant dissipation mechanism. Further, typical r-mode frequencies are of the order of stellar rotational frequencies ($1s^{-1} < \omega < 10^3 s^{-1}$), which are comparable to the weak interaction time scales. Further, since timescales associated with strong interaction processes are very fast compared to weak interaction processes, bulk viscosity that is relevant for r-mode instability will be dominated by the weak processes.

Bulk viscosity is produced when the mode oscillations induce perturbations in density of the stellar matter and drive the system away from β-equilibrium. As a result energy is dissipated from the system as the weak interaction tries to restore the equilibrium. While for hadronic neutron star matter, modified Urca processes ($n + n \to n + p + e^- + \bar{\nu}_e$) involving leptons are important, it has been noted that the damping of the instability is dominated by large bulk viscosity arising due to non-leptonic processes involving hyperons [76–78]. The corresponding viscosities are not only stronger, the temperature dependence is also different (varying as T^{-2} instead of T^6) which makes the hyperon bulk viscosity important at lower temperatures. Bulk viscosities of dense baryonic, kaonic and quark matter has been calculated under various assumptions as well as conditions over last few years and applied to the study of mode damping. [63, 76–89].

We would like to analyse the role of hyperon bulk viscosity in the damping of r-modes in a neutron star with a hyperonic core scenario. We will use a chiral model for the neutron star matter including the lowest lying octet of baryons and evaluate bulk viscosity within this model.

1.2 QGP in relativistic heavy ion collisions

Heavy ion collisions are the only means by which we can create hot/dense nuclear matter in a laboratory. Depending upon the energy that can be attained, we can create hot quark-gluon matter (as in RHIC and LHC) or hot and dense matter (as in proposed FAIR); see Fig. [1.1]. We are interested in the production scenario of hot, almost baryon free, QGP formed in the RHIC and LHC experimental conditions. In a heavy ion collision, two nuclei are accelerated to relativistic speeds and they collide each other depositing huge amount of energy. Thus generated entropy ultimately manifests as new particles which we observe in the detectors. We can broadly divide heavy ion collision scenario into three temporal regions [14]:

Pre-equilibrium stage ($0 < \tau < \tau_0$): Collision of the nuclei results in the production of hot quarks and gluons as the nucleons degrees of freedom are destroyed due to the impact and lot of entropy is generated in the center. We still don't have a clear understanding about the entropy production associated with the heavy ion collision at $\tau = 0$. In this state after a certain time τ_0 (< 1 fm) system attains thermalisation. Again, the actual mechanism behind this thermalisation is unknown. Models like color glass condensate (CGC) etc. are used to explain this pre-equilibrium stage, eventhough these theories has drawbacks [90, 91]. The main reason for these ambiguities are due to the inherent non-Abelian nature of the underlying theory, QCD. So what we assume is that after τ_0, we have a hot thermalised plasma formed in heavy ion collision.

QGP phase ($\tau_0 < \tau < \tau_f$): At this phase, the hot fireball created in the heavy ion collision will be in a thermalised state. Deconfined system is now in the form of hot QGP. There can be a possibility of having thermally equilibrated but chemically non-equilibrated phase. Since the local thermal equilibrium is attained we can use hydrodynamics to describe the evolution of the system from the initial time τ_0. The fireball undergoes an expansion, governed by relativistic hydrodynamical equations, subsequently may cool up to the critical temperature T_c. In this thesis we will be focusing on this stage of the heavy ion collision.

Mixed/Hadronic phase and freeze-out ($\tau_f < \tau < \tau_{fr}$): At T_c system will be in a mixed phase and now the entropy of the system decreases due to conversion of QGP into hadrons, while maintaining the temperature T_c. Further below temperatures, subsequently hadronisaton will take place. Applicability of hydrodynamics ceases to exist when system reaches the freeze-out time τ_{fr}. Freeze-out is defined by the space-time hyper-surface where mean-free path of the particles becomes larger than the system size. At this juncture, local equilibrium is no longer maintained so the particles fly away. It is to be noted that different particle species reaches freeze-out in different times, in reality.

1.2.1 Relativistic hydrodynamics

Enrico Fermi in 1951 suggested using thermodynamics and statistical prescriptions for studying the multiple particle production in heavy ion collision [92]. In his seminal papers (1953, 1955), Soviet physicist Lev Landau used relativistic hydrodynamics to prescribe the expansion of strongly interacting matter in heavy ion collisions [93, 94]. In this *Landau picture*, two nucleons with relativistic speeds collide each other with zero impact parameters (central collision) in center-of-mass reference frame. They get significantly slowed down, stick together and produce hot baryon rich particles at the center. And thereafter hydrodynamical expansion of this matter takes place mainly along the incident beam axis (say, z-axis). For high energy collisions like that in RHIC and LHC, we have to replace this picture by that of Björken [95]. In *Björken picture*, the two Lorentz contracted nuclei collide and pass-through each other creating baryon free hot quark-gluon matter at the center, which will undergo a longitudinal (one dimensional) expansion along the incident beam axis.

Hydrodynamics is valid when the mean free path of the particles in the system (λ) is shorter compared to the size of the system (L). In other words the interaction between the constituent particles should be frequent enough to establish the equilibrium of the system under consideration. The mean free path, which is the distance travelled by the particle in between successive collisions is written as

$$\lambda = \frac{1}{\sigma\rho} \tag{1.26}$$

where σ is the interaction cross section and ρ is the density of the medium. Now the condition for applicability of hydrodynamics can be expressed as $L \gg l \gg \lambda$, where l being the size of the fluid element. Equivalently, in terms of *Knudsen number*, $K_n = \lambda/L \ll 1$. Let us calculate K_n in the context of RHIC ($Au - Au$, $\sqrt{s} = 200$ GeV). With the central density taken as $\rho = n_0 = 0.153$ fm^{-3} and corresponding nucleon-nucleon cross section given by $\sigma_{NN} = 45$ mb $= 4.5$ fm^2, we have $\lambda \sim 1.45$ fm. Now size of the system is given by $L = 2\ R_A$, where $R_A = 1.2A^{1/3}$ fm, is the radius of the (Au, A=197) nucleus. Therefore, $K_n \sim 0.1 < 1$, so that a nucleon will undergo almost ten collisions before passing through the nucleus.

In order to formulate the relativistic hydrodynamics, we need to construct the energy-momentum tensor $T^{\mu\nu}$ for the fluid. The information about the state of the fluid is represented via the 4-velocity u^μ and any two thermodynamic quantities e.g.; energy density ε and pressure P of the fluid. We use the approach of Landau and Lifshitz in the following [96]. The energy-momentum tensor for an *ideal* relativistic fluid is defined as

$$T^{\mu\nu} = (\varepsilon + P)\, u^\mu\, u^\nu \; - P\, g^{\mu\nu} = \varepsilon\, u^\mu\, u^\nu \; - P\, \Delta^{\mu\nu} \tag{1.27}$$

where ε and P are the energy density and pressure of the fluid element respectively. 4-velocity $u^\mu = \gamma(1, \vec{v})$ (with $\gamma = \frac{1}{\sqrt{1-\vec{v}^2}}$) is constrained by the relation $u^\mu u_\mu = 1$ with $g^{\mu\nu} = (+1, -1, -1, -1)$. We note that *all* the thermodynamic quantities are defined in the rest frame of the fluid. The operator $\Delta^{\mu\nu} = g^{\mu\nu} - u^\mu\, u^\nu$ acts as a projection perpendicular to four velocity; $u_\mu \Delta^{\mu\nu} = 0$. In the local rest frame of the fluid; i.e.; $u^\mu = (1, \vec{0})$, energy-momentum tensor takes the form

$$T^{\mu\nu} = \begin{pmatrix} \varepsilon & 0 & 0 & 0 \\ 0 & P & 0 & 0 \\ 0 & 0 & P & 0 \\ 0 & 0 & 0 & P \end{pmatrix}. \tag{1.28}$$

Now the hydrodynamic equations are obtained from the following energy-momentum conservation statement:

$$\partial_\mu T^{\mu\nu} = 0. \tag{1.29}$$

Apart from the energy-momentum conservation we may need to incorporate the information regarding the particle number conservation also. In order to write an equation for the conservation of particle number, i.e.; continuity equation, we need to define the four dimensional particle density flux $n^\mu = n u^\mu$ with n being the particle number density. In the case of high temperature the particle number may not be conserved due to pair creation and annihilation. In such cases we can take n to be a conserved number like net baryon number, n_B. Now the relativistic generalisation of the continuity equation is obtained by taking the 4-divergence of

n^μ and equating it to zero:

$$\partial_\mu n^\mu = 0. \tag{1.30}$$

By projecting Eq. (1.29) along the direction of u^μ and noting $u^\mu u_\mu = 1$ and $u^\mu \partial_\nu u_\mu = 0$, we find

$$u_\nu \partial_\mu T^{\mu\nu} = u_\mu \partial^\mu \varepsilon + (\varepsilon + P)\, \partial_\mu u^\mu = 0. \tag{1.31}$$

Next, projecting Eq. (1.29) along the perpendicular direction of u^μ, we get

$$\Delta_{\nu\alpha} \partial_\mu T^{\mu\nu} = (\varepsilon + P)\, u_\mu \partial^\mu u_\alpha - \Delta_{\alpha\nu} \partial^\nu P = 0. \tag{1.32}$$

The above two equations can be written in the following form,

$$D\varepsilon + (\varepsilon + P)\, \Theta = 0 \tag{1.33}$$

$$(\varepsilon + P)\, Du^\alpha - \nabla^\alpha P \,= 0 \tag{1.34}$$

where we denote $D \equiv u^\mu \partial_\mu$, $\Theta \equiv \partial_\mu\, u^\mu$ and $\nabla_\alpha = \Delta_{\mu\alpha} \partial^\mu$. Here we note that in the local rest frame of the fluid, D and ∇_i becomes time and spatial derivatives respectively.

Using the thermodynamic relations,

$$\begin{aligned} \varepsilon + P &= Ts + \mu\, n \\ d\varepsilon &= Tds + \mu\, dn \end{aligned} \tag{1.35}$$

where s being entropy density and μ being chemical potential; along with Eq. (1.30), from Eq. (1.33) it is easy to see that

$$\partial_\mu s^\mu = 0, \tag{1.36}$$

where $s^\mu = s\, u^\mu$ is the entropy flux. This is the statement of entropy conservation for an ideal fluid.

Eqs. (1.33 & 1.34) along with Eq. (1.30) are the fundamental equations for ideal relativistic fluids. The Eq. (1.34) is the relativistic generalisation of Euler's equation for non-relativistic ideal fluids and Eq. (1.33) gives the energy dissipation. In the non-relativistic limit ($|\vec{v}| \ll 1$) neglecting terms of the order $\mathcal{O}(|\vec{v}|^2)$ and above, we have

$$D \,\simeq\, \partial_t + \vec{v}\,.\,\vec{\nabla},\;\; \Theta \,\simeq\, \vec{\nabla}\,.\,\vec{v} \;\;\&\;\; \nabla^i \,\simeq\, -(\vec{\nabla} + \vec{v}\,\partial_t). \tag{1.37}$$

At this juncture we would like to note that basically there are only five equations: Eqs. (1.29 & 1.30) for the seven unknowns in the theory: u^μ, n, ε, P. So in order to close the system we need to have more equations. This is achieved by providing the EoS, which relates energy density and pressure: $\varepsilon = \varepsilon(P)$. Besides, the 4-velocity u^μ satisfies the relation $u_\mu u^\mu = 1$.

These equations are a set of coupled non-linear partial differential equations and it is rather difficult to find the general analytic solution. In the present treatise, we intend to apply these equations for a few well motivated but simple scenarios only.

1.2.2 Björken picture of expansion

Motivated by the empirical or experimental results, in 1983 J. D. Björken gave a model for expanding thermalised plasma created in heavy ion collisions [95]. This model is based on certain assumptions, namely a) the existence of a central plateu in the inclusive particle production with respect to the space-time rapidity; $\frac{dN}{d\eta_s} \sim$ const., b) that the receding nuclei carry all the baryon numbers creating baryon-less hot matter in between them, c) expansion of the thermalised matter formed along the longitudinal direction and d) boost invariant scaling flow of the matter formed. However, in reality there is a significant transverse flow observed at RHIC.

We will be interested in the initial stages of the central collision of the nuclei. Since the hot matter formed expands along longitudinal direction initially, as an approximation we can drop the transverse expansion at early times. After a time equal to the transverse size of the nucleus i.e.; $R_A = 1.2A^{1/3}$ fm (A- atomic mass number of the nucleus), transverse flow will be generated [12].

In what follows we use Björken's scenario to describe the one dimensional boost invariant expanding flow, where we use the convenient parametrization of the co-ordinates

$$t = \cosh\eta_s \quad \& \quad z = \tau\,\sinh\eta_s \tag{1.38}$$

using the proper time (τ) and space-time rapidity (η_s),

$$\tau = \sqrt{t^2 - z^2} \quad \& \quad \eta_s = \frac{1}{2}\ln\left[\frac{t+z}{t-z}\right]. \tag{1.39}$$

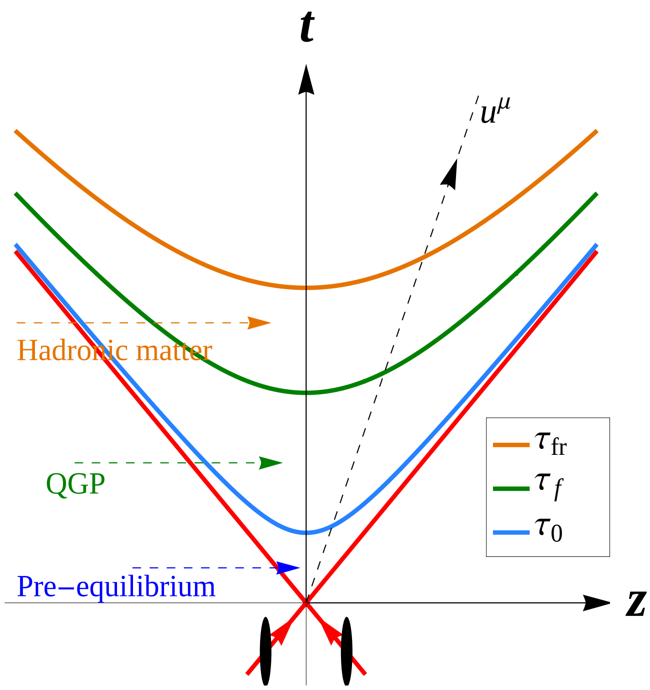

Figure 1.2: *Space-time picture of nuclear collision in Björken model*

Now the 4-velocity in this one dimensional analysis is obtained as,

$$\begin{aligned} u^\mu &= \frac{dx^\mu}{d\tau} = \gamma\,(1,0,0,v_z) = (t/\tau,0,0,z/\tau) \\ &= (\cosh\eta_s,0,0,\sinh\eta_s). \end{aligned} \tag{1.40}$$

Here we note that $v_z = z/t$ and $\tau = t/\gamma$. This prescription of the flow is called as *Björken's scaling flow* or simply *Björken flow*. The transformation of the derivatives from (t,z) to (τ,η_s) coordinates is given by

$$\begin{pmatrix} \partial_t \\ \partial_z \end{pmatrix} = \begin{pmatrix} \cosh\eta_s & -\sinh\eta_s \\ -\sinh\eta_s & \cosh\eta_s \end{pmatrix} \begin{pmatrix} \partial_\tau \\ \frac{1}{\tau}\partial_{\eta_s} \end{pmatrix} . \tag{1.41}$$

Also with this scaling flow we have

$$D = \frac{\partial}{\partial\tau} \quad \text{and} \quad \Theta = \frac{1}{\tau}. \tag{1.42}$$

Now within Björken flow relativistic Euler equation: Eq. (1.34) gives

$$\frac{\partial P(\tau,\eta_s)}{\partial\eta_s} = 0. \tag{1.43}$$

Thus the pressure (and other thermodynamics quantities also) is a function of τ only. Next, the entropy equation Eq. (1.36) becomes

$$\frac{\partial s}{\partial\tau} + \frac{s}{\tau} = 0, \tag{1.44}$$

implying

$$s\,\tau = s(\tau_0)\,\tau_0, \tag{1.45}$$

with τ_0 being the proper initial time.
The energy dissipation equation i.e.; Eq. (1.33) under Björken flow

$$\frac{\partial\varepsilon}{\partial\tau} + \frac{\varepsilon + P}{\tau} = 0. \tag{1.46}$$

So far our consideration doesn't depend on any EoS. To get further insight into the scaling flow solutions we use *ideal* EoS of relativistic weakly interacting massless quarks and gluons (Appendix A), characterised by

$$P = c_s^2\,\varepsilon = \varepsilon/3. \tag{1.47}$$

Here $c_s = \sqrt{\frac{\partial P}{\partial \varepsilon}} = \frac{1}{\sqrt{3}}$ is the speed of sound in the medium. In this case pressure of the system is given as (with zero baryon chemical potential i.e.; $\mu_B = 0$)

$$P = a\,T^4\,; \quad a = \left(16 + \frac{21}{2}N_f\right)\,\frac{\pi^2}{90}, \tag{1.48}$$

where N_f is the number of flavors considered. $\varepsilon(\tau)$ and $T(\tau)$ can be obtained by solving Eq. (1.46) and is given by [95],

$$\varepsilon = \varepsilon_0\,\left(\frac{\tau_0}{\tau}\right)^{1+c_s^2}, \tag{1.49}$$

$$T = T_0\,\left(\frac{\tau_0}{\tau}\right)^{c_s^2}, \tag{1.50}$$

where τ_0 and T_0 are the initial time and temperature. So the temperature gets reduced by a longitudinal expansion according to Björken flow described by the Eq. (1.50). From this, one can estimate the time system takes to reach the critical temperature, if τ_0 and T_0 are known.

Although we will restrict ourself to the central collisions, in reality, off-central collisions happen in experiments and result in important observables like *the elliptic flow*. Elliptic flow is quantified by the flow parameter, the second Fourier coefficient in the azimuthal distribution of produced particles in momentum space, v_2 [97]. In elliptical flow, the initial spatial anisotropy is converted into final momentum space anisotropy of observed particles.

1.2.3 Viscosity in heavy ion collisions

Ideal hydrodynamics is successfully used to model QGP formed in heavy ion collisions and to compare with the observables (see Ref. [98] for a review). Having analysed the *ideal* flow of QGP, a natural question one may ask is about the viscosity of the QGP, as non-viscous flows are unnatural.

First thing one need to address here is the nature of dissipative hydrodynamics needed to describe the system, as there are various dissipative hydrodynamics theories available [99]. First order Navier-Stokes dissipative hydrodynamics formalism was applied in the context of heavy ion collisions to study the viscous plasma properties [100, 101]. However, Navier-Stokes formalism is known to have several issues like acausal propagation of information [102] and unphysical instabilities [103]. Further, while applied to heavy ion collision scenario Navier-Stokes formalism gives unphysical reheating of the fireball. However, if one employs second order theories, like that of Israel-Stewart [104–106], such artifacts are removed [107].

Shear viscosity of QGP matter produced in RHIC and LHC is under extensive investigation. RHIC experimental results of elliptical flow parameter v_2 (which indicates the collectivity of the flow) show that matter produced in RHIC exhibits strong collective flow [108] indicating a very low value for the ratio shear viscosity (η) to entropy density (s). Lot of efforts has been gone into extract the shear viscosity of QGP formed in RHIC and now in LHC. Using causal viscous hydrodynamics a comparison between theoretical and experimental results is done leading to the result that this value of η/s should not be much larger than $1/4\pi$ [109]; the conjectured lower bound of η/s for *any* system, known as KSS bound [110]. Thus the QGP produced in RHIC experiments is believed to be in a form of *the most perfect liquid* in nature [111], since this value of η/s is the smallest for any known liquid [112]. It might be mentioned here that it is the value of the quantity η/s, which measures the "perfectness" of the fluid under consideration; that is low for QGP. If we consider the shear viscosity η alone, it is high for QGP, for e.g.; several orders of magnitude higher than that of water [112]. Situation can differ if one goes to the LHC energies as matter will be produced at much high temperature there and one may expect a change in the value of η/s.

It is only very recently realized that the effect of bulk viscosity can bring complications in the hydrodynamical description of the heavy-ion collisions. Since bulk viscosity ζ scaled like $\varepsilon - 3P$, at very high energy ζ was set to zero as the matter might be following the ideal gas type EoS: $\varepsilon = 3P$ [46]. But during its course of expansion the fireball temperature can approach values close to T_c. Recent lQCD results [7] show that the quark-gluon matter do not satisfy ideal EoS near T_c and the ratio ζ/s show a strong peak around T_c [113]. The bulk viscosity contribution in this regime can be much larger than that of the the shear viscosity. Recently the role of bulk viscosity in heating and expansion of the fireball was analyzed using one dimensional hydrodynamics [114, 115]. Another complication that bulk viscosity brings in hydrodynamics of heavy ion collisions is phenomenon of *cavitation* [115]. Cavitation arises when the fluid pressure becomes smaller than the vapour pressure. Since the bulk viscosity (and also shear viscosity) contributes to the pressure gradient with a negative contribution, it may be possible for the effective fluid pressure to become zero. Once the cavitation sets in, the hydrodynamical description breaks down. It was shown in Ref. [115] that cavitation may happen in RHIC experiments when the effect of bulk viscosity is included in manner consistent with the lQCD results. It was shown that the cavitation may significantly reduce the time of hydrodynamical evolution. We also would also like to study the effect of viscosity on the chemical equilibration of the plasma.

We would like to explore the effects of viscosities- both bulk and shear, on hydrodynamic evolution of QGP at RHIC and LHC energies, using causal second order hydrodynamics. Further, we would also like to understand the effect of viscosities on the thermal particles (photon and dilepton) produced from the QGP phase.

1.3 Organisation of the thesis

The thesis is organised as follows:

After a brief introduction in Chapter 1, in Chapter 2, we introduce the chiral model that includes the hyperons, which we shall use to obtain the EoS needed to study the equilibrium structure of the neutron star. In the subsequent sections, we derive the bulk viscosity of the hyperonic matter and discuss their role in damping of r-mode instability in the specific model of neutron star with a hyperon core.

In Chapter 3, we move from cold and dense matter to hot QGP created in heavy ion collisions. We first give a brief review of causal relativistic dissipative hydrodynamics and its application in describing the viscous expansion of the QGP in heavy ion collisions. We also discuss the properties of the QGP produced in heavy ion collisions like bulk viscosity, shear viscosity and EoS.

In Chapter 4, we numerically solve the equations of causal hydrodynamics in (1+1)-dimensions for the initial conditions relevant for RHIC and LHC. In this chapter we discuss various physical problems related with the chemical non-equilibration, fragmentation/cavitation caused by the presence of finite shear or bulk viscosity etc.

Chapter 5, consists of studying the consequences of the above stated physical situations due to the presence of finite viscosity on electromagnetic probes of the QGP, namely thermal photons and dileptons.

Finally, in Chapter 6, we summarise our results and also discuss the future scope for further studies.

Chapter 2

Bulk viscosity of the hyperonic matter and r-mode instability

2.1 Effective chiral model for hyperons

The effective chiral model that we shall consider is a generalisation of the model considered in Ref. [57] to include the lowest lying octet of baryons (n, p, Λ^0, $\Sigma^{-,0,+}$, $\Xi^{-,0}$). They interact via the exchange of the pseudo-scalar mesons π, the scalar meson σ, the vector meson ω and the iso-vector $\rho-$meson. Lagrangian density under consideration is given by [57]:

$$
\begin{aligned}
\mathscr{L} \;=\; & \bar{\Psi}_B \left[i\gamma_\mu \partial^\mu - g_{\omega B}\gamma_\mu \omega^\mu - \frac{1}{2} g_{\rho B} \vec{\rho}_\mu \cdot \vec{\tau}\gamma^\mu - g_{\sigma B}\left(\sigma + i\gamma_5 \vec{\tau}\cdot\vec{\pi}\right)\right] \Psi_B \\
& + \frac{1}{2}\left(\partial_\mu \vec{\pi}\cdot\partial^\mu\vec{\pi} + \partial_\mu\sigma\partial^\mu\sigma\right) - \frac{\lambda}{4}\left(x^2 - x_0^2\right)^2 - \frac{\lambda B}{6}\left(x^2 - x_0^2\right)^3 - \frac{\lambda C}{8}\left(x^2 - x_0^2\right)^4 \\
& - \frac{1}{4} W_{\mu\nu}W^{\mu\nu} + \frac{1}{2} {g_{\omega B}}^2 x^2 \omega_\mu \omega^\mu - \frac{1}{4}\vec{R}_{\mu\nu}\cdot\vec{R}^{\mu\nu} + \frac{1}{2} m_\rho^2 \vec{\rho}_\mu \cdot \vec{\rho}^\mu \; . \qquad (2.1)
\end{aligned}
$$

The first line of the above Lagrangian density represents the interaction of baryons Ψ_B with the aforesaid mesons. In the next line, we have the kinetic and the non-linear terms in the pseudo-scalar-isovector pion field '$\vec{\pi}$', the scalar field 'σ', and with chiral invariant $x^2 = \vec{\pi}^2 + \sigma^2$. Finally in the last line, we have the field strength and the mass term for the vector field 'ω' and the iso-vector field '$\vec{\rho}$' meson; with $W_{\mu\nu} = \partial_\mu\omega_\nu - \partial_\nu\omega_\mu$ and $\vec{R}_{\mu\nu} = \partial_\mu\vec{\rho}_\nu - \partial_\nu\vec{\rho}_\mu$. The terms in Eq. (2.1) with the subscript B should be interpreted as sum over the states of lowest baryonic octet. In this paper, we shall be concerned only with the normal non-pion condensed state of matter and, so we take $\langle\vec{\pi}\rangle = 0$ and pion mass $m_\pi = 0$.

The potential $V(\sigma, \pi)$ in Eq. (2.1), given by

$$V(\sigma,\pi) = \frac{\lambda}{4}\left(x^2 - x_0^2\right)^2 + \frac{\lambda B}{6}\left(x^2 - x_0^2\right)^3 + \frac{\lambda C}{8}\left(x^2 - x_0^2\right)^4, \tag{2.2}$$

generates the vacuum expectation value for σ by spontaneously breaking the chiral symmetry, $\langle 0|\sigma|0\rangle = x_0$. Then, mass acquired by the σ particle is given by

$$m_\sigma^2 = \frac{\partial^2 V}{\partial \sigma^2}|_{\sigma=x_0} = 2\lambda x_0^2, \tag{2.3}$$

where $\lambda = (m_\sigma^2 - m_\pi^2)/(2f_\pi^2)$, where f_π being the pion decay constant. Now, the interaction of the scalar and the pseudo-scalar mesons with the vector boson generates a dynamical mass for the vector bosons through spontaneous breaking of the chiral symmetry with scalar field getting the vacuum expectation value x_0. Then the masses of the baryons, the scalar and the vector mesons, are respectively given by

$$m_B = g_{\sigma B} x_0, \quad m_\sigma = \sqrt{2\lambda} x_0, \quad m_\omega = g_{\omega B} x_0 \ . \tag{2.4}$$

We could have taken an interaction of the $\rho-$meson with the scalar and the pseudo-scalar mesons similar to the omega meson. However, a dynamical mass generation mechanism of the $\rho-$meson in a similar manner will not generate the correct symmetry energy. Therefore, we have taken an explicit mass term for the isovector $\rho-$meson similar to what was considered in earlier works [54, 57].

The equations of motion for the fields can be written now. The Euler-Lagrangian equations for the meson fields are,

$$\left[\partial_\mu \partial^\mu - \sum_B {g_{\omega B}}^2 \omega_\mu \omega^\mu\right] x = -\sum_B g_{\sigma B} \bar{\Psi}_B \Psi_B - \frac{\partial V}{\partial x}, \tag{2.5}$$

$$\partial_\mu W^{\mu\nu} + {g_{\omega B}}^2 x^2 \omega^\nu = \sum_B g_{\omega B} \bar{\Psi}_B \gamma^\nu \Psi_B, \tag{2.6}$$

$$\partial_\mu R_i^{\mu\nu} + m_\rho^2 \rho_i^\nu = \sum_B g_{\rho B} \bar{\Psi}_B \gamma^\nu I_{iB} \Psi_B; \tag{2.7}$$

and the Dirac equation for the baryons reads as

$$\left[i\gamma^\mu \partial_\mu - g_{\omega B}\gamma^\mu \omega_\mu - \frac{1}{2} g_{\rho B} \gamma^\mu \vec{\rho}_\mu \cdot \vec{\tau} - g_{\sigma B}\ x\right] \Psi_B = 0. \tag{2.8}$$

Here in Eq. (2.7) we have used $\vec{\tau} = \sum_{i=1}^{3} 2 I_B^i$, where I_B^i is the ith component of isospin of each baryon species (See Table 2.1). In Eq. (2.8) mass term appears as $g_{\sigma B}\ x$ and we call it as the *effective mass* m_B^* of the baryon.

Table 2.1: *Baryonic octet*

B	Mass (MeV)	Q_B	I_3
p, n	938	1, 0	1/2, -1/2
Λ^0	1116	0	0
$\Sigma^{-,0,+}$	1193	-1, 0, 1	-1, 0, 1
$\Xi^{-,0}$	1318	-1, 0	-1/2, 1/2

We use relativistic mean field theory (RMFT) approximation to evaluate the meson fields in our present calculation. In the mean field treatment, meson fields are replaced by classical constant fields while retaining the quantum nature of the baryonic fields Ψ_B. We refer Section 1.1.1 for more details. Under RMFT approximation, we have,

$$x \;\rightarrow\; \langle x \rangle \;= x_0, \tag{2.9}$$

$$\omega^\mu \;\rightarrow\; \langle \omega^\mu \rangle \;= \delta^{\mu 0}\omega_0, \tag{2.10}$$

$$\rho^{i\mu} \;\rightarrow\; \langle \rho^{i\mu} \rangle \;= \delta^{3i}\delta^{\mu 0}\rho_{03}. \tag{2.11}$$

Dirac equation for Ψ_B now becomes,

$$\left[i\gamma^\mu\partial_\mu - g_{\omega B}\gamma^0\omega_0 - g_{\rho B}\gamma^0\rho_{03}I_{3B} - m_B^*\right]\Psi_B = 0, \tag{2.12}$$

and this equation can be treated as the corresponding equation in the Walecka model i.e.; Eq. (1.9). Using similar procedure, see Eqns. (1.9 - 1.15), we can obtain the general solution to Eq. (2.12),

$$\Psi_B(x) = \sum_{\vec{k}\ r} \frac{1}{\sqrt{2V\mathcal{K}^0}} \left[a_{\vec{k}\ r} U_r(\vec{k})\, e^{-iE^+t + i\vec{k}\cdot\vec{x}} + b^\dagger_{\vec{k}\ r} V_r(\vec{k})\, e^{-iE^-t - i\vec{k}\cdot\vec{x}}\right], \tag{2.13}$$

with eigenvalues of particle (E^+) and antiparticle (E^-) given as,

$$E^{(\pm)} = g_\omega\omega_0 + g_{\rho B}\rho_{03}I_{3B} \pm \sqrt{\vec{k}^2 + M^{*2}}, \tag{2.14}$$

where $\mathcal{K}^0 = \sqrt{\vec{k}^2 + M^{*2}}$. As before, $a_{\vec{k}\ r}$ ($b^\dagger_{\vec{k}\ r}$) is the annihilation (creation) operator for baryons (anti-baryons). The spinors are normalised as in Eq. (1.15), with M^* being replaced by $m_B^* = g_{\sigma B}x$. Again we note that, we are describing nuclear matter inside neutron star, $T \simeq 0$, and we don't consider antiparticles in the present problem.

We now calculate the baryon density n_B and the scalar density n_{SB} for a baryon species,

$$n_B = \langle \psi^\dagger \psi \rangle = \frac{\gamma}{(2\pi)^3} \int_o^{k_{F_B}} d^3k, \tag{2.15}$$

$$n_{SB} = \langle \bar{\psi} \psi \rangle = \frac{\gamma}{(2\pi)^3} \int_o^{k_{F_B}} \frac{m_B^* d^3k}{\sqrt{\vec{k}^2 + m_B^{\star 2}}}, \tag{2.16}$$

where k_{F_B} is the fermi momentum of the baryon and $\gamma = 2$ is the spin degeneracy factor.

The field equations for vector meson i.e.; Eq. (2.6), and iso-vector meson i.e.; Eq. (2.7), in RMFT framework become,

$$\omega_0 = \sum_B \frac{n_B}{g_{\omega B} x^2} \ , \tag{2.17}$$

$$\rho_{03} = \sum_B \frac{g_{\rho B}}{m_\rho^2} I_{3B} n_B \ . \tag{2.18}$$

respectively.

The scalar field Eq. (2.5) within RMFT can be written in terms of the variable $Y = x/x_0$ with $x = \sqrt{\langle \sigma^2 + \vec{\pi}^2 \rangle}$ as [57]

$$\sum_B \left[(1 - Y^2) - \frac{B}{c_{\omega B}} (1 - Y^2)^2 + \frac{C}{c_{\omega B}^2} (1 - Y^2)^3 + \frac{2 c_{\sigma B} c_{\omega B} n_B^2}{m_B^2 Y^4} - \frac{2 c_{\sigma B} n_{SB}}{m_B Y} \right] = 0, \tag{2.19}$$

where the effective mass of the baryonic species is $m_B^\star \equiv Y m_B$ and $c_{\sigma B} \equiv g_{\sigma B}^2 / m_\sigma^2$ are the $c_{\omega B} \equiv g_{\omega B}^2 / m_\omega^2$ are the usual scalar and vector coupling constants respectively. Similarly, in the present model describing dense matter, the $\omega-$meson mass is generated dynamically. This vector meson mass enters in Eq. (2.19) through the ratio $c_\omega = (g_\omega / m_\omega)^2 \equiv 1/{x_0}^2$. Various parameters of the model for the nuclear matter case (the meson nucleon couplings, $C_\sigma, C_\omega, C_\rho$ and the non-linear couplings B and C) are fitted from nuclear matter saturation properties [54, 56, 57]. It was shown recently that these parameters are rather constrained by the nuclear matter saturation properties like the binding energy per nucleon, saturation density, the nuclear incompressibility, as well as the asymmetry energy, the effective mass of the nucleon and the pion decay constant f_π.

Now we proceed to find the energy density and pressure (EoS) corresponding to this model. Noting that $\partial\mathscr{L}/\partial\partial_\mu\Psi_B = i\bar{\Psi}_B\gamma^\mu$, we can write under RMFT,

$$T^{\mu\nu} = -g^{\mu\nu}\mathscr{L} + i\bar{\Psi}_B\gamma^\mu\partial^\nu\Psi_B; \tag{2.20}$$

so that from Eq. (1.21),

$$\varepsilon = \langle\mathscr{H}\rangle = \langle T^{00}\rangle = i\langle\bar{\Psi}_B\gamma^0\partial^0\Psi_B\rangle - \langle\mathscr{L}\rangle \tag{2.21}$$

$$P = \frac{1}{3}\langle T^{ii}\rangle = \frac{1}{3}i\langle\bar{\Psi}_B\gamma^i\partial^i\Psi_B\rangle + \langle\mathscr{L}\rangle. \tag{2.22}$$

Therefor, for a given baryon density, the total energy density 'ε' and the pressure 'P' can be written in terms of the dimensionless variable $Y = x/x_0$ as

$$\begin{aligned}\varepsilon = {} & \frac{2}{\pi^2}\int_0^{k_{F_B}} k^2 dk\sqrt{k^2 + m_B^{\star 2}} + \frac{m_B^2(1-Y^2)^2}{8c_{\sigma B}} - \frac{m_B^2 B}{12c_{\omega B}c_{\sigma B}}(1-Y^2)^3 \\ & + \frac{m_B^2 C}{16c_{\omega B}^2 c_{\sigma B}}(1-Y^2)^4 + \frac{1}{2Y^2}c_{\omega B}n_B^2 + \frac{1}{2}m_\rho^2\rho_{03}^2 + \frac{1}{\pi^2}\sum_{\lambda=e,\mu^-}\int_0^{k_\lambda} k^2 dk\sqrt{k^2+m_\lambda^2}\,,\end{aligned} \tag{2.23}$$

$$\begin{aligned}P = {} & \frac{2}{3\pi^2}\int_0^{k_{F_B}} \frac{k^4 dk}{\sqrt{k^2 + m_B^{\star 2}}} - \frac{m_B^2(1-Y^2)^2}{8c_{\sigma B}} + \frac{m_B^2 B}{12c_{\omega B}c_{\sigma B}}(1-Y^2)^3 \\ & - \frac{m_B^2 C}{16c_{\omega B}^2 c_{\sigma B}}(1-Y^2)^4 + \frac{1}{2Y^2}c_{\omega_B}n_B^2 + \frac{1}{2}m_\rho^2\rho_{03}^2 + \frac{1}{3\pi^2}\sum_{\lambda=e,\mu^-}\int_0^{k_\lambda} \frac{k^4 dk}{\sqrt{k^2+m_\lambda^2}},\end{aligned} \tag{2.24}$$

where the last term in both equations represents the non-interacting lepton contribution; $\mathscr{L}_l = \sum_{l=e,\mu^-}\bar{\Psi}_l(i\gamma^\mu\partial_\mu - m_l)\Psi_l$. Neutron stars, generally, are considered to be made of mostly neutrons, some of them β-decay and subsequently an equilibrium is reached between neutrons, protons and electrons: $\mu_p + \mu_e = \mu_n$. At higher densities one can have muons also when $\mu_e = \mu_\mu$. Hyperons start to appear in neutron star core when the nucleon chemical potential is large enough to compensate the mas differences between nucleon and hyperons.

The meson field equations for the σ, ω and $\rho-$mesons, Eqs. (2.17 - 2.19), are then solved self-consistently at a fixed baryon density to obtain the respective field strengths. The EoS for the $\beta-$equilibrated hyperon rich matter is obtained with the requirements of conservation of total baryon number and charge neutrality condition given by [57]

Table 2.2: *Parameter set for the model.*

$c_{\sigma N}$ (fm^2)	$c_{\omega N}$ (fm^2)	$c_{\rho N}$ (fm^2)	B (fm^2)	C (fm^4)	K (MeV)	$m_N^\star/m_N$
6.79	1.99	4.66	-4.32	0.165	300	0.85

$$\sum_B Q_B n_B + \sum_l Q_l n_l = 0, \tag{2.25}$$

where n_B and n_l are the baryon and the lepton (e, μ^-) number densities with Q_B and Q_l as their respective electric charges. Further, we can relate chemical potential of each baryons in terms of two independent chemical potentials μ_n and μ_e, as

$$\mu_B = \mu_n - Q_B\,\mu_e. \tag{2.26}$$

The resulting EoS is discussed in Refs. [57, 116] in detail. It was further observed that the parameters of the model were sternly constrained and turned to be consistent with the constraints on nuclear equation of state from heavy ion collision data [116, 117]. Using general relativistic stellar structure equations, neutron star sequences, both rotating and non-rotating; has been considered in Ref. [116]. Where, global properties of resulting neutron star with hyperonic core, has been studied. In this calculation we use EoS corresponding to $m_N^*/m_N = 0.85$, as shown in Fig. 2.1. Parameter set for the model is given in Table 2.2. In this model, all the baryons start to appear if we go upto 10 times normal nuclear matter density n_0 [116]. First, around $2n_0$ Σ^- followed by Λ^0 hyperons start to appear, whereas other baryons comes after $4n_0$ only.

2.2 Hyperon bulk viscosity

Bulk viscosity characterizes the response of the system to an externally oscillating change in the volume. The volume expansion or contraction leads to a change in density or the chemical potential of the system. This drives the system out of chemical equilibrium. The equilibrium is restored by the microscopic processes.

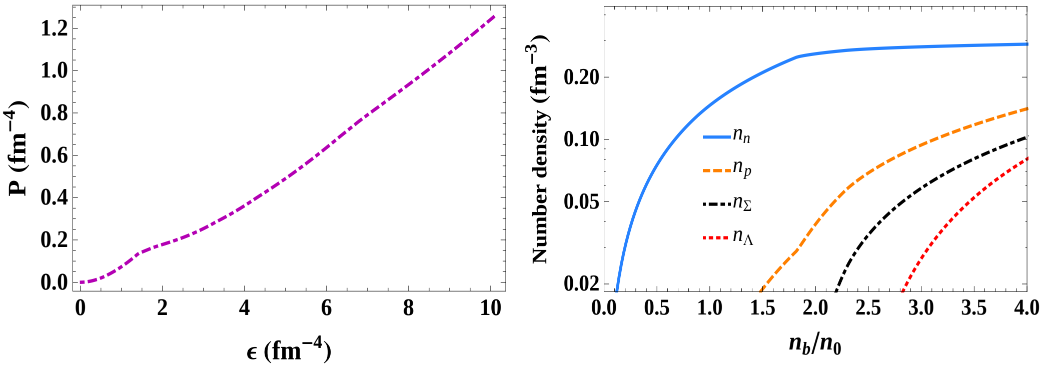

Figure 2.1: *EoS and corresponding particle densities*

If the equilibrium time scales are comparable to the oscillating time scales, there will be energy dissipation. In the context of neutron star, the typical oscillation frequencies are less than a kilo hertz. Therefore, the microscopic processes that will be relevant are the weak processes.

It is already known that the non-leptonic processes containing hyperons lead to high values of bulk viscosity for rotating neutron stars with temperature $\sim 10^9 - 10^{10}$K [76, 78]. We note that hyperons can contribute to bulk viscosity also through semi-leptonic processes like their direct Urca. These effects has been considered in Ref. [118] and is shown to contribute to the bulk viscosity as comparable as the nucleon initiated direct Urca processes. However their contribution is negligible compared to the more efficient non-leptonic weak interaction processes [76, 79, 119]. The leptonic processes are suppressed by smaller phase space factors. Thus the relevant reactions which are going to give a lower limit on the rates (or upper limit on bulk viscosity) are

$$n + n \longleftrightarrow p + \Sigma^- \tag{2.27}$$

$$n + p \longleftrightarrow p + \Lambda^0 \tag{2.28}$$

$$n + n \longleftrightarrow n + \Lambda^0 \tag{2.29}$$

The coefficient of bulk viscosity relates difference between the perturbed pressure P and the thermodynamic pressure $\tilde{P}$ to the macroscopic expansion of the fluid as

$$P - \tilde{P} = -\zeta \vec{\nabla} \cdot \vec{v} \tag{2.30}$$

where $\vec{v}$ is the velocity of the fluid element and ζ is the coefficient of bulk viscosity, which, in general, is complex in nature [96].

The relativistic expression for the real part of ζ, which corresponds to the damping, can be calculated in terms of microscopic equilibrium restoring reaction rates [78, 96]. Within a relaxation time approximation, the real part of ζ is given as [96],

$$\zeta = \frac{P\left(\gamma_\infty - \gamma_0\right)\tau}{1 + \left(\omega\tau\right)^2} \tag{2.31}$$

where γ_∞ and γ_0 are the "infinite" and "zero" frequency adiabatic index respectively. ω is the angular frequency of the perturbation in co-rotating frame and τ is the net equilibrium restoring microscopic relaxation time. The expression for $\gamma_\infty - \gamma_0$ is

$$\gamma_\infty - \gamma_0 = -\frac{{n_B}^2}{P}\frac{\partial P}{\partial n_n}\frac{d\tilde{x}}{dn_B} \tag{2.32}$$

Here n_B corresponds to the total baryon density and $\tilde{x} = \frac{n_n}{n_B}$ is the neutron fraction.Thus the difference $\gamma_\infty - \gamma_0$ can be calculated from a given equation of state. The angular frequency ω of the r - mode (l=2, m=2) in a co-rotating frame is given in terms of the angular velocity Ω of the rotating star as $\omega = \frac{2m}{l(l+1)}\Omega$ [66].

The prominent reactions involving the lightest hyperons, Σ^- and Λ^0, which have higher population in a given star are as given by Eqs. (2.27 & 2.28). The rates of these reactions can be calculated from the tree-level Feynman diagrams involving the exchange of a W boson.

We are not be considering the other reaction $n + n \longleftrightarrow n + \Lambda^0$ since it has no simple W-boson exchange picture. We shall discuss more regarding this in Section III. The relaxation time τ (at a temperature T), when both Σ^- and Λ^0 are present, is given by [78, 82]

$$\frac{1}{\tau} = \frac{(k_B T)^2}{192\pi^3}\left(k_\Sigma \left\langle|\mathcal{M}_\Sigma^2|\right\rangle + k_\Lambda \left\langle|\mathcal{M}_\Lambda^2|\right\rangle\right)\frac{\delta\mu}{n_B \delta x_n} \tag{2.33}$$

where k_B is the Boltzmann's constant and k_Λ and k_Σ are the Fermi momenta of these hyperons. $\delta\mu \equiv \delta\mu_n - \delta\mu_\Lambda$ is the chemical potential imbalance. $\delta x_n = x_n - \tilde{x_n}$ is the small difference between the perturbed and equilibrium values of the neutron fraction. $\langle|\mathcal{M}^2|\rangle$ are the angle averaged, squared, summed over initial spinors matrix elements of the reactions calculated from the Feynman diagrams. We refer

[78, 82] for the expressions for $\langle|\mathcal{M}_\Sigma^2|\rangle$ and $\langle|\mathcal{M}_\Lambda^2|\rangle$. We note that the contribution from Λ hyperons will not be present in Eq. (2.33) while considering a neutron star medium before the appearance of Λ.

The factor $\delta\mu/n_B\delta x_n$ is determined from the constraints imposed by the electric charge neutrality and the baryon number conservation given respectively as

$$\delta x_p - \delta x_\Sigma = 0 \tag{2.34}$$

$$\delta x_n + \delta x_\Lambda + \delta x_p + \delta x_\Sigma = 0 \tag{2.35}$$

together with the condition that the non-leptonic strong interaction reaction

$$n + \Lambda^0 \longleftrightarrow p + \Sigma^- \tag{2.36}$$

which has a higher rate, is in equilibrium compared to weak interaction processes giving rise to the bulk viscosity. Equilibrium of this reaction implies that both the reactions given by Eqs. (2.27 & 2.28) have equal chemical potential imbalance,

$$\delta\mu \equiv \delta\mu_n - \delta\mu_\Lambda = 2\delta\mu_n - \delta\mu_p - \delta\mu_\Sigma. \tag{2.37}$$

Using these constraints, we can write,

$$\begin{aligned}\frac{\delta\mu}{n_B\delta x_n} &= \alpha_{nn} + \frac{(\beta_n - \beta_\Lambda)(\alpha_{np} - \alpha_{\Lambda p} + \alpha_{n\Sigma} - \alpha_{\Lambda\Sigma})}{2\beta_\Lambda - \beta_p - \beta_\Sigma} \\ &\quad -\alpha_{\Lambda n} - \frac{(2\beta_n - \beta_p - \beta_\Sigma)(\alpha_{n\Lambda} - \alpha_{\Lambda\Lambda})}{2\beta_\Lambda - \beta_p - \beta_\Sigma}\end{aligned} \tag{2.38}$$

where $\alpha_{ij} = \left(\frac{\partial\mu_i}{\partial n_j}\right)_{n_k, k\neq j}$ and $\beta_i = \alpha_{ni} + \alpha_{\Lambda i} - \alpha_{pi} - \alpha_{\Sigma i}$. These expressions are for the case when both the Σ^- and Λ^0 hyperons are present. One can not use the reaction given by Eq. (2.36) while considering the region where we have only Σ^- hyperons. In that case, instead of Eq. (2.38), we have

$$\begin{aligned}\frac{2\delta\mu}{n_B\delta x_n} &= 4\alpha_{nn} - 2(\alpha_{pn} + \alpha_{\Sigma n} + \alpha_{np} + \alpha_{n\Sigma}) \\ &\quad +\alpha_{pp} + \alpha_{\Sigma p} + \alpha_{p\Sigma} + \alpha_{\Sigma\Sigma}.\end{aligned} \tag{2.39}$$

Now the α_{ij}'s can be found out using the expression for baryon chemical potential and the equations of motion of the mesonic fields given by Eqs. (2.17 & 2.18). In general, the form of the α_{ij} is given as,

$$\begin{aligned}\alpha_{ij} &= \frac{m_i^* m_i}{\sqrt{k_{F_i}^2 + m_i^{*2}}}\frac{\partial Y}{\partial n_j} + \frac{g_{\omega i}}{g_{\omega j}}\frac{1}{(Yx_0)^2} \\ &\quad -\frac{2g_{\omega i}x_0}{(Yx_0)^3}\left(\sum_B \frac{\rho_B}{g_{\omega B}}\right)\frac{\partial Y}{\partial n_j} + \frac{1}{2m_\rho^2}(g_{\rho i}g_{\rho j})(I_{3i}I_{3j})\end{aligned} \tag{2.40}$$

for $i \neq j$ and

$$\begin{aligned}\alpha_{ii} &= \frac{m_i^* m_i}{\sqrt{k_{F_i}^2 + m_i^{*2}}} \frac{\partial Y}{\partial n_i} + \frac{\pi^2}{k_{F_i}\sqrt{k_{F_i}^2 + m_i^{*2}}} + \frac{1}{(Yx_0)^2} \\ &- \frac{2g_{\omega i}x_0}{(Yx_0)^3}\left(\sum_B \frac{\rho_B}{g_{\omega B}}\right)\frac{\partial Y}{\partial n_i} + \frac{1}{2}(\frac{g_{\rho i}I_{3i}}{m_\rho})^2. \end{aligned} \tag{2.41}$$

As before, Y is the scalar field expectation value in the medium in units of its vacuum expectation value. Further, $\frac{\partial Y}{\partial n_i}$ are calculated from the scalar field Eq. (2.19) and are given by

$$\frac{\partial Y}{\partial n_i} = \frac{1}{D}\left(\frac{2c_{\sigma i}c_{\omega i}\rho_i}{m_B^2 Y^4} - \frac{c_{\sigma i}m_i^*}{m_i Y\sqrt{k_{F_i}^2 + m_i^{*2}}}\right) \tag{2.42}$$

with

$$\begin{aligned} D &= \sum_B \left[\, Y + \frac{2B}{c_{\omega B}}(Y^2-1)Y + \frac{3C}{c_{\omega B}^2}(Y^2-1)^2 Y - \frac{c_{\sigma B}\rho_{SB}}{m_B Y^2} + \frac{4c_{\sigma B}c_{\omega B}\rho_B^2}{m_B^2 Y^5} \right. \\ &\left. + \frac{c_{\sigma B}}{m_B Y}\frac{\gamma}{(2\pi)^3}\int_o^{k_{F_B}} d^3k \frac{k^2 m_B}{(k^2 + m_B^{*2})^{3/2}} \,\right] \end{aligned} \tag{2.43}$$

Using Eqs. (2.39 - 2.43), one can compute the relaxation time from Eq. (2.33) and hence the bulk viscosity given in Eq. (2.31), for a given equation of state.

2.3 r-mode damping in a neutron star

As mentioned in the introduction Section 1.1.2, the r-modes correspond to the axial modes where the restoring force is the Coriolis force. In a rotating star emission of these waves causes the modes to grow. This instability can get damped due to the various viscosities of the stellar matter. This happens when the damping time scales associated with these viscous processes are comparable to the gravitational radiation (GR) time scale [63].

We need the expressions for the time scales associated with the dissipative processes and GR in order to understand the nature of the damping of the r-modes. The imaginary part of the dissipative time scale (which causes the damping) is given by [78, 127]

$$\frac{1}{\tau_i} = -\frac{1}{2\tilde{E}}\left(\frac{d\tilde{E}}{dt}\right)_i \tag{2.44}$$

where i labels the various dissipative phenomena like hyperonic bulk viscosity (B), bulk viscosity due to Urca processes (U), shear viscosity (η) GR etc. In the above, $\tilde{E}$ is energy of the r-mode in the co-rotating frame. This can arise both from velocity perturbation as well as the perturbation of the gravitational potential. For a slowly rotating star, the dominant contribution is from the velocity perturbation and is given as

$$\tilde{E} = \frac{1}{2} \int \rho |\delta \vec{v}|^2 d^3x, \tag{2.45}$$

with, $\rho(r)$ being the mass density of the star. Assuming the spherical symmetry, mode energy can be reduced into an one dimensional integral [63] as

$$\tilde{E} = \frac{1}{2} \alpha^2 \Omega^2 R^{-2l+2} \int_0^R \rho(r) r^{2l+2} dr. \tag{2.46}$$

with $l = m = 2$ for the r-modes and R denotes the radius of the star. α is the dimensionless amplitude coefficient of the mode, which gets canceled out in the τ calculation. This energy is dissipated both by gravitational radiation as well as thermodynamic transport of the fluid [61, 65, 66]. The dissipation rate due to the bulk viscosity effects is given by

$$\frac{d\tilde{E}_B}{dt} = -\int \text{Re}\ \zeta \ |\vec{\nabla} \cdot \delta \vec{v}|^2 d^3x. \tag{2.47}$$

Here, in general, $|\vec{\nabla} \cdot \delta \vec{v}|^2$ depends upon the radial and the angular co-ordinates. In slowly rotating stars, to the lowest order, ζ depends only on the radius. Therefore, to the lowest order in Ω, it is possible to write the bulk viscosity dissipation rate in Eq. (2.47) as an one dimensional integral by defining a quantity which is the angle averaged expansion squared $\left\langle |\vec{\nabla} \cdot \delta \vec{v}|^2 \right\rangle$. In terms of this quantity, Eq. (2.47) can be written as

$$\frac{d\tilde{E}_B}{dt} = -4\pi \int_0^R \text{Re}\ \zeta(r) \left\langle |\vec{\nabla} \cdot \delta \vec{v}|^2 \right\rangle r^2 dr. \tag{2.48}$$

where $\left\langle |\vec{\nabla} \cdot \delta \vec{v}|^2 \right\rangle$ can be determined numerically [120]. However Refs. [78, 82] give an analytic expression

$$\langle |\vec{\nabla} \cdot \delta \vec{v}|^2 \rangle = \frac{\alpha^2 \Omega^2}{690} \left(\frac{r}{R} \right)^6 \left[1 + 0.86 \left(\frac{r}{R} \right)^2 \right] \left(\frac{\Omega^2}{\pi G \bar{\rho}} \right)^2, \tag{2.49}$$

which fits to the numerical data. Here G is the gravitational constant and $\bar{\rho}$ is the mean density of the non-rotating star.

Now with the knowledge of density profile $\rho(r)$ of the star, it is straightforward to find out the bulk viscosity damping time scales from equations Eq. (2.49), Eq. (2.48), Eq. (2.46) and Eq. (2.44), once we know the bulk viscosity coefficient $\zeta(r)$. In the case of bulk viscosity time scale arising due to hyperons (τ_B), we can get $\zeta(r)$ from Eq. (2.31) . Similarly we can find out the time scale (τ_U) associated with modified Urca processes, with the help of the expression for associated bulk viscosity ζ_U given by [121]

$$\zeta_U = 1.46\ \rho(r)^2\omega^{-2}\left[\frac{k_BT}{1MeV}\right]^6\ \mathrm{g/(cm\ s)}. \tag{2.50}$$

The shear viscosity time scale is given by [63]

$$\frac{1}{\tau_\eta} = \frac{(l-1)(2l+1)}{\int_0^R dr\rho(r)r^{2l+2}}\int_0^R dr\eta r^{2l}, \tag{2.51}$$

where η can be calculated from the prominent nn scattering and is given by [88]

$$\eta = 2\times 10^{18}\rho_{15}^{9/4}T_9^{-2}\ \mathrm{g/(cm\ s)}. \tag{2.52}$$

Here $\rho_{15} = \rho/(10^{15}\ \mathrm{g/cm^3})$ and $T_9 = T/(10^9\ \mathrm{K})$ are density and temperature respectively, casted in dimensionless forms. Finally, the gravitational radiation time scale (τ_{GR}) is given by [63],

$$\frac{1}{\tau_{GR}} = -\frac{32\pi G\Omega^{2l+2}}{c^{2l+3}}\frac{(l-1)^{2l}}{[(2l+1)!!]^2}\left(\frac{l+2}{l+1}\right)^{2l+2}\times\int_0^R \rho(r)r^{2l+2}dr. \tag{2.53}$$

The evolution of the r-mode due to dissipative viscous effects and GR can be studied by defining the overall r-mode time scale τ_r [63, 78, 122],

$$\frac{1}{\tau_r(\Omega,T)} = \frac{1}{\tau_{GR}(\Omega)} + \frac{1}{\tau_B(\Omega,T)} + \frac{1}{\tau_U(\Omega,T)} + \frac{1}{\tau_\eta(\Omega,T)}. \tag{2.54}$$

It appears in the decay of the mode as e^{-t/τ_r} and when $\tau_r > 0$, the mode is stable. Now from Eq. (2.53) we can see that $\tau_{GR} < 0$, which is indicative of the fact that GR allows the modes to grow and drives them to instability, while τ_B, τ_U and τ_η are positive and thus they try to dampen the mode. We can define the critical angular velocity Ω_C as $1/\tau_r(\Omega_C,T) = 0$; for a star at a given temperature T. Now if the angular velocity of the star is greater than Ω_C then the star is unstable and will be subjected to GR emission while stars with angular velocities smaller than Ω_C will be stable.

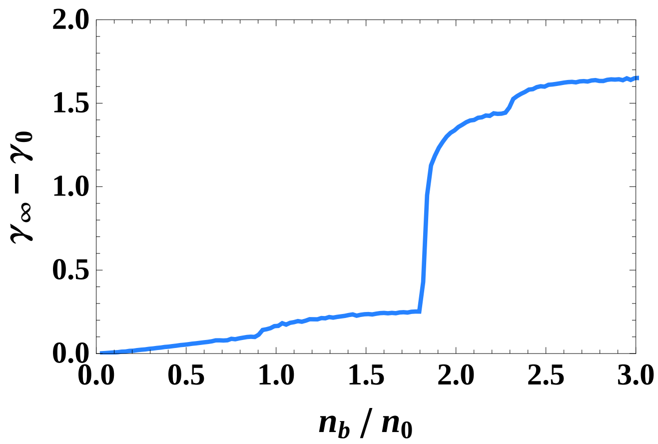

Figure 2.2: *Thermodynamic factor $\gamma_\infty - \gamma_0$ that appears in the expression for hyperon bulk viscosity, is plotted against the normalised baryon density.*

2.4 Results and discussions

Now with the EoS discussed in Section 2.1 we set out to find the coefficient of bulk viscosity as given by Eq. (2.31). The parameters in the effective chiral model that we have used are given in Table 2.2. The parameters were so chosen that they satisfy the constraints on the equation of state from the flow data in heavy ion collisions [116]. The resulting EOS is plotted in Fig. [2.1]. To calculate the bulk viscosity, we first need to calculate $\gamma_\infty - \gamma_0$, the difference between fast and slow adiabatic indices, from Eq. (2.32). This expression can be calculated with the help of EoS alone. In Fig. [2.2], we plot $(\gamma_\infty - \gamma_0)$ as a function of the normalized baryon density (n_b/n_0), where $n_0 = 0.153\ \text{fm}^{-3}$ is the nuclear matter saturation density. The sudden rises in the graph can be attributed to the appearance of hyperons with increase of baryon density at the cost of neutron number density n_n.

Since we have Σ^- and Λ hyperons formed in the system with lowest threshold densities, we consider the non leptonic reactions represented by the Eq. (2.27) and Eq. (2.28) and calculate the relaxation time as given by the Eq. (2.33). We note that we have not considered the reaction Eq. (2.29) and further there are several reactions which are going to contribute to the net reaction rate [80, 82]. The reason for this is that the rate for the process given in Eq.(2.29) is estimated to be an order of magnitude higher than the process given by Eq. (2.28). This leads to sub-

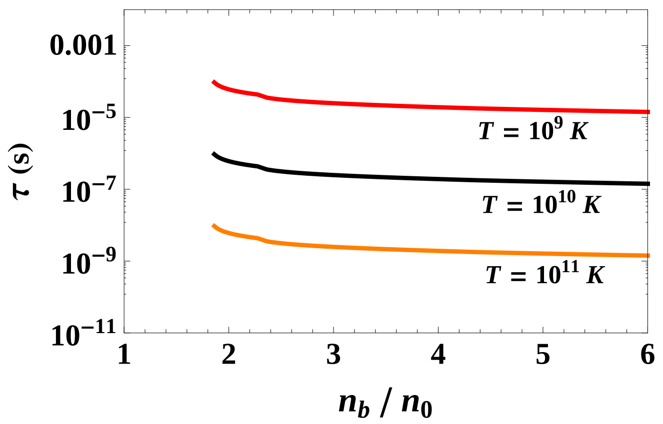

Figure 2.3: *Relaxation time τ (in seconds) for the non-leptonic processes causing hyperon bulk viscosity is plotted for various temperatures T.*

dominant contribution to the relaxation time and hence to the bulk viscosity [76]. Thus what we are calculating is a lower limit of the net rate which will correspond to an upper limit on the bulk viscosity. The matrix elements are calculated with the values of Fermi momenta and effective masses of various baryonic species obtained from the EoS. Here we use axial-vector coupling values $g_{np} = -1.27$, $g_{p\Lambda} = -0.72$ and $g_{n\Sigma} = 0.34$ measured in β-decay of baryons at rest and Fermi coupling constant $G_F = 1.166 \times 10^{-11}$ MeV^{-2} and sin$\theta_C = 0.222$ (where θ_C is the Cabibbo weak mixing angle) [?]. Then, we calculate $\frac{\delta\mu}{n_B \delta x_n}$ from Eq. (2.38) for the densities where both the hyperons are present ($n_B/n_0 > 2.36$), and, from Eq. (2.39) for lower densities where there is only Σ–hyperon present ($n_B/n_0 = 1.86 - 2.36$). Further, Eqs. (2.40 - 2.43) are evaluated using the EoS under consideration. We can thus calculate the relaxation time for relevant temperatures. We show the calculated behavior of relaxation time (in seconds) with temperature in Fig. [2.3]. It is clear that the relaxation time increases considerably with the decrease of temperature. For a given temperature, the relaxation time is seen to decrease when both the hyperons are present, as compared to the case of presence of a singe species of hyperons (Σ), since in this case τ value will be less according to Eq. (2.33).

We then compute the coefficient of bulk viscosity responsible for the mode damping in neutron stars from the expression given by Eq. (2.31). The value of maximum frequency Ω_K is the Keplerian angular frequency of the rotating star

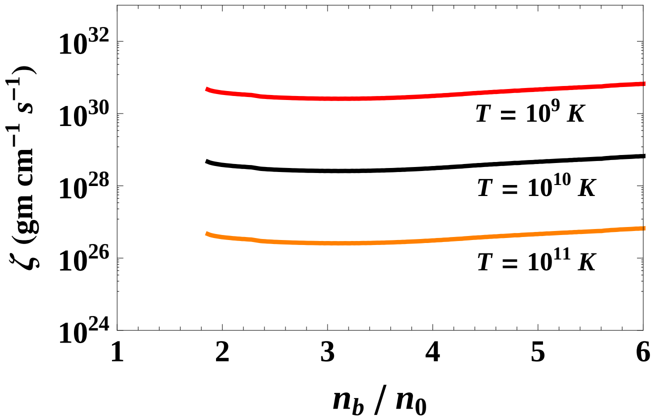

Figure 2.4: *Hyperon bulk viscosity ζ in units of g/(cm s) is plotted as a function of normalized baryon density for various temperatures.*

and is set by the onset of mass shedding from the equator of the star [123]. The bulk viscosity coefficient is calculated for the relevant temperatures and is plotted against the normalized baryon density in Fig. [2.4]. The behavior of the hyperon bulk viscosity is similar to that of the corresponding relaxation time as is expected from Eq. (2.31). The high value of the bulk viscosity coefficient at the temperature 10^9 K is indicative of the fact that hyperon bulk viscosity plays a major role in the suppression of the r-modes. We note that our bulk viscosity values are order of magnitude less than the values obtained by [78]. It could be due to the fact that unlike their work we are not considering the effect of hyperon superfluidity in this calculation. It might also be noted that the non-superfluid hyperonic bulk viscosity calculated in [83] uses an EoS based on a model, where only Λ hyperons are present at the relevant density.

We next study the effect of hyperon bulk viscosity on the r-modes. Here we need to calculate the dissipation time scale due to hyperon bulk viscosity as well as due to other dissipative phenomena. If this time scale is greater than the gravitational radiation time scale, then the r mode is not stable and suppressed. In order to calculate the dissipative timescales from Eqs. (2.44 - 2.53) we need to know the density profile $\rho(r)$, of the neutron star under consideration. We need to know the Kepler frequency of the rotating star also. We use Tolman-Oppenheimer-Volkoff equations to construct the non-rotating stellar configurations. The maximum mass of the neutron star in this case is found to be 1.65 $M_\odot$ with a radius of 16.7 km.

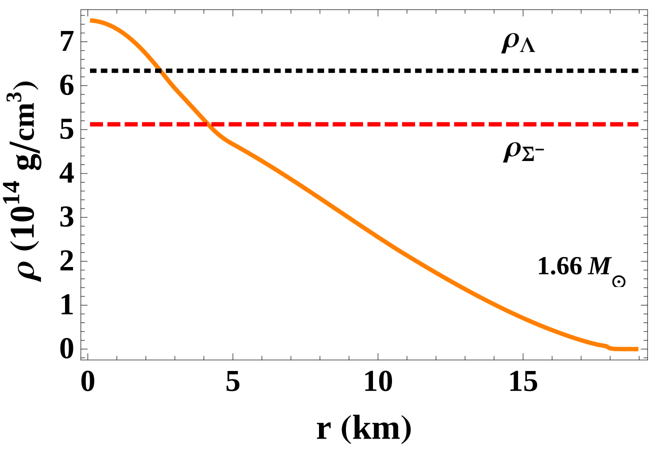

Figure 2.5: *Density of the star, ρ (in units of g/cm^3), as a function of distance r (in km) from the centre (r= 0) to the radius of the star (r = R). Threshold densities corresponding to the formation of Σ^- and Λ^0 hyperons are also plotted.*

We use Hartle's slow rotation approximation to calculate the global properties of rotating neutron star [124, 125]. We get the maximum mass and radius (R) of the rotating star to be 1.66 $M_\odot$ and 18.9 km respectively. The Kepler frequency in this case is found to be Ω_K = 3998 Hz. A typical density profile of the rotating star is shown in the Fig. [2.5]. This profile corresponds to a central density of 7.48×10^{14} gm/cm^3. We have also indicated the densities corresponding to the appearance of the hyperons, i.e., threshold densities of both Σ and Λ hyperons in the graph. From centre of the star upto a density of $\rho = 6.34 \times 10^{14}$ gm/cm^3, we have the presence of both the hyperons in the star (i.e., up to a distance 2.5 km from the centre). The presence of Σ alone is there upto $\rho = 5.1 \times 10^{14}$ gm/cm^3 (another 1.7 km) making a hyperon core of radius 4.2 km in the neutron star. Hyperon bulk viscosity time scale, and, hence its effects on r-mode is very sensitive to the hyperonic core's constituent structure and its radius.

For the rotating neutron star with a mass of 1.66 $M_\odot$ and Ω_K = 3998 Hz as considered above, we next evaluate the various dissipative time scales associated with the r-mode damping. The dissipative time scale of hyperonic bulk viscosity, denoted by τ_B can be calculated from Eqs. (2.44 - 2.49) with the help of density profile of the star. Here hyperonic bulk viscosity (ζ) as a function of radius is obtained from our previous calculations of ζ for the EoS together with the knowledge of stellar density profile i.e., $\zeta(\rho(r))$. The time scale associated with *modified*

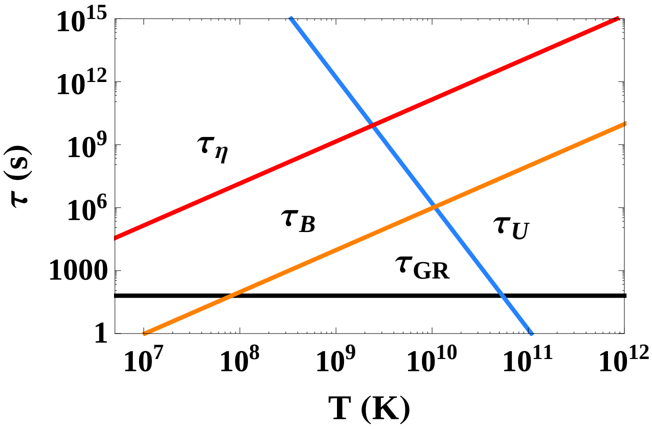

Figure 2.6: *The temperature dependence of damping time scales (in seconds) due to hyperonic bulk viscosity τ_B, modified Urca bulk viscosity τ_U and shear viscosity τ_η. τ_{GR} represents the temperature independent gravitational radiation time scale. (The star is considered to be rotating with the Kepler frequency Ω_K here).*

Urca processes τ_U, is calculated in the same manner as for τ_B, by using the Eq. (2.50) instead of hyperonic bulk viscosity. Next, we estimate the shear viscosity dissipative time scale τ_η using the Eqs. (2.51 & 2.52). Finally, the gravitational radiation time scale τ_{GR} associated with the r-mode can be calculated with the help of density profile using Eq. (2.53). Fig. [2.6] shows the calculated time scales as functions of temperature, for the star rotating with Ω_K. From Fig. [2.6], we observe that in the non-superfluid hyperonic matter, r-modes get substantially damped due to hyperonic bulk viscosity only at low temperatures ($T < 10^8$ K), whereas the *modified* Urca bulk viscosity suppresses the r-modes rapidly only at high temperatures $T > 5 \times 10^{10}$ K. The role of shear viscosity in suppressing the modes is not prominent in this temperature range. Consequently, the effect of r-mode instability will be prominent in the temperature window $(10^8 - 5 \times 10^{10})$ K. The hyperon bulk viscosity suppresses the instability for temperatures below 10^8K while modified Urca processes suppress the instability beyond $10^{10}K$.

Now we are in a position to calculate the critical angular velocity Ω_C of the neutron star. Ω_C is obtained by solving Eq. (2.54); $\frac{1}{\tau_r(\Omega_C,T)} = 0$, for a particular value of T. At this frequency, the energy fed into the r-mode per unit time by gravitational radiation is equal to the energy dissipated per unit time. A star

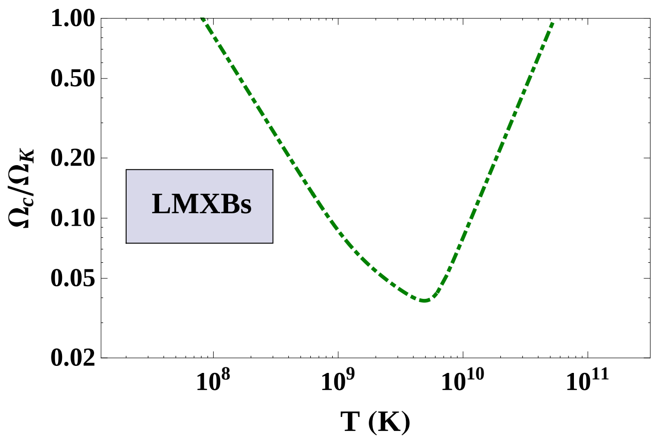

Figure 2.7: *Critical angular velocities (normalized to the Kepler frequency Ω_K = 3998* Hz*) for a neutron star with mass of 1.66 $M_\odot$ is shown as a function of hyperon core temperature. The shaded region represents the majority of the observed LMXBs.*

rotating above this critical frequency will be subjected to r-mode instability. We have shown the Ω_C (scaled to Ω_K) in Fig. [2.7] for the temperature regime of interest. Since Ω_K determines the maximum allowed rotation rate for the star, stable rotation at any temperature will have $\Omega_C/\Omega_K = 1$ as an upper bound. In this figure, the region above Ω_C curve is unstable and a star rotating in this region will be rapidly spun down to an angular frequency below Ω_C. As expected the instability window exists in the temperature regime $(10^8 - 5 \times 10^{10})$ K, where gravitational radiation is dominant and not substantially suppressed, which shows that the neutron star with hyperonic core is unstable in this region. In the low temperature regime hyperonic bulk viscosity damps the r-mode effectively whereas nucleon dominated modified Urca bulk viscosity is the cause of mode damping at high temperatures. The minima of Ω_C curve occurs at $T \approx 5 \times 10^{10}$ K with $\Omega_C \approx .04\ \Omega_K$, which is indicative of the fact that the r-mode instability is rather strong in the present hyperon core scenario. The shaded box in the Fig. [2.7] is where most of the observed Low Mass X-ray Binaries (LMXBs) are found. They have a core temperature in the range of $(2 \times 10^7 - 3 \times 10^8)$ K with rotation rate between 300 to 700 Hz [88, 126]. In our case, LMXBs are placed in the stable region, unlike conventional neutron stars with *npe* matter [127].

2.5 Conclusions

Rotating equilibrium configurations of self gravitating fluids are subjected to various possibilities of instabilities at large rotation periods. In the present work, we have investigated the r-mode instability which is known to limit the angular velocities of rapidly rotating stars. The r-mode and the related instabilities are damped by various viscosities of the matter in the interior of the neutron star. Thus the microscopic models describing the matter in the interior of the star get constrained by the observations of the rapidly rotating pulsars.

In the present work, we have confined our attention to the case of neutron star with a hyperonic core. For the description of the matter in the core of the neutron star, we have used an effective chiral hadronic model generalised to include the lowest lying octet of baryons. The parameters of the model are chosen that are consistent with the flow data in heavy ion collisions, nuclear matter properties as well as observation of high mass neutron stars. In the present work, we have computed the coefficient of bulk viscosity due to the the hyperonic matter in the core of a neutron star and the resulting effects on the r-mode instability. It turns out that hyperon bulk viscosity within the model is effective in damping the instability for temperatures below 10^8K . Beyond a temperature of about 10^{10}K, the bulk viscosity due to modified Urca processes become effective in damping the r-mode instability. Shear viscosity of hadronic matter becomes effective in damping only at low temperatures. Within the model it turns out that the the bulk viscosity in normal hyperonic matter does play an important role in spinning down fast rotating neutron stars. However, superfluid hyperonic matter or quark matter in the core can change this conclusion. With lower value of bulk viscosity (compared to Ref. [78]) due to non-superfluid hyperon matter considered in our model, the corresponding damping of r-mode is less effective. Similarly, compared to Ref. [83] we have a wider window of instability. The reasons for this are, firstly due to the presence of Σ hyperons along with Λ in our model; in contrast to Ref. [83], where only Λ hyperons are there in the stellar core. Further, the difference could also be due to a different stellar energy density profile resulting from a rather softer EoS of the present model as compared to Ref. [83].

We have not considered in the present work the phase transition to quark matter which could be most likely in a color superconducting phase. The role of quark matter in the context of r-mode characteristics has been dealt with in Ref. [88] which shows that the r-mode instability gets suppressed by both normal quark matter as well as gapped quark matter in the color flavor locked phase. Further, the neutron stars are also endowed with strong magnetic fields the effects of which on the r-modes have not been included in the present work. Ultra strong magnetic field seem to increase the instability window for quark matter [89]. It will thus be interesting to examine the scenario with a phase transition to quark matter and the effect of magnetic fields in the context of r-modes for a hybrid star with a crust of hadronic matter.

Chapter 3

Relativistic dissipative hydrodynamics

3.1 Relativistic viscous hydrodynamics

A general introduction to relativistic formulation of dissipative hydrodynamics can be found in Refs. [96, 128–130]. When the hydrodynamical evolution changes the local thermodynamic distributions, microscopic processes try to revert it back. If this doesn't happen very fast, distributions will start to deviate from its original forms.

In order to develop the relativistic viscous hydrodynamics we write the energy momentum tensor as

$$T^{\mu\nu} = \varepsilon\, u^\mu\, u^\nu\ - P\,\Delta^{\mu\nu} + \Pi^{\mu\nu} + 2W^{(\mu}\, u^{\nu)}, \tag{3.1}$$

where (...) denotes the symmetrization; $U_{(\mu}\,V_{\nu)} = \frac{1}{2}\,(U_\mu\,V_\nu + U_\nu\,V_\mu)$. The last two terms in the expression for $T^{\mu\nu}$ are the terms representing the dissipation. Here $\Pi^{\mu\nu}$ denotes the the viscous contributions and $W^\mu = q^\mu + \frac{(\varepsilon+P)}{n} J^\mu$; where q^μ denotes the heat vector and J^μ denotes the modifications due to dissipative effects in particle flux density 4-vector:

$$n^\mu = nu^\mu + J^\mu. \tag{3.2}$$

Equations of motion for the dissipative fluid can be found, as in the case of *ideal* case, by taking 4-divergence of $T^{\mu\nu}$ and n^μ and equating to zero.

At this point we would like to discuss about the proper frame and velocity u^μ. In relativistic considerations since energy flux and mass flux are interrelated, it is not possible to define velocity in terms of the mass flux as in the non-relativistic case. Two choices for the definition of 4-velocities are particularly useful and used in the literature. One is known as *Landau-Lifshitz frame* where there is no energy flow in the rest frame and in this choice we take u^μ parallel to the energy flow,

$$u_\nu T^{\mu\nu} = \varepsilon u^\mu. \tag{3.3}$$

In this frame $W^\mu = 0$, implying that there is a non-zero baryon flow related to the heat conduction in the rest frame, $q^\mu = -\frac{\varepsilon+P}{n} J^\mu$. Another choice for u^μ is known as *Eckart frame* [131]. In this frame we have no baryon flow in the rest frame and therefore u^μ is parallel to the particle flux,

$$n^\mu = n u^\mu. \tag{3.4}$$

In this frame $J^\mu = 0$ making $W^\mu = q^\mu$.

Since we deal with the systems (QGP produced at LHC and RHIC) with net baryon number zero ($n = 0$), natural choice for our purpose is *Landau-Lifshitz frame* as *Eckart frame* is ill-defined in this scenario. Now we will consider the case where there is no heat conduction in the fluid, $q^\mu = 0$. Now we don't have to consider Eq. (3.2) anymore. Now by the definition of the proper frame ($W^\mu = 0$): $T^{00} = \varepsilon$ and $T^{0\,i} = 0$; from Eq. (3.1) we have, $\Pi^{00} = 0$ and $\Pi^{0\,i} = 0$. Since, at the proper frame $u^0 = 1$ and $u^i = 0$, we can write

$$u_\mu \Pi^{\mu\nu} = 0. \tag{3.5}$$

Since above equations are tensor ones they are valid for *any* frame. Projecting 4-divergence of the energy-momentum tensor along and perpendicular to the 4-velocity we get,

$$\begin{aligned} u_\nu \partial_\mu T^{\mu\nu} &= u_\mu \partial^\mu \varepsilon + (\varepsilon + P)\,\partial_\mu u^\mu + u_\nu\,\partial_\mu \Pi^{\mu\nu} = 0, && (3.6) \\ \Delta_{\nu\alpha}\partial_\mu T^{\mu\nu} &= (\varepsilon + P)\,u_\mu \partial^\mu u_\alpha - \Delta_{\alpha\nu}\partial^\nu P + \Delta_{\alpha\nu}\,\partial_\mu \Pi^{\mu\nu} = 0. && (3.7) \end{aligned}$$

Now the last term in the first equation can be simplified using Eq. (3.5) as

$$u_\nu\,\partial_\mu \Pi^{\mu\nu} = -\Pi^{\mu\nu}\,\partial_\mu u_\nu = -\Pi^{\mu\nu}\partial_{(\mu}\,u_{\nu)} = -\Pi^{\mu\nu}\nabla_{(\mu}\,u_{\nu)},$$

where we have used the relation $\partial_\mu = \nabla_\mu + u_\mu D$. So the fundamental equations for relativistic viscous hydrodynamics are given by,

$$D\varepsilon + (\varepsilon + P)\,\Theta - \Pi^{\mu\nu}\nabla_{(\mu}\,u_{\nu)} = 0\,, \tag{3.8}$$

$$(\varepsilon + P)\,Du^\alpha - \nabla^\alpha P \,+\, \Delta^\alpha_\nu\,\partial_\mu \Pi^{\mu\nu} = 0\,. \tag{3.9}$$

Until now we have not specified the form of the viscous stress tensor $\Pi^{\mu\nu}$. This can be done by writing the entropy 4-flux s^μ and demanding the validity of second law of thermodynamics,

$$\partial_\mu s^\mu \geq 0\,. \tag{3.10}$$

One can have different order prescriptions for s^μ, resulting in different expressions for $\Pi^{\mu\nu}$, which together with Eqs. (3.8 & 3.9) give different viscous hydrodynamics theories.

3.1.1 First order: Navier-Stokes formalism

We follow standard Landau-Lifshitz approach [96], in which the entropy 4-flux contains terms *first order* or linear in dissipative quantities and on the absence of dissipative effects it should reduce to the ideal case su^μ. Therefore we write,

$$s^\mu = su^\mu - \beta\,\Pi^{\mu\nu}u_\nu = su^\mu, \tag{3.11}$$

because of Eq. (3.5). Now writing the second law of thermodynamics i.e.; Eq. (3.10), we have,

$$\partial_\mu s^\mu = Ds + s\,\Theta = \frac{D\varepsilon}{T} + \frac{(\varepsilon + P)}{T}\,\Theta = \frac{1}{T}\Pi^{\mu\nu}\nabla_{(\mu}\,u_{\nu)} \geq 0, \tag{3.12}$$

where we have used the thermodynamics relations Eq. (1.35) together with Eq. (3.8).

Now we split viscous stress tensor $\Pi^{\mu\nu}$ in to a traceless part $\pi^{\mu\nu}$ (i.e.; with $\pi^\mu_\mu = 0$) and a part with non-vanishing trace Π:

$$\Pi^{\mu\nu} = \pi^{\mu\nu} \,-\, \Delta^{\mu\nu}\,\Pi. \tag{3.13}$$

Now the Eq. (3.5) implies,

$$u_\mu \pi^{\mu\nu} = 0 \;\text{ with }\; \pi^\mu_\mu = 0. \tag{3.14}$$

Let us write the traceless part of $\nabla_{(\mu}u_{\nu)}$ as $\nabla_{\langle\mu}u_{\nu\rangle}$;

$$\nabla_{\langle\mu}u_{\nu\rangle} \equiv 2\nabla_{(\mu}u_{\nu)} - \frac{2}{3}\Delta_{\mu\nu}\nabla_\alpha u^\alpha. \tag{3.15}$$

Now the Eq. (3.12) becomes

$$\partial_\mu s^\mu = \frac{1}{2T}\pi^{\mu\nu}\nabla_{\langle\mu}u_{\nu\rangle} - \frac{1}{T}\Pi\nabla_\alpha u^\alpha \geq 0 \tag{3.16}$$

and this inequality can be easily assured by taking

$$\pi^{\mu\nu} = \eta\nabla^{\langle\mu}u^{\nu\rangle},\ \ \Pi = -\zeta\nabla_\alpha u^\alpha;\ \ \zeta \geq 0,\, \eta \geq 0. \tag{3.17}$$

In the non-relativistic limit, one can see that, with the above expressions the viscous stress tensor, Eq. (3.9) takes the familiar Navier-Stokes equations. This enables us to identify the coefficients $\eta(\varepsilon, n)$ and $\zeta(\varepsilon, n)$ as the shear and bulk viscosity coefficient respectively. So the *first order* relativistic dissipative hydrodynamics is described by the Eqs. (3.8, 3.9, 3.13 & 3.17).

The Navier-Stokes hydrodynamics is known to have acausal behavior such as propagation of information in infinite speed [102], which is undesirable in a relativistic theory. The solution to this problem was first suggested by Cattaneo [102], by introducing relaxation times in the equations making the theory causal. However this was done in an *ad hoc* manner and a strong theoretical basis was missing from his theory. It has also been shown that Navier-Stokes relativistic theories exhibit unphysical instabilities [103]. All these problems can be avoided by going to second order theories.

3.1.2 Second order: Israel-Stewart formalism

An extension of the relativistic Navier-Stokes hydrodynamics to higher order was done by Müller [132], Isreal and Stewart [104–106]. Detailed calculations can be found in Ref. [128] and in papers of Rischke and Muronga, who introduced this causal relativistic theory of Israel-Stewart to heavy-ion physics [107, 129, 133–136]. In the *second order* theories we allow the entropy 4-flux s^μ to have terms upto the second order in dissipative quantities (Π and $\pi^{\mu\nu}$). Assuming that the deviations from the equilibrium are small so that higher orders can be neglected, we write,

$$s^\mu = su^\mu - \frac{\beta_0}{2T}\Pi^2 u^\mu - \frac{\beta_2}{2T}\pi^{\alpha\beta}\pi_{\alpha\beta}\, u^\mu; \tag{3.18}$$

where $\beta_0 > 0$ and $\beta_2 > 0$ are thermodynamic coefficients corresponding to Π and $\pi^{\alpha\beta}$ contributions respectively. In this case Eq. (3.10) implies

$$\begin{aligned} \partial_\mu s^\mu &= \frac{\pi^{\alpha\beta}}{2T}\left[\nabla_{\langle\alpha}u_{\beta\rangle} - 2\beta_2 D\pi_{\alpha\beta} - 2\pi_{\alpha\beta}T\,\partial_\mu\left(\frac{u^\mu\beta_2}{2T}\right)\right] \\ &\quad -\frac{\Pi}{T}\left[\nabla_\alpha u^\alpha + \beta_0 D\Pi + \Pi T\,\partial_\mu\left(\frac{u^\mu\beta_0}{2T}\right)\right] \geq 0; \end{aligned} \tag{3.19}$$

where we have used the equations of motion along with the thermodynamic relations Eq. (1.35). Now second law of thermodynamics can be satisfied in the simplest way by assuming

$$\begin{aligned} \pi_{\alpha\beta} &= \eta\left[\nabla_{\langle\alpha}u_{\beta\rangle} - 2\beta_2 D\pi_{\alpha\beta} - 2\pi_{\alpha\beta}T\,\partial_\mu\left(\frac{u^\mu\beta_2}{2T}\right)\right], \\ \Pi &= \zeta\left[-\nabla_\alpha u^\alpha - \beta_0 D\Pi - \Pi T\,\partial_\mu\left(\frac{u^\mu\beta_0}{2T}\right)\right]. \end{aligned} \tag{3.20}$$

We can see that in the limit $\beta_{0,2} \to 0$, we get back the first order Navier-Stokes expressions for $\pi^{\alpha\beta}$ and Π- Eq. (3.17). Here the coefficients β_0 and β_2 are related with the relaxation time by

$$\tau_\Pi = \zeta\,\beta_0\,,\;\; \tau_\pi = 2\eta\,\beta_2; \tag{3.21}$$

and in principle these should be calculated by the underlying theory. Rewriting Eq. (3.20) in terms of these relaxation times, we get

$$D\pi_{\alpha\beta} = -\frac{1}{\tau_\pi}\left[\pi_{\alpha\beta} - \eta\nabla_{\langle\alpha}u_{\beta\rangle} + 2\pi_{\alpha\beta}\eta T\,\partial_\mu\left(\frac{u^\mu\beta_2}{2T}\right)\right], \tag{3.22}$$

$$D\Pi = -\frac{1}{\tau_\Pi}\left[\Pi + \zeta\nabla_\alpha u^\alpha + \Pi\zeta T\,\partial_\mu\left(\frac{u^\mu\beta_0}{2T}\right)\right]. \tag{3.23}$$

The above Eqs. (3.8, 3.9, 3.13, 3.22 & 3.23) describe the *second order causal* Israel-Stewart relativistic dissipative hydrodynamics. One can see that the key difference between second order theory with that of first order Navier-Stokes theory is the presence relaxation times. Unlike Navier-Stokes theory, dissipative terms in second order theory are differential evolution or dynamical equations. These dynamical equations show that the dissipative fluxes relax to their steady state values through the relaxation times. These relaxation times in the second order theory ensures the causality [137]. The new thermodynamic coefficients introduced in the theory i.e.; τ_π and τ_Π are to be calculated from the underlying theory like kinetic theory, as for the case of η and ζ. Ignoring the terms which are the product of irreversible flows with the gradients of equilibrium thermodynamic quantities in the above equations we get [130],

$$D\pi_{\alpha\beta} \approx -\frac{1}{\tau_\pi}\left[\pi_{\alpha\beta} - \eta\nabla_{\langle\alpha}u_{\beta\rangle}\right], \tag{3.24}$$

$$D\Pi \approx -\frac{1}{\tau_\Pi}\left[\Pi + \zeta\nabla_\alpha u^\alpha\right]. \tag{3.25}$$

From the above equations it is clear that in the second order evolution equations, the viscous stresses relaxes into the first order Navier-Stokes values from its initial values.

One can obtain Israel-Stewart hydrodynamical equations from the kinetic theory as well [128, 135, 136]. Kinetic theory of viscous ultra-relativistic fluids is still under development. In kinetic theory formulation we can see that some more terms are coming into the viscosity equations [137, 138]. The general shear stress equation of second order Israel-Stewart theory from kinetic theory formulation (corresponding to Eq. (3.24)) is given as [138];

$$\tau_\pi\Delta^\alpha_\mu\Delta^\beta_\nu D\pi^{\alpha\beta} + \pi^{\alpha\beta} = \eta\nabla^{\langle\alpha}u^{\beta\rangle} - 2\tau_\pi\pi^{\mu(\alpha}\Omega^{\beta)}_\mu. \tag{3.26}$$

Since τ_π multiplies all the second order terms in the above equation, we can consider it as a second order coefficient and is related to η. For a relativistic massless Boltzmann gas, using kinetic theory one gets [138],

$$\beta_2 = \frac{\tau_\pi}{2\eta} = \frac{3}{4P}. \tag{3.27}$$

The extra terms in Eq. (3.26) will not contribute to the entropy production so that the Eq. (3.19) will remain same. Since these terms cannot be calculated from the entropy based argument discussed above, kinetic theory based formulation is more general. The viscosity equations in kinetic theory formulation matches with Eq. (3.20) only when the fluid under consideration has no *vorticity*, $\Omega^{\mu\nu} \equiv -\frac{1}{2}\left(\nabla_\mu u_\nu - \nabla_\nu u_\mu\right) = 0$ and $Du^\mu = 0$. It should be noted that when we consider *Björken flow*, $\Omega^{\mu\nu}$ and Du^μ are zero. Therefore it really does not matter whether we use Eq. (3.24) or Eq. (3.26) for our purpose.

Form of the second order Israel-Stewart equations remains the same irrespective of the frame that we choose (*Lanadu-Lifshitz* or *Eckart*), whereas the second order coefficients are found to be frame dependent [139]. It ought to be mentioned that there exists other theories derived with modified entropy current and work in this direction can be found in Refs. [140–142].

Further, it has been shown that for a conformal fluid there will be additional terms in the equation corresponding to shear viscosity [143]. Since QGP at high temperatures $(1.5-2)T_c$ behave more and more conformal, as suggested by lattice QCD results [7], we would be including these terms in the shear viscosity equation. Including terms up to second order in gradients, the general form of the shear viscous tensor in flat space is then given as [143],

$$\begin{aligned}\pi^{\alpha\beta} = \eta\nabla^{\langle\alpha}u^{\beta\rangle} - \tau_\pi \left[\Delta^\alpha_\mu\Delta^\beta_\nu D\pi^{\alpha\beta} + \frac{4}{3}\pi^{\alpha\beta}\Theta\right] \\ -\frac{\lambda_1}{2\eta^2}\pi^{\langle\alpha}_\mu\pi^{\beta\rangle\mu} + \frac{\lambda_2}{2\eta}\pi^{\langle\alpha}_\mu\Omega^{\beta\rangle\mu} - \frac{\lambda_3}{2}\Omega^{\langle\alpha}_\mu\Omega^{\beta\rangle\mu}.\end{aligned} \tag{3.28}$$

Here λ_1, λ_2 and λ_3 are additional second order coefficients for a conformal fluid and they must be calculated from the underlying theory. As seen before τ_π gives us the estimate how fast $\pi^{\mu\nu}$ relaxes to first order value $\eta\nabla^{\langle\alpha}u^{\beta\rangle}$ from the starting value. The coefficients λ_1 tells about the non-linearity of the viscous effects whereas $\lambda_{2,3}$ has to do with the vorticity of the fluid. The explicit calculations for the second order coefficients are done using AdS/CFT correspondence for a strongly coupled $\mathcal{N} = 4$ supersymmetric Yang-Mills (SYM) theory and their results are [143–146]:

$$\tau_\pi = \tau_\Pi = \frac{2(2-\ln 2)}{T}\frac{\eta}{s}\,,\ \lambda_1 = \frac{\eta}{2\pi T}\,,\ \lambda_2 = -\frac{\eta\ln 2}{\pi T}\ \&\ \lambda_3 = 0. \tag{3.29}$$

Here bulk viscosity relaxation time $\tau_\Pi = \tau_\pi$ was found using a strongly interacting non-conformal field theory [147]. On the other hand, for a weakly coupled QCD, explicit calculations indicate [148]

$$\tau_\pi = \frac{5.0...5.9}{T}\frac{\eta}{s}. \tag{3.30}$$

For more details of the calculations of these coefficients and review of the results we refer Ref. [149].

We would also like to note that this second order theory is derived under the assumption that the system is close to the equilibrium and dissipative fluxes are small compared to the equilibrium values:

$$|\Pi| \ll P \quad \text{and} \quad \sqrt{\pi_{\alpha\beta}\pi^{\alpha\beta}} \ll \mathrm{P}\,. \tag{3.31}$$

So the validity or the applicability of the second order hydrodynamics depends on this condition.

3.2 Viscous expansion of QGP

Let us consider the viscous expansion of the QGP formed in heavy-ion collisions. We need to apply the Björken flow described in Section 1.2.2 to dissipative hydrodynamics to get the governing equations.

Let us consider the form of $T^{\mu\nu}$ in the rest frame, $u^\mu = (1, \vec{0})$ of the fireball. With the help of the Eqs. (3.1, 3.13 & 3.14) we can write [129, 150]

$$T^{\mu\nu} = \begin{pmatrix} \varepsilon & 0 & 0 & 0 \\ 0 & P_\perp & 0 & 0 \\ 0 & 0 & P_\perp & 0 \\ 0 & 0 & 0 & P_z \end{pmatrix} \tag{3.32}$$

where the effective pressure of the expanding fluid in the transverse and longitudinal directions are respectively given by

$$\begin{aligned} P_\perp &= P + \Pi + \frac{1}{2}\Phi, \\ P_z &= P + \Pi - \Phi. \end{aligned} \tag{3.33}$$

Here $\Phi = \pi^{00} - \pi^{zz}$ and Π are the non-equilibrium contributions to the equilibrium pressure P coming from shear and bulk viscosities respectively. Respecting the symmetries in the transverse directions the traceless shear tensor has the form $\pi^{ij} = \mathrm{diag}(\Phi/2, \Phi/2, -\Phi)$. It is clear from the above equations that the effect of viscosity is to alter the equilibrium pressure and the effective pressure is anisotropic unlike the ideal case.

In order to study the dynamics of the system we need to study the structure of $T^{\mu\nu}$ in a moving frame. Using $u^\mu = (\cosh\eta_s, 0, 0, \sinh\eta_s)$ and Eqs. (3.1, 3.13 & 3.14) we can find $T^{\mu\nu}$. The non-vanishing terms of the shear stress tensor are given as

$$\begin{aligned}\pi^{00} &= -\Phi\,\sinh^2\eta_s,\;\pi^{11}=\pi^{22}=\frac{\Phi}{2},\;\pi^{33}=-\Phi\,\cosh^2\eta_s,\\ \pi^{03} &= \pi^{30}=-\Phi\,\sinh\eta_s\,\cosh\eta_s.\end{aligned} \tag{3.34}$$

Now we can write the general form of the energy-momentum tensor in a moving frame,

$$T^{\mu\nu}=\begin{pmatrix}\mathcal{W}\cosh^2\eta_s-P_z & 0 & 0 & \mathcal{W}\cosh\eta_s\sinh\eta_s\\ 0 & P_\perp & 0 & 0\\ 0 & 0 & P_\perp & 0\\ \mathcal{W}\cosh\eta_s\sinh\eta_s & 0 & 0 & \mathcal{W}\sinh^2\eta_s+P_z\end{pmatrix}, \tag{3.35}$$

where $\mathcal{W}=\varepsilon+P_z$ is the effective enthalpy.

We have already seen from Section 1.2.2 that (1+1)-dimensional scaling solution gives thermodynamic quantities as a function of only one variable τ. Now let us look at the energy-dissipation equation, i.e.; Eq. (3.8) in this context. We already know the ideal part i.e.; Eq. (1.46), and the viscous part $\Pi^{\mu\nu}\nabla_{(\mu}u_{\nu)}$ can be calculated using Eqs. (1.40 - 1.42 & 3.34) as

$$\Pi^{\mu\nu}\nabla_{(\mu}u_{\nu)}=\pi^{\mu\nu}\partial_\mu u_\nu-\Pi\,\Theta=\frac{\Phi}{\tau}-\frac{\Pi}{\tau}. \tag{3.36}$$

Now the Eq. (3.8) becomes [107],

$$\frac{\partial\varepsilon}{\partial\tau}+\frac{\varepsilon+P}{\tau}-\frac{\Phi}{\tau}+\frac{\Pi}{\tau}=0, \tag{3.37}$$

and this is the fundamental equation that governs the effect of dissipation in expanding plasma. One can define a ratio $\mathfrak{R}$ of non-dissipative term to dissipative term, as an analogy to *Reynolds number* [153, 154]

$$\mathfrak{R}\equiv\frac{(\varepsilon+P)}{\Phi+\Pi} \tag{3.38}$$

so that Eq. (3.41) can be written as

$$\frac{\partial\varepsilon}{\partial\tau}=(\mathfrak{R}^{-1}-1)\,\frac{\varepsilon+P}{\tau}. \tag{3.39}$$

We can study the general effect of dissipation by looking into this equation. It is clear that system energy-density decreases (increases) for $\mathfrak{R}>1$ ($\mathfrak{R}<1$) and

$\mathfrak{R} = 1$ corresponds to the case when energy-density (and other thermodynamic quantities) remains the same.

In Eq. (3.37) various viscous theories will give corresponding expressions for the viscous parts Φ and Π. Let us analyse these cases separately.

Ideal case

In the ideal case we have $\Phi = \Pi = 0$, and from Section 1.2.2 we know the energy-dissipation equation, Eq. (1.33).

First order

In the first order Navier-Stokes theory, the expressions for viscous terms within Björken flow can be found from Eq. (3.17) and is given by

$$\Pi = -\frac{\zeta}{\tau} \quad \text{and} \quad \Phi = \frac{4\eta}{3\tau}, \tag{3.40}$$

so that energy-dissipation equation takes the form,

$$\frac{\partial\varepsilon}{\partial\tau} + \frac{\varepsilon + P}{\tau} = \frac{\left(\frac{4}{3}\eta + \zeta\right)}{\tau^2}. \tag{3.41}$$

From Eq. (3.16) we can find the entropy equation and is given as

$$\frac{\partial s}{\partial\tau} + \frac{s}{\tau} = \frac{s}{\mathfrak{R}\tau}, \tag{3.42}$$

where $\mathfrak{R}^{-1} = \frac{\left(\frac{4}{3}\eta+\zeta\right)}{Ts\tau}$. In the case of perfect fluid $\mathfrak{R}^{-1}$ is zero and from the above equation we get $s\tau$ as a constant (Eq. (1.45)).

First order dissipative hydrodynamics in the context of heavy-ion physics was studied in detail in Refs. [100, 101, 151–154].

Second order

When we use causal dissipative second order hydrodynamics of Isreal-Stewart to study the expanding plasma in the fireball, instead of expressions as in Navier-Stokes theory, we have *dynamical* or *evolution* equations for Φ and Π governed by their relaxation times τ_π and τ_Π, i.e.; Eqs. (3.28 & 3.25) within Björken flow:

$$\frac{\partial\Phi}{\partial\tau} = -\frac{\Phi}{\tau_\pi} + \frac{2}{3}\frac{1}{\beta_2\tau} - \frac{1}{\tau_\pi}\left[\frac{4\tau_\pi}{3\tau}\Phi + \frac{\lambda_1}{2\eta^2}\Phi^2\right] \tag{3.43}$$

$$\frac{\partial\Pi}{\partial\tau} = -\frac{\Pi}{\tau_\Pi} - \frac{1}{\beta_0\tau}. \tag{3.44}$$

Where we used the fact that within Björken flow, $\Omega^{\mu\nu} = 0$ and $Du^{\mu} = 0$, and $\lambda_3 = 0$. In second order hydrodynamics, Eqs. (3.37, 3.43, 3.44) describe the dissipative evolution of the fireball in heavy ion collisions. As with the ideal case, we need to supplement this set of equations with EoS to close the system. Additionally we have to prescribe the viscosities of the medium under consideration also. Second order relativistic hydrodynamics models have been used extensively to describe the role of viscosity on the fireball evolution in heavy ion collisions [109, 155–161]. We refer [129, 134, 137, 162] for more details on the recent developments in the theory and its application to relativistic heavy-ion collisions.

Now in order to understand the dissipative scaling flow solutions better we consider an ultra-relativistic (*ideal*) EoS of massless quarks and gluons (Appendix A): $P = c_s^2\varepsilon = \varepsilon/3 = a\,T^4$. Generally in the context of heavy ion collision, the effect of bulk-viscosity ζ is neglected for a system obeying such an EoS. This is because here ζ scales like $c_s^2 - \frac{1}{3}$, where c_s^2 is the speed of sound [46].

We have already seen from Section 1.2.2 that for ideal hydro (1+1)-scaling solution is given by Eq. (1.50): $T = T_0\ \left(\frac{\tau_0}{\tau}\right)^{1/3}$, with T_0 and τ_0 being initial values of temperature and time respectively.

In the first order hydrodynamics, with $\varepsilon = 3P$ EoS, energy-dissipation equation Eq. (3.41) with $\zeta = 0$ becomes

$$\frac{\partial T}{\partial \tau} = -c_s^2 \left[\frac{1}{\tau} - \frac{4}{3}\left(\frac{\eta}{s}\right)\frac{1}{T\tau^2}\right]. \tag{3.45}$$

This equation can be solved analytically for the case of constant η/s and the solution is [107, 154],

$$T(\tau) = T_0\left[\frac{\tau_0}{\tau}\right]^{1/3}\left[1 + \frac{2\eta}{3s\tau_0 T_0}\left(1 - \left[\frac{\tau_0}{\tau}\right]^{2/3}\right)\right]. \tag{3.46}$$

It is clear that effect of viscosity is to reduce the rate at which temperature of the system drops, compared to the ideal fluid case. This function has a maximum at the τ value

$$\tau_{max} = \tau_0\left[\frac{1}{3} + \frac{s}{\eta}\frac{T_0\tau_0}{2}\right]^{-3/2}. \tag{3.47}$$

For times greater than τ_{max} we have a decreasing temperature of the expanding fireball with time, as expected. But $\tau < \tau_{max}$ system will show a reheating, which is unphysical. Apart from the other problems with the first order theory discussed

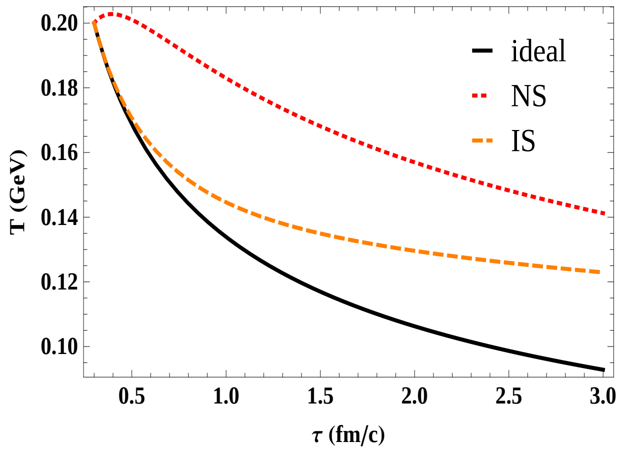

Figure 3.1: *Temperature evolution in first order (NS) and second order (IS) dissipative hydrodynamics. Ideal case is also shown. One can see that first order gives unphysical reheating at early times whereas second order hydro is devoid of such artifacts.*

in Section 3.1.1, this unphysical artifact is also removed by going into second order theories [107, 138].

Since only the effect of shear viscosity appears with *ideal* EoS, in the second order theories we need to solve two equations: energy dissipation equation Eq. (3.37) with $\zeta = 0$ and shear stress evolution equation Eq. (3.43) in order to study the scaling solution. We need to provide relaxation coefficient τ_π, which for the massless particles is given by Eq. (3.27). We take $\lambda_1 = \frac{\eta}{2\pi T}$ as in Eq. (3.29) and $\eta/s = 0.3$. We provide following initial conditions: $T_0 = 0.2$ GeV, $\tau_0 = 0..3$ fm/c and we take $\Phi(\tau_0) = 0$. After numerically solving the equations we plot the resulting temperature profile in Fig. [3.1]. For comparison we have plotted the temperature profiles for the first order; Eq. (3.46) and ideal hydrodynamics; Eq. (1.50) also. One can see that for sufficiently lower times first order hydro gives rise to unphysical reheating whereas second order is devoid of such artifacts. One can also see that effects of dissipation on the system are: a) to increase the temperature b) to decrease the cooling rate.

We would like to end this section by mentioning how the applicability condition for viscous hydrodynamics will look like in the Björken flow. In this context conditions expressed in Eq. (3.31) becomes,

$$|\Pi| \ll P \quad \text{and} \quad \sqrt{\pi_{\alpha\beta}\pi^{\alpha\beta}} = \sqrt{\frac{3}{2}}\,\Phi \ll \mathrm{P}\,. \tag{3.48}$$

This conditions has a significant impact on the initial conditions for Φ and Π. In the theory as we have two differential equations for these stresses, we need to provide the initial values Φ_0 and Π_0 at initial time τ_0. We don't know exactly what are these values, however, in the limiting case we know it should be less than P_0. This ensures that initial *Reynolds number* $\mathfrak{R} > 1$, which in turn makes sure that thermodynamic variables will always be decreasing in the second order theory; Eq. (3.39). So unlike first order theories in the second order we have conditions which ensures the application of the theory in its valid domains. For more detailed analysis of the applicability of second order hydrodynamics in the context of heavy-ion collisions we refer Ref. [163].

Having set up the causal second order dissipative relativistic hydrodynamical equations dictating the expansion of the fireball formed in the heavy ion collisions, we know turn our attention to the properties of the system like EoS and viscosities which are important inputs needed for the hydrodynamical treatment of the expanding QGP.

3.3 Non-ideal effects

In this session we will concentrate on the thermodynamic quantities that we need to input in the hydrodynamical model to study the expanding QGP formed in nucleus-nucleus collisions. The hot matter formed in the heavy ion collisions expands and subsequently cools. After reaching the critical temperature it eventually gets hadronised. At high temperatures we use weakly coupled QCD to study the thermodynamic properties. However, the maximum temperature attained in nucleus-nucleus collision experiments is not very high e.g.; at LHC maximum temperature ~ 600 MeV and RHIC ~ 350 MeV. We are interested in an experimentally accessible regime of QCD matter where it is near the critical temperature T_c. The thermodynamic properties of the matter near T_c cannot be studied using perturbative analysis, as we do in the high temperature regimes, as the QCD coupling constant is large in this region. So one has to rely upon some other techniques to extract thermodynamic and transport properties of the hot QCD matter at these strongly interacting regimes. One of the successful ways of doing calculation is using lattice QCD (lQCD) techniques and other recent one being AdS/CFT correspondence.

In lQCD approach; originally proposed by Wilson in 1974 [4], QCD is defined on a space-time lattice leading to a gauge-invariant regularised theory and allows a non-perturbative numerical investigation. Thus lQCD provides a framework for studying non-perturbative phenomena like QGP phase transition and confinement [164].

AdS/CFT correspondence (or gauge/gravity duality) allows us to map a strongly coupled finite temperature conformal gauge theory in d dimension onto a weakly coupled gravity theory in $d+1$ dimension with a blackhole. Most useful for our purpose being correspondence between $\mathcal{N} = 4$ SYM in 4 dimensions to a string theory in 5 dimensions $AdS_5 \times S^5$ (5-dimensional Anti de Sitter space times a 5-dimensional sphere) [165–167]. So the problems that are difficult to handle in strongly coupled systems like QGP, are transported onto a higher dimensional gravitational theory; where it become easy to handle. One then maps back the solutions onto the real 4-dimensional flat space-time. For a recent review on the AdS/CFT techniques and its application with the heavy-ion collision physics, we refer readers to Ref. [149].

3.3.1 EoS from lQCD ($\varepsilon \neq 3P$)

Most reliable calculations of the thermodynamic quantities of QCD matter at the regimes close to phase-transition in QGP comes from the lQCD calculation techniques. From the recent lattice results we have a picture how energy density and pressure of QCD matter at thermal equilibrium and with zero chemical potential behave [6, 7, 168, 169]. In Fig. [3.2], we plot temperature dependence of ε and $3P$ (in units of T^4) obtained from lQCD calculation by Bazavov *et al.* [7] with critical temperature being 190 MeV. From the figure one can see that the pressure (energy density) increases rapidly above T_c indicating a rise in number of degrees

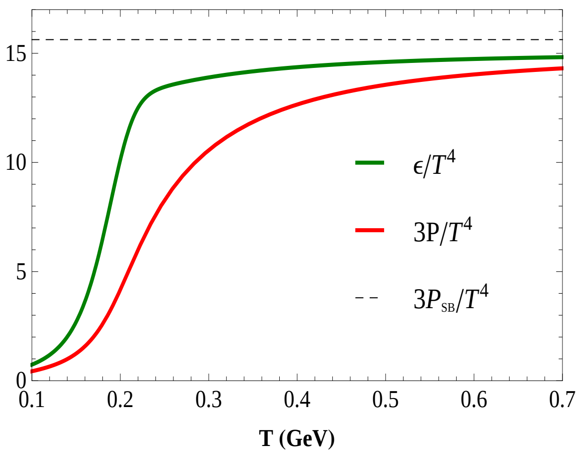

Figure 3.2: *Energy density ε/T^4 and pressure $3P/T^4$ as functions of temperature T. The dashed line denotes value of pressure in ideal EoS limit $3P_{SB}/T^4$. Around critical temperature ($T_c = .190$ GeV) sudden rise in these quantities are seen due to increase in number f degrees of freedom. Results are from Ref. [7].*

of freedom; and almost remains constant at higher temperatures but below the ideal non-interacting value of pressure (Stefan-Boltzmann limit) i.e.; Eq. (1.48). Only at asymptotic values of temperature ($T < 10^8$ GeV) the pressure from lQCD reaches the ideal limit and we observe a difference $\sim 20\%$ between the ideal limit and lQCD results as high as 1 GeV [149, 170]. Another important quantity that one calculates in lQCD is the thermal expectation value of the trace of the energy-momentum tensor $\langle \Theta^\mu_\mu \rangle = \varepsilon - 3P$, known as trace anomaly. For a conformal theory this quantity is zero. What one observes is rise in $\langle \Theta^\mu_\mu \rangle / T^4$ around T_c owing to the more steady rise of ε/T^4 compared to $3P/T^4$. Large value of trace anomaly is necessarily indicative of the strong interaction among the constituents of the QCD matter. At high temperatures trace anomaly falls off indicating a more and more conformal (scale-invariant) behavior of QGP.

The important point that one should note from these studies is, since QCD matter is more and more conformal at high temperatures, one can use conformal theories with AdS/CFT techniques to get an insight into real world QGP.

We use the recent lattice QCD result of Bazavov *et al.* [7] for equilibrium EoS (*non-ideal*: $\varepsilon - 3P \neq 0$) with zero baryon chemical potential, which becomes significantly important near the critical temperature. Parametrised form of their

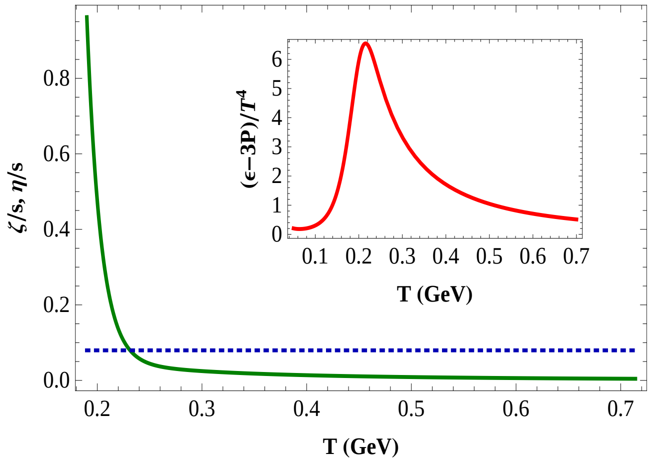

Figure 3.3: $(\varepsilon - 3P)/T^4$, ζ/s *and* $\eta/s = 1/4\pi$ *as functions of temperature* T*. One can see around* $T_c = .190$ *GeV, departure of equation of state from ideal case is large and* $\zeta \gg \eta$*.*

result for trace anomaly in units of T^4 is given by [7]

$$\frac{\varepsilon - 3P}{T^4} = \left(1 - \frac{1}{\left[1 + \exp\left(\frac{T - c_1}{c_2}\right)\right]^2}\right)\left(\frac{d_2}{T^2} + \frac{d_4}{T^4}\right) , \tag{3.49}$$

where values of the coefficients are $d_2 = 0.24$ GeV^2, $d_4 = 0.0054$ GeV^4, $c_1 = 0.2073$ GeV, and $c_2 = 0.0172$ GeV. The functional form of the pressure is given by [7]

$$\frac{P(T)}{T^4} - \frac{P(T_0)}{T_0^4} = \int_{T_0}^{T} dT' \, \frac{\varepsilon - 3P}{T'^5} , \tag{3.50}$$

with $T_0 = 50$ MeV and $P(T_0) = 0$ [115].

From Eq. (3.49) and Eq. (3.50) we get ε and P in terms of T. A crossover from QGP to hadron gas around the temperature 200-180 MeV is predicted by this model. Throughout the analysis we keep the critical temperature T_c to be 190 MeV until and unless specified.

Now we need to specify the viscosity prescriptions used in the hydrodynamical model.

3.3.2 Shear viscosity

First theoretical investigations to find out shear viscosity of QCD matter can be found in Refs. [151, 171]. Using relativistic kinetic theory it was estimated that for a weakly coupled QCD shear viscosity $\eta \sim T^3/(\alpha_s^2 \ln \alpha_s^{-1})$ [151] and it was suggested that Kubo formula should be used to calculate viscosities near T_c [171]. At the high temperature regime of QCD, explicit calculations by Arnold, Moore and Yaffe gave the expressions for shear viscosity upto leading logarithmic accuracy [172, 173]. E.g.; for massless quarks with $N_f = 0$ and $N_C = 3$ we have,

$$\eta = \frac{27.126\, T^3}{g^4 \ln (2.765 g^-1)}, \tag{3.51}$$

where $g^2 = 4\pi\alpha_s$. However these results are uncertain upto a great extent, due to its strong dependence on coupling constant and Debye mass [138, 162].

In order to understand the shear viscosity near phase transition (non-perturbative regime), studies were done using AdS/CFT correspondence techniques. $\mathcal{N} = 4$ SYM theory with large $N_C \to \infty$ and strong coupling $g^2 N_C \to \infty$ limit, η/s was calculated and it was found to be a constant $\eta/s = 1/4\pi$ [174]. Finite-coupling corrections (large but finite coupling constant $g^2 N_C$) of this result were calculated by Buckel *et al.* and is given by [175]

$$\frac{\eta}{s} = \frac{1}{4\pi}\left(1 + \frac{135\zeta(3)}{8(2g^2N_C)^{3/2}} + ...\right), \tag{3.52}$$

where $\zeta(3) \approx 1.202..$ is Apérys constant. Similar calculations were done in the weak coupling regime also and the results suggested that the η/s is not constant but smaller compared to weak QCD results [176].

After a close study with various strongly coupled field theories, it was found that the constant nature of η/s was not confined to $\mathcal{N} = 4$ SYM theory but for a large class of gauge theories with a gravity dual [110, 177, 178]. Universal nature of this result is manifested with the fact that it applies to many field theories in the strongly coupled and large N_C limit, regardless of conformal or non-conformal, supersymmetric or non-supersymmetric etc. This led Kovtun, Son and Starinets to conjecture [110] that

$$\frac{\eta}{s} = \frac{1}{4\pi} \tag{3.53}$$

(written in units $\hbar = c = k_B = 1$, otherwise $\eta/s = \hbar/4\pi k_B$) is *an absolute lower bound on the value of* η/s *for all systems in nature*; now known as *KSS bound*. The fact that the finite corrections to the η/s in Eq. (3.52) are positive also indicates the validity of KSS bound [110]. Experimental studies also support this bound as we are yet to come across a system with $\eta/s < 1/4\pi$ [179]. It is worth mentioning that recently there are some AdS/CFT studies where violation of KSS bound is discussed [180].

The measurements of the elliptical flow parameter v_2 of QGP formed at RHIC show a strong collectivity in the flow [181–183] indicating a very low value of $\eta/s \sim 1/4\pi$ [109].

There are some lQCD based efforts to determine η/s of QGP [184, 185]. However these results suffer from huge associated errors [149]. However it is interesting to note that the results of these studies are in accordance with observed bound on the values of QGP shear viscosity from flow experiments and respect the KSS bound also.

3.3.3 Bulk viscosity

We are interested in the effect of bulk viscosity on the hydrodynamical evolution of the plasma. Generally the effect of bulk viscosity is neglected in the heavy ion collision scenarios, since we use an ultra-relativistic $\varepsilon = 3P$ EoS to describe the system [46]. In the weak coupling limit of QCD, by explicit calculations, it was shown that bulk viscosity $\zeta \sim \alpha_s^2 T^3/\ln \alpha_s^{-1}$ [186] and can be neglected compared to the shear viscosity $\eta \sim T^3/(\alpha_s^2 \ln \alpha_s^{-1})$ [151, 172, 173]. It is due to the fact that at high temperatures QCD is more and more conformal.

But as seen from the previous session, lQCD results indicate medium having an EoS deviating from *ideal* ($\varepsilon = 3P$) case more and more near T_c indicating the non-conformal nature of the plasma. Speed of sound of the medium also has a change from the *ideal* EoS case ($c_s^2 = \frac{1}{3}$) here [7, 168]. So we can expect that near T_c bulk viscosity may not be zero as it is related to the speed of the sound in the medium. There exists several mechanisms that can contribute for bulk viscosity in a system [187]. Using linear sigma model it was shown in Ref. [187] that near the QCD phase transition, ratio of bulk viscosity to entropy density (ζ/s) gets a maximum. Further studies also confirmed this by examining the temperature dependence of ζ/s by relating it to the lQCD results for trace anomaly $\varepsilon - 3P$ [188–192]. All these recent studies point out that near critical temperature the effect of bulk viscosity

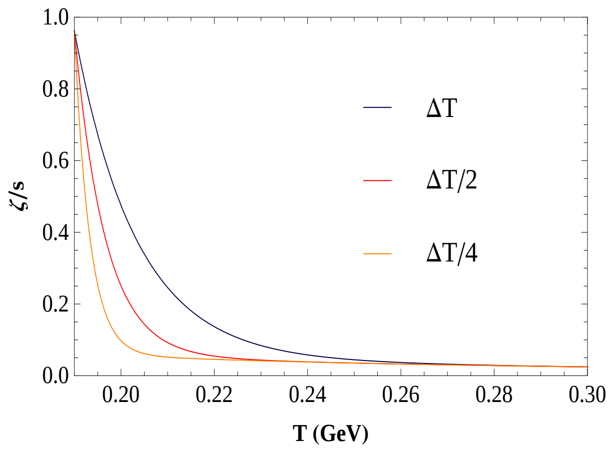

Figure 3.4: *Various bulk viscosity scenarios by changing the width of the curve through the parameter ΔT in Eq. (3.54).*

becomes prominent $\zeta \gg \eta$ and cannot be ignored. We would like to note that these studies are not conclusive about the strength of ζ/s.

We use recent lQCD calculation results of Meyer [113], for determining ζ/s. His result indicate the existence a peak of ζ/s near T_c, although the height and width of this curve are not well understood. We use the parametrization of Meyer's result given in Ref. [115]:

$$\frac{\zeta}{s} = a \exp\left(\frac{T_c - T}{\Delta T}\right) + b\left(\frac{T_c}{T}\right)^2 \quad \text{for } T > T_c, \tag{3.54}$$

where the parameter $a = 0.901$ controls the height, $\Delta T = T_c/14.5$ controls the width of the ζ/s curve and $b = 0.061$. We will change these values to explore the various cases of ζ/s to account for the uncertainty of the height and width of the curve.

Since in conformal field theories $\zeta = 0$, there are attempts of calculating bulk viscosity using non-conformal field theory and gauge/string duality [193, 194]. Buchel has calculated a bound on bulk viscosity using such attempts and is given by [195]

$$\zeta \geq 2\left(\frac{1}{3} - c_s^2\right)\eta. \tag{3.55}$$

We would like to note that this result indicate a value for ζ/s which is considerably less than lQCD estimates described before.

In Fig. [3.3] we plot the trace anomaly $(\varepsilon - 3P)/T^4$ and ζ/s for desired temperature range. We also plot the constant value of $\eta/s = 1/4\pi$ for a comparison. It is clear that the *non-ideal* EoS deviates from the *ideal* case ($\varepsilon = 3P$) significantly around the critical temperature. Around same temperature ζ/s starts to dominate over η/s significantly. We would like to note that these results are qualitatively in agreement with Ref. [114]. In Fig. [3.4] we show the change in bulk viscosity profile by varying the width of the ζ/s curve by keeping the height intact.

3.4 Conclusions

In this chapter we reviewed the relativistic dissipative hydrodynamics of first order (Navier-Stokes) and second order (Israel-Stewart type) in the context of heavy ion collisions. We discussed the problems with the first order theories and need for using the second order theories. We also reviewed the results for bulk viscosity and shear viscosity prescriptions available for QGP matter.

In next chapter, we will look the hydrodynamical evolution in presence of these viscosity prescriptions using second order causal hydrodynamics.

Chapter 4

Hydrodynamic evolution at early stages and cavitation

We would like to study how the viscosity prescriptions, both shear and bulk, discussed in Section 3.3, affect the expanding fireball produced in RHIC/LHC energies, within causal second order hydrodynamics framework. From Section 3.2, we know the equations dictating the longitudinal viscous expansion of the medium, and they are:

$$\frac{\partial \varepsilon}{\partial \tau} = -\frac{1}{\tau}(\varepsilon + P + \Pi - \Phi)\,, \tag{4.1}$$

$$\frac{\partial \Phi}{\partial \tau} = -\frac{\Phi}{\tau_\pi} + \frac{2}{3}\frac{1}{\beta_2 \tau} - \frac{1}{\tau_\pi}\left[\frac{4\tau_\pi}{3\tau}\Phi + \frac{\lambda_1}{2\eta^2}\Phi^2\right]\,, \tag{4.2}$$

$$\frac{\partial \Pi}{\partial \tau} = -\frac{\Pi}{\tau_\Pi} - \frac{1}{\beta_0 \tau}. \tag{4.3}$$

Here Φ and Π denote the contributions from shear and bulk viscosities respectively. Apart from these three equations (4.1 - 4.3), we need to provide the EoS and viscosity prescriptions to study the hydrodynamical evolution of the system.

4.1 Cavitation

Let us recall that the effective longitudinal pressure within second order hydrodynamics is defined as Eq. (3.33),

$$P_z = P + \Pi - \Phi,$$

with P being equilibrium hydrodynamic pressure. As both shear viscosity and bulk viscosity contributions are always negative, large values of Π or/and Φ can make P_z negative. During the course of expansion when P_z vanishes, the fluid will break apart into fragments and the hydrodynamic treatment will become invalid [115]. Phenomenon of cavitation is known to occur in liquids [196], when the pressure of an expanding liquid becomes less than its vapour pressure. The condition that the longitudinal pressure $P_z = 0$ defines the onset condition for the *cavitation* and the time at which $P_z = 0$ is called the cavitation time τ_c. One can have the following intuitive picture for the cavitation. Consider an expanding fluid scenario in the low viscosity regime where the collective flow is pushing the system outward. Next, consider that there is a sharp rise in the viscosity as the expanding fluid cools down. In such a situation, the emergence of a strong viscous force will try to halt the collective flow. However, due to causality, it cannot suddenly overcome the collective flow globally. But, it is possible for the viscous force to overcome the flow locally. This may result in breaking up of the fluid into fragments and the conditions for the applicability of second order hydrodynamics may not be satisfied any more. However, our formulation in the 1+1 boost invariant approximation cannot describe the characteristics of the fragmentation. Nonetheless, it can give us *the onset condition for the cavitation.* One of the signatures of such fragmentation condition could be in terms of the HBT correlations [197, 198]. Nevertheless, our condition of cavitation is also the condition for the validity of second order hydrodynamics. One of the limitations of this approach is that the effects of transverse flow cannot be incorporated. However it should also be noted that the effect of transverse flow could remain small as cavitation can restrict the time for hydrodynamical evolution.

In this chapter we intend to address three distinct cases:

- Hydrodynamic evolution at RHIC energies: effect of finite bulk viscosity ζ/s and shear viscosity $\eta/s = 1/4\pi$, within lQCD inspired EoS.
- Hydrodynamic evolution at LHC energies: effect of finite temperature dependent η/s, within lQCD inspired EoS.
- Hydrodynamic evolution at both RHIC and LHC energies: effect of finite

shear viscosity $\eta/s = 1/4\pi$ on chemically equilibrating plasma with ideal massless gas $\varepsilon = 3P$ EoS.

4.2 Bulk viscosity, cavitation and hydrodynamics at RHIC

Only recently, the effect of bulk viscosity was considered in hydrodynamic evolution at RHIC energies, using (1+1)-dimensional hydrodynamics. It can be shown with lQCD result for a temperature dependent ζ/s that during evolution effective pressure of the system can go to zero much before the system temperature reaches T_c and thereby trigger the *cavitation* [114, 115].

In our analysis we use lQCD results for ζ/s, whereas for η/s we take the minimal value as suggested by the RHIC experiments [109]. Information about viscosity coefficients η and ζ are obtained from Eqs. (3.53 & 3.54) using $s = (\varepsilon + P)/T$. The second order coefficients in the hydrodynamical equations are being taken from the strongly coupled $\mathcal{N} = 4$ SYM theory results given in Eq. (3.29). In order to close the hydrodynamical equations we use the *non-ideal* EoS obtained from lQCD i.e.; Eq. (3.49) and Eq. (3.50). Near the critical temperature $T_c = 190$ MeV, ζ/s has a peak and is much larger than η/s, as we had seen in Fig. [3.3].
In order to understand the temporal evolution of temperature $T(\tau)$, pressure $P(\tau)$ and viscous stresses - $\Phi(\tau)$ and $\Pi(\tau)$, we numerically solve the hydrodynamical equations describing the longitudinal expansion of the plasma: Eqs. (4.1 - 4.3).
We need to specify the initial conditions to solve the hydrodynamical equations, namely τ_0, T_0, $\Phi(\tau_0)$ & $\Pi(\tau_0)$. We use the initial values relevant for RHIC (Au+Au, $\sqrt{s} = 200$ GeV) experiments: $\tau_0 = 0.5$ fm/c and $T_0 = 0.310$ GeV; taken from Ref. [199]. The initial values of viscous stresses are not known exactly and in literature people consider values ranging from zero to Navier-Stokes values Eq. (3.40) [114]. We will take initial values of viscous contributions as $\Phi(\tau_0) = 0$ and $\Pi(\tau_0) = 0$. We would like to note that our hydrodynamical results are in agreement with that of Ref. [115].

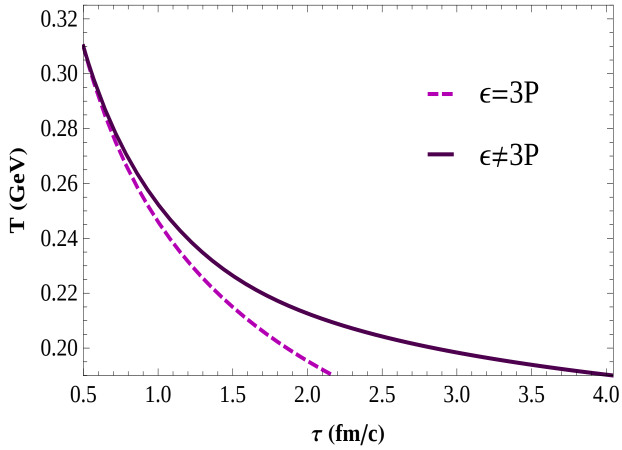

Figure 4.1: *Temperature profile using massless (ideal) and non-ideal EoS in RHIC scenario. Viscous effects are neglected in both cases. System evolving with non-ideal EoS takes a significantly larger time to reach T_c as compared to ideal EoS scenario. We note that initial entropy in both the cases are different.*

4.2.1 Hydrodynamics with *ideal* and *non-ideal* EoS

Fig. [4.1] shows plots of temperature versus time for the *ideal* and *non-ideal* equation of states. The temperature profiles are obtained from the hydrodynamics without incorporating the effect of viscosity. Here we consider the *ideal* EoS of a relativistic gas of massless quarks and gluons (Appendix A). The pressure of such a system is given by Eq. (1.48), where we take $N_f = 2$ in our calculations. From Section 1.2.2 we have seen that for such a system temperature profile within Björken flow is given by Eq. (1.50): $T = T_0 \left(\frac{\tau_0}{\tau}\right)^{1/3}$. The figure shows system with *non-ideal* EoS takes almost the double time than the system with *ideal* massless EoS to reach T_c. So even when the effect of viscosity is not considered, inclusion of the *non-ideal* EoS makes significant change in temperature profile of the system. However, we note here that although we have taken same initial temperature, the initial entropy is not the same, it is larger for the *non-ideal* EoS case. Subsequent difference will be there in the final entropies also.

Next we analyse the viscous effects on the temperature profile. We consider possible combinations of Φ and Π in *non-ideal* EoS case and study the corresponding temperature profiles as shown in Fig. [4.2]. As expected viscous effects is slowing down temperature evolution. For the case of non zero bulk and shear viscosities

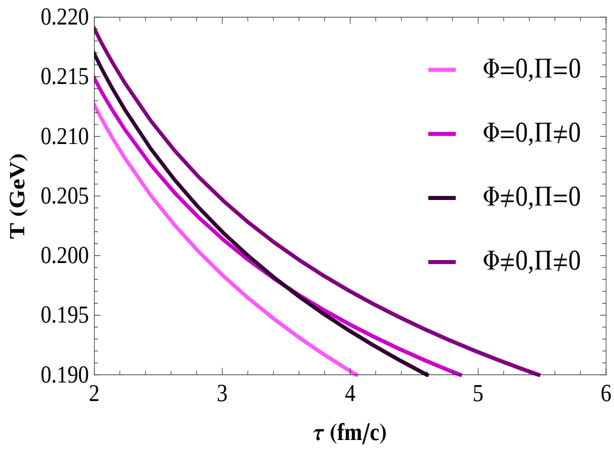

Figure 4.2: *Figure shows time evolution of temperature with non-ideal EoS for different combinations of bulk (Π) and shear (Φ) viscosities. Non zero value of bulk viscosity refers to Eq. (3.54) and non-zero shear viscosity is calculated from Eq. (3.53).*

$(\Pi \neq 0;\ \Phi \neq 0)$, temperature takes the longest time to reach T_c as indicated by the top most curve. This is about 35% larger than the case without viscosity (the lowest curve). The remaining two curves show that the bulk viscosity dominates over the shear viscosity when the value of T approaches T_c and this makes the system to spend more time around T_c. However the intersection point of the two curves may vary with values of a and ΔT as highlighted by Fig. [3.4].

4.2.2 Bulk viscosity driven cavitation at RHIC

Now we analyse the effective longitudinal pressure P_z of the system. We have already discussed that, large values of shear or bulk stress can drive, $P_z \approx 0$ triggering cavitation. Recent experiments at RHIC suggest η/s to its smallest value $\sim 1/4\pi$. Such a small value of η/s alone is inadequate to induce cavitation. Now we vary the bulk viscosity values by changing the height and width of ζ/s curve, via a and ΔT, and carefully analyse P_z.

In Figs. [4.3 & 4.4] we plot P_z and T as functions of the proper time for different values of ΔT while keeping a (=0.901) fixed. As may be inferred from Fig. [4.3], higher value of ΔT leads to a shorter cavitation time. For the base values $a = 0.901$ and $\Delta T = T_c/14.5$ we find that around $\tau_c = 2.5$ fm/c, P_z becomes zero as shown

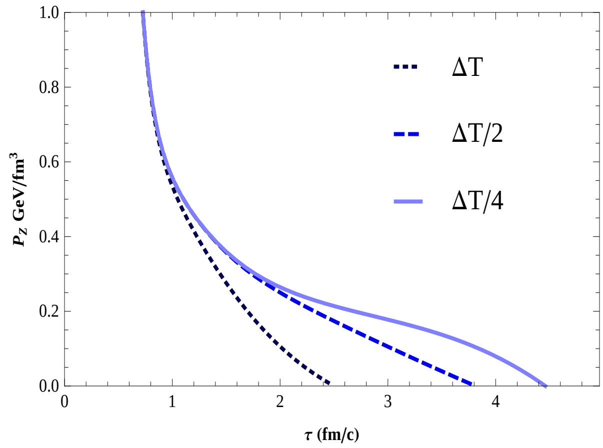

Figure 4.3: *Longitudinal pressure P_z for various viscosity cases shown in Fig. [3.4].*

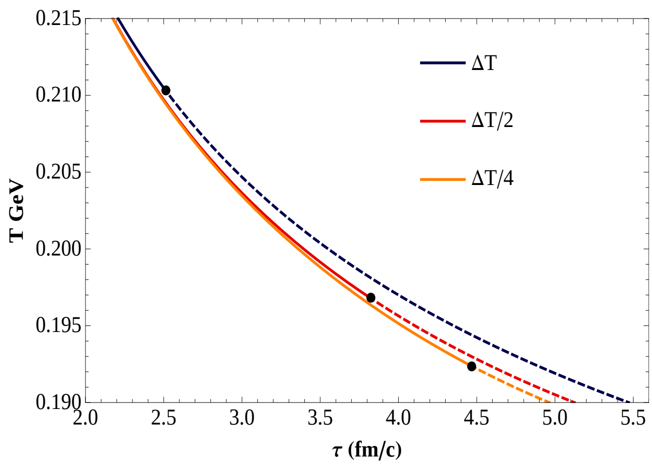

Figure 4.4: *Temperature is plotted as a function of time. With peak value (a) of ζ/s remains same while width (ΔT) varies. In all the three curves, solid lines end at cavitation time τ_c denoted by a dark circle. The dashed lines in each curves show how the system would evolve till T_c if cavitation is ignored. Figure shows that larger the width parameter shorter the cavitation time.*

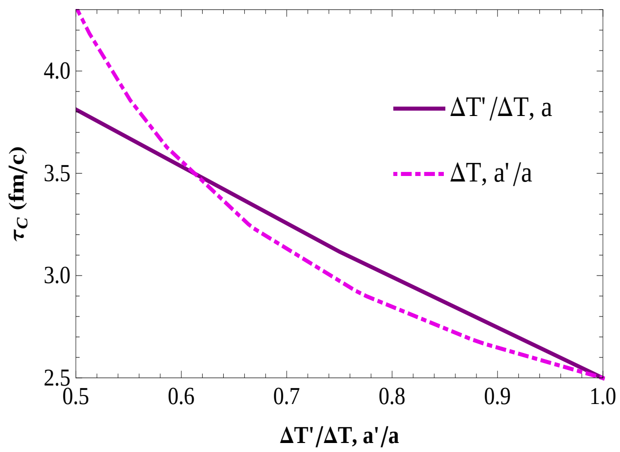

Figure 4.5: *Cavitation time τ_c as a function of different values of height (a') and width ($\Delta T'$) of ζ/s curve.*

by the lowest curve in Fig. [4.3]. In this case, the cavitation occurs when the temperature reaches the value about 210 MeV, as may be seen in Fig. [4.4]. Had we ignored the cavitation, the system would have taken a time τ_f = 5.5 fm/c to reach T_c, which is significantly larger than τ_c. This shows that cavitation occurs rather abruptly without giving any sign in the temperature profile of the system. The hydrodynamic evolution without implementing the cavitation constraint can lead to over-estimation of the evolution time and the particle production.

We have carried out a similar analysis shown in Figs. [4.3 & 4.4] by keeping ΔT fixed ($= T_c/14.5$) and varying parameter a. In Fig. [4.5] we show the cavitation times corresponding to changes in a and ΔT (denoted by a' and $\Delta T'$). The dashed curve in Fig. [4.5] shows τ_c as a function of a, while keeping ΔT fixed. The curve shows that τ_c decreases with with increasing a. The solid line shows how τ_c varies while keeping a fixed and changing ΔT.

Further, we also consider $\eta/s = 1/4\pi$ and ζ/s as function of T as in Ref. [115] for LHC energies. It is found that the cavitation does not occur in this case unlike the results for RHIC energies [115, 200, 201]. One may naively expect that when the system temperature reach $T \sim T_c$, the bulk viscosity become large enough to drive cavitation. However, the cavitation occurs when the viscous stress (Π and/or Φ) has a peak in its temporal profile. The height of the peak is determined by τ_0, T_0 and the initial values of ζ/s or η/s. For LHC energies, we find that even at the peak value of the viscous stress Π, the condition $\Pi < P$ is satisfied and therefore cavitation does not occur.

4.3 Shear viscosity, cavitation and hydrodynamics at LHC

Presently the shear viscosity of the strongly-interacting matter produced in the heavy-ion collision experiments at LHC and RHIC is under extensive investigations. It has been argued that in order to explain the collective flow data from RHIC, η/s cannot be larger than twice the KSS-bound [109]. It is generally expected that η/s for QGP has a minimum at the critical temperature T_c, while it increases with the temperature beyond T_c [184, 202, 203].

It must be noted that the applications of the viscous hydrodynamics discussed above regard η/s as independent of temperature. However, recently it has been argued that constant η/s is in sharp contrast with the observed fluid behavior in nature where it can depend on temperature [179, 202]. It has been demonstrated that the temperature-dependence of η/s can strongly influence the transverse momentum spectra and elliptical flow in the heavy-ion collision experiments at LHC [202, 204]. It should be emphasized here that the ratio of bulk viscosity to entropy density ζ/s as a function of temperature was already considered by several authors and interesting consequences like *cavitation* were studied [115, 197, 200, 205]. A similar analysis with a temperature-dependent η/s has not been performed so far, which we intend to address here. Cavitation has also been studied recently with a holographic formulation of sQGP [206].

In this work we use η/s prescriptions arising from lattice QCD (lQCD) as in Ref. [202], virial theorem type of arguments [203] as well as the analytical expressions for η/s as given in Ref.[204]. We show that the large values of η/s, relevant for LHC energies, can make the effective pressure of the fluid very small in a time less than 2 fm/c. This would cause cavitation in the fluid which in turn would limit the applicability of hydrodynamics. It must be noted that the cavitation at RHIC energies studied in Refs. [115, 200, 201] earlier was driven by the high values of the bulk viscosity near the critical temperature. However, the bulk viscosity can play an insignificant role in the temperatures $T >> T_c$. In the present study we for the first time demonstrate that for LHC energies cavitation is solely driven by the shear viscosity.

4.3.1 Hydrodynamics and temperature dependent η/s at LHC

We treat the longitudinally expanding plasma within second order hydrodynamics in our analysis i.e.; Eqs. (4.1 - 4.3). One may argue against the validity of applying (1+1)-dimensional flow, in studying the relativistic heavy-ion collisions by ignoring the transverse flow. As will be shown later for a central collision at LHC energies the cavitation sets during the initial stage of the collision in a time less than 2 fm/c. Since the transverse flow is expected to be negligible during the earlier stages of a heavy-ion collision, it will not have a significant effect on the cavitation time.

We recall from Section 3.1.2 that the last term with brackets on the right-hand side of the equation describing the evolution of shear stress Φ, i.e.; Eq. (4.2):

$$\frac{\partial \Phi}{\partial \tau} = -\frac{\Phi}{\tau_\pi} + \frac{2}{3}\frac{1}{\beta_2 \tau} - \frac{1}{\tau_\pi}\left[\frac{4\tau_\pi}{3\tau}\Phi + \frac{\lambda_1}{2\eta^2}\Phi^2\right]$$

is due to the conformal symmetry. Here we take the lQCD result for EoS, as in previous study i.e.; Eqs. (3.49 & 3.50). At LHC energies the bulk viscosity is expected to be negligible as $\varepsilon \approx 3P$ and one can ignore Eq. (4.3). Effective longitudinal pressure P_z in Eq. (3.33) and in the absence of the bulk stress is given by $P_z = P - \Phi$.

We use recent lQCD estimate for η/s in QGP sector calculated by Nakamura *et al.* [184]. The resulting η/s from lQCD has the expected minimum near the critical temperature T_c. It should be noted that recent lattice studies indicate a crossover rather than a phase-transition [6]. However, for the present work this may not be an issue since we are interested in temperature dependence of η/s where T_c is a parameter. We use the parametrization of η/s given in Ref. [207], where the minimum value of η/s is $1/4\pi$. Another prescription for shear viscosity that we use is from Ref. [203], where using virial expansion techniques, the authors

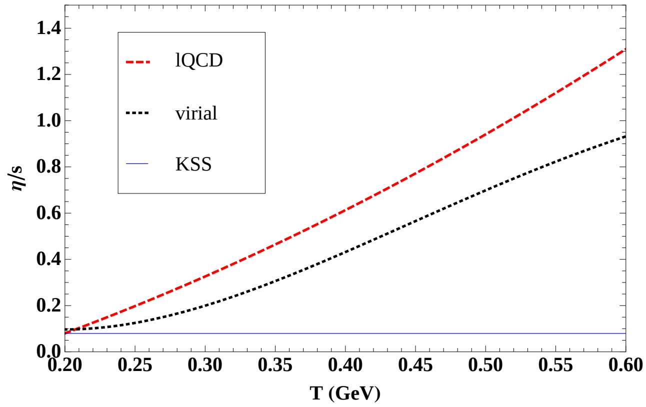

Figure 4.6: *Different prescriptions of η/s as function of temperature, with T_c=0.2 GeV. The horizontal curve show $\eta/s = 1/4\pi$ obtained from the AdS/CFT correspondence.*

calculate η/s in QGP. Fig. [4.6] shows the plots of various η/s prescriptions versus temperature with T_c =0.2 GeV. The top curve shows values of η/s obtained from the lattice results, while the middle curve corresponds to η/s values obtained from the virial expansion. The horizontal line corresponds to the KSS value. Finally, we consider the temperature-dependent forms of η/s as given in Ref. [204]: $(\eta/s)_1 = 0.2 + 0.3\,\frac{T-T_{chem}}{T_{chem}}$, $(\eta/s)_2 = 0.2 + 0.4\,\frac{(T-T_{chem})^2}{T_{chem}^2}$ and $(\eta/\mathrm{s})_3 = 0.2 + 0.3\sqrt{\frac{\mathrm{T}-\mathrm{T_{chem}}}{\mathrm{T_{chem}}}}$, with $T_{chem} = 0.165$ GeV.

It ought to be mentioned that in the relativistic viscous hydrodynamic literature there is some ambiguity regarding the value of the relaxation times associated with shear and bulk viscosities. In this work we have taken the relaxation time for shear viscosity, Eq. (3.30): $\tau_\pi = \frac{5\eta/s}{T}$; which is motivated by kinetic theory. In addition we also solve Eqs. (4.1 & 4.2) by taking Eq. (3.29): $\tau_\pi = \frac{2\eta/s}{T}(2-\ln 2) \approx \frac{2.6\eta/s}{T}$ with $\lambda_1 = \frac{\eta}{2\pi T}$, inspired by results from strongly coupled $\mathcal{N}$=4 SYM theory.

4.3.2 Shear viscosity driven cavitation

Next we present the numerical solutions for the equations of hydrodynamics. First we consider the case with temperature-dependent η/s taken from lQCD calculations. Fig. [4.7] shows the plots of longitudinal pressure P_z versus the proper time for the cases of pure Israel-Stewart type (IS) hydro by neglecting the conformal terms in Eq. (4.2) and with conformal terms (IS+C). In the case of IS we use τ_π

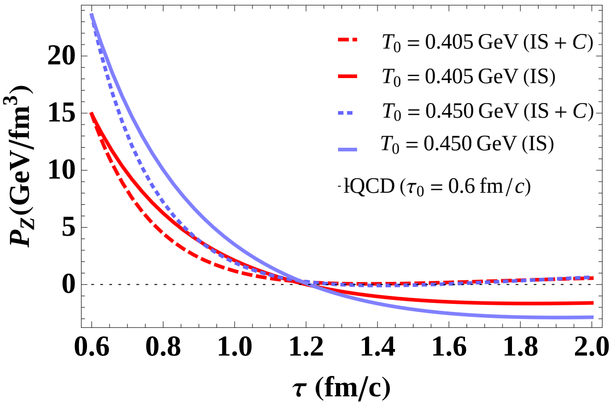

Figure 4.7: *The longitudinal pressure P_z as function of time for IS and IS+C hydrodynamics. Initial time is taken to be 0.6 fm/c with initial temperatures 0.405 and 0.450 GeV. $\eta/s(T)$ is obtained from the lQCD curve shown in Fig. [4.6].*

from the kinetic theory and from the supersymmetric Yang-Mills theory when we consider IS+C case. We plot P_z for these two cases with the initial temperatures 0.405 and 0.450 GeV. The starting time τ_0 is chosen to be 0.6 fm/c. Let us first consider the case with $T_0 = 0.405$ GeV. From the figure it is clear that longitudinal pressure becomes negative in the IS case around cavitation time $\tau_c = 1.20$ fm/c. The temperature T_{cav} at which the cavitation occurs is about 0.333 GeV which is much larger than the critical temperature T_c . Thus the cavitation can take place very early during the evolution. This, we believe, provides *a posteriori* justification for neglecting the transverse flow; as the hydrodynamic treatment may not be valid for the time larger than τ_c. Further, if we include the conformal terms in Eq. (4.2) together with the relaxation time obtained from supersymmetric Yang-Mills (IS+C), the cavitation time increases marginally and becomes τ_c=1.53 fm/c. Similarly T_{cav}=0.316 GeV is less than the cavitation temperature without the conformal terms. Next we consider a higher initial temperature $T_0 = 0.450$ GeV. Here also we observe cavitation for both IS and IS+C cases as in the previous case with $T_0 = 0.405$ GeV. For IS case cavitation happens at a time $\tau_c = 1.21$ fm/c which is only marginally greater than the corresponding $T_0 = 0.405$ GeV case considered previously. However, here $T_{cav} = 0.369$ GeV is higher than the previous case. This difference is expected since the initial temperature for the latter case is also larger. IS+C case with $T_0 = 0.450$ GeV, cavitation sets in at $\tau_c = 1.29$ fm/c

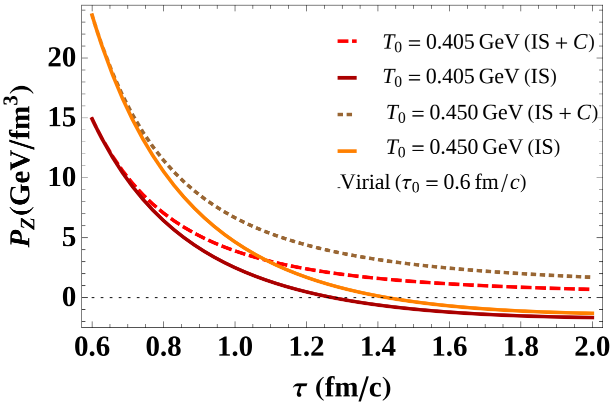

Figure 4.8: *The longitudinal pressure P_z as function of time for IS and IS+C hydrodynamics. Initial time is taken to be 0.6 fm/c with initial temperatures 0.405 and 0.450 GeV. $\eta/s(T)$ taken from the virial expansion techniques curve in Fig. [4.6].*

with T_{cav}=0.365 GeV. Again we note that there is not much difference between the cavitation times in IS and IS+C cases.

In Fig. [4.8], we show P_z as a function of time by taking η/s values using the virial expansion techniques given in Ref. [203]. Values for τ_0 and T_0 are same as in Fig. [4.7]. Here in the IS case with $T_0 = 0.450$ GeV we can see that cavitation sets in around 1.43 fm/c when the system temperature is 0.353 GeV. However, as one can see from Fig. [4.8], when we include conformal terms (IS+C case) cavitation scenario is avoided. Next we lower the initial temperature to 0.405 GeV and consider the IS case. Here system reaches a negative longitudinal pressure stage at $\tau_c = 1.27$ fm/c with $T_{cav} = 0.329$ GeV. But with conformal terms included, as one can see from the figure, the longitudinal pressure remains positive although it assumes a very small value by 2 fm/c. Since the values of η/s for the virial expansion techniques are systematically smaller than η/s for the lQCD results as shown in Fig. [4.6], the corresponding cavitation time is larger than that shown in Fig. [4.7]. However, the cavitation temperature T_{cav} is smaller than the corresponding cases discussed in Fig. [4.7].

Further, we have changed the values of the initial time by considering the case $\tau_0 = 0.3$ fm/c and $\tau_0 = 1.0$ fm/c. These results are summarized in Table 4.1. For $\tau_0 = 0.3$ fm/c and $T_0 = 0.560$ GeV case, the cavitation occurs around $\tau_c = 0.6$ fm/c

LHC		IS ($\tau_\pi = \frac{5\eta/s}{T}$)			IS+C ($\tau_\pi = \frac{2.6\eta/s}{T}$)		
		τ_f	τ_c	T_{cav}	τ_f	τ_c	T_{cav}
τ_0=0.3 fm/c	η/s lQCD	21.18	0.57	0.421	14.21	0.52	0.434
T_0=0.506 GeV	η/s virial	20.61	0.63	0.410	13.93	0.93	0.374
τ_0=0.3 fm/c	η/s lQCD	31.58	0.57	0.465	20.31	0.52	0.479
T_0=0.560 GeV	η/s virial	25.06	0.68	0.444	18.12	1.20	0.385
τ_0=0.6 fm/c	η/s lQCD	12.40	1.20	0.333	10.83	1.53	0.316
T_0=0.405 GeV	η/s virial	15.30	1.27	0.329	11.88	-	-
τ_0=0.6 fm/c	η/s lQCD	18.36	1.21	0.369	15.63	1.29	0.365
T_0=0.450 GeV	η/s virial	19.84	1.43	0.353	16.07	-	-
τ_0=1.0 fm/c	η/s lQCD	10.48	-	-	9.98	-	-
T_0=0.350 GeV	η/s virial	13.04	2.16	0.283	11.17	-	-

Table 4.1: *Column IS corresponds to the case when the conformal terms are neglected from the hydrodynamics equations. In this case the relaxation time τ_π from the kinetic theory is taken in to account. The column IS+C corresponds to the case when the conformal terms and τ_π obtained from the supersymmetric Yang-Mills theory are included in the equations of hydrodynamics. The cavitation time τ_c and τ_f are measured in the unit of fm/c and the cavitation temperature T_{cav} is shown in the units of GeV. τ_c and T_{cav} are left blank when there is no cavitation.*

for the lQCD η/s while it occurs around $\tau_c = 0.68$ fm/c for η/s obtained from the virial expansion. For the case with $\tau_0 = 1.0$ fm/c and $T_0 = 0.350$ GeV, for η/s from virial expansion, the cavitation occurs around $\tau_c = 2.16$ fm/c. However, in this case when the η/s values from lQCD are used there is no cavitation. We would like to note that the table shows no entries for τ_c and T_{cav} for certain cases. For such instances the longitudinal pressure remains positive and there is no cavitation. Table 4.1 indicates for the given initial conditions there are *more number of no-cavitation instances when the conformal terms* in the equations of the hydrodynamics are taken into account.

We also summarise the results for τ_f, the total time taken by the system to reach T_c by ignoring the cavitation in Table 4.1. One can see that with $T_0 = 0.405$

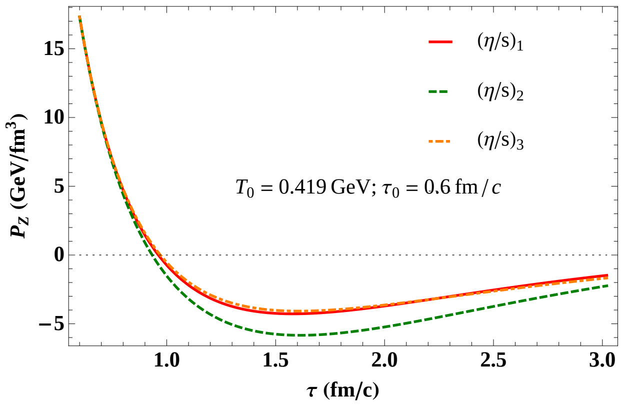

Figure 4.9: *Cavitation with various η/s prescriptions considered by Shen et.al. in Ref. [204]. The initial temperature is taken to be 0.419 GeV with initial time* 0.6 *fm/c.*

GeV for lQCD (virial) case τ_f=12.40 (15.30) fm/c without the conformal term and τ_f=10.83 (11.88) fm/c if the term is included. Thus the inclusion of the conformal terms reduces τ_f. We would like to emphasize that in this work we have taken a rather conservative initial value $\Phi(\tau_0)$=0 so that the initial value of the longitudinal pressure is always positive [208]. Instead if one includes the first-order (Navier-Stokes) initial value $\Phi(\tau_0) = 4\eta(T_0)/(3\tau_0)$, then the cavitation can occur at even earlier time and higher temperature.

Next, we repeat our analysis using the temperature-dependent η/s prescriptions given in Ref. [204]. With the same initial conditions as in Ref. [204] we find that the longitudinal pressure becomes negative very early $\sim$ 1 fm/c for *all* the cases they have considered. Fig. [4.9] shows P_z versus τ for initial temperature $T_0 = 0.419$ GeV and $\tau_0 = 0.6$ fm/c. In this case also cavitation sets in early in about $\tau_c \sim$ 1 fm/c.

We have further considered the effect of anomalous viscosity (η_A), which may be important during the early time evolution in the hydrodynamics [209]. We use an effective shear viscosity $\eta^{-1} = \eta_A^{-1} + \eta_C^{-1}$ as discussed in Ref. [209]. Here, η_C the collisional viscosity is taken from lQCD and for η_A/s we use the expression from Ref. [209]. In this case, (with $\tau_0 = 0.6$ fm/c and $T_0 = 450$ MeV), cavitation sets in at a time 1.46 fm/c when the system is at a temperature 351 MeV. The initial value of anomalous viscosity to entropy density ratio is $\sim$ 0.23. The results are

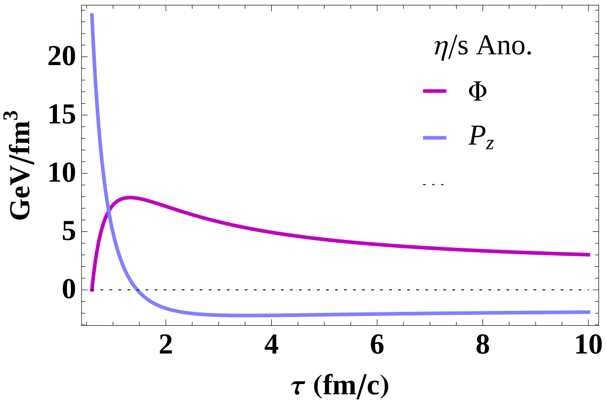

Figure 4.10: *Cavitation along with anomalous viscosity. The longitudinal pressure P_z and Φ as function of time. The initial temperature is taken to be 0.450 GeV with initial time* 0.6 *fm/c.*

presented in Fig. [4.10], where we plot the shear stress term Φ and longitudinal pressure P_z as a function of proper time. As is clear from Fig. [4.10] the shear stress Φ increases sharply from its initial value. The maximum value of Φ and the time it takes to reach that value strongly depend upon τ_π. This sharp rise of Φ result in a sharp reduction of P_z, which, finally becomes negative at τ_c.

4.4 Chemically non-equilibrated dissipative parton plasma

Plasma created in heavy-ion collision can be in a state of chemical non-equilibrium eventhough it is in thermal (kinetic) equilibrium. Chemical equilibration of the parton plasma formed in nucleus-nucleus collisions was studied using rate equations for quarks and gluons [210]. In this model QGP formed at RHIC and LHC conditions was considered to be far away from the chemical equilibrium. This study was done using ideal hydrodynamics with the Björken flow. In this section we analyse the role of a finite shear viscosity in chemical non-equilibration. Recent studies from RHIC indicate a minimal finite value of shear viscosity to entropy density $\eta/s \sim 1/4\pi$ of the QGP formed [109, 111]. We ignore the bulk viscosity in the relativistic limit when the $\varepsilon = 3P$ EoS is obeyed [46]. However, the bulk viscosity can be important near the critical temperature (see Section 3.3.3) . Therefor we consider chemical equilibration of a dissipative parton plasma with the minimal value of $\eta/s \approx 1/4\pi$ in RHIC and LHC scenarios.

We assume that after a time τ_{iso}, the partons produced from the nucleus-nucleus collision have a isotropic momentum distribution. To describe the chemical non-equilibration while maintaining the kinetic equilibrium, one can use the parton distribution of the form (for $\tau > \tau_{iso}$) [210, 211]:

$$f(p,T)_{q,g} = \lambda_{q,g}(\tau)\frac{1}{e^{u\cdot p/T(\tau)} \pm 1}, \tag{4.4}$$

where p^μ and u$^\mu$ are the four momentum and four-velocity of the partons in local co-moving reference frame. Temperature T is a time-dependent quantity and the distribution is multiplied by time and another dependent quantity called fugacity $\lambda_{q,g}(\tau)$ to describe deviations from the chemical equilibrium. The fugacity parameter become unity when the chemical-equilibrium is reached and in general it has the range $0 \leq \lambda_{q,g} \leq 1$. The scattering processes $gg \leftrightarrow ggg$ and $gg \leftrightarrow q\bar{q}$ give the most dominant mechanism for the chemical equilibration. The master equations describing evolution the parton density are given by

$$\partial_\mu(n_g u^\mu) = \frac{1}{2}\sigma_3 n_g^2\left(1 - \frac{n_g}{\tilde{n}_g}\right) - \frac{1}{2}\sigma_2 n_g^2\left(1 - \frac{n_q^2\tilde{n}_g^2}{\tilde{n}_q^2 n_g^2}\right), \tag{4.5}$$

$$\partial_\mu(n_q u^\mu) = \frac{1}{2}\sigma_2 n_g^2\left(1 - \frac{n_q^2\tilde{n}_g^2}{\tilde{n}_q^2 n_g^2}\right), \tag{4.6}$$

where $\tilde{n}_i(i = q, g)$ is parton density with unit fugacity [210] and $\sigma_2 = \langle\sigma(gg \leftrightarrow q\bar{q})\rangle$ and $\sigma_3\langle\sigma(gg \leftrightarrow ggg)\rangle$ are thermally averaged scattering cross sections. It should be noted here that when equation for n_g and n_q are added one gets the total number density n and the term with $\frac{1}{2}\sigma_2 n_g^2\left(1 - \frac{n_q^2\tilde{n}_g^2}{\tilde{n}_q^2 n_g^2}\right)$ will drop out. This is due to the the scattering process $gg \leftrightarrow q\bar{q}$ loss in the gluon density is equal to the gain in quark density and vice verse.

We use ultra-relativistic $\varepsilon = 3P$ EoS to describe the system and therefor bulk viscosity will be absent in the system [46]. Now the energy density ϵ and number density n of the system can be calculated using Eq. (4.4) as given below

$$n = (\lambda_g a_1 + \lambda_q b_1)T^3, \quad \varepsilon = (\lambda_g a_2 + \lambda_q b_2)T^4 \tag{4.7}$$

where $a_1 = 16\xi(3)/\pi^2$, $a_2 = 8\pi^2/15$ for the gluons and $b_1 = 9\xi(3)N_f/\pi^2$, $b_2 = 7\pi^2 N_f/20$ for the quarks.

To describe evolution of the energy density and the shear stress we use second order dissipative hydrodynamics of Israel-Stewart described in Section 3.2. Energy dissipation is governed by Eq. (3.37) and for Φ evolution we use Eq. (3.22) in Björken flow and is given by [107]

$$\frac{\partial \Phi}{\partial \tau} = -\frac{\Phi}{\tau_\pi} - \frac{1}{2}\Phi\left(\frac{1}{\tau} + \frac{1}{\beta_2}T\frac{\partial}{\partial \tau}(\frac{\beta_2}{T})\right) + \frac{2}{3}\frac{1}{\beta_2 \tau}\,, \tag{4.8}$$

where $\tau_\pi = 2\beta_2\eta$ denotes the relaxation time and $\beta_2 = 9/(4\varepsilon)$ (Eq. (3.27)).

Using Eqs. (3.37, 4.8, 4.4-4.7) following evolution equations for T, Φ and $\lambda_{q,g}$ can be obtained [241]:

$$\frac{\dot{T}}{T} + \frac{1}{3\tau} = -\frac{1}{4}\frac{\dot{\lambda}_g + b_2/a_2\dot{\lambda}_q}{\lambda_g + b_2/a_2\lambda_q} + \frac{\Phi}{4\tau}\frac{1}{(a_2\lambda_g + b_2\lambda_q)T^4}\,, \tag{4.9}$$

$$\dot{\Phi} + \frac{\Phi}{\tau_\pi} = \frac{8}{27\tau}\left[a_2\lambda_g + b_2\lambda_q\right]T^4 - \frac{\Phi}{2}\left[\frac{1}{\tau} - 5\frac{\dot{T}}{T} - \frac{\dot{\lambda}_g + b_2/a_2\dot{\lambda}_q}{\lambda_g + b_2/a_2\lambda_q}\right] \tag{4.10}$$

$$\frac{\dot{\lambda}_g}{\lambda_g} + 3\frac{\dot{T}}{T} + \frac{1}{\tau} = R_3\left(1 - \lambda_g\right) - R_2\left(1 - \frac{\lambda_q^2}{\lambda_g^2}\right)\,, \tag{4.11}$$

$$\frac{\dot{\lambda}_q}{\lambda_q} + 3\frac{\dot{T}}{T} + \frac{1}{\tau} = R_2\frac{a_1}{b_1}\left(\frac{\lambda_g}{\lambda_q} - \frac{\lambda_q}{\lambda_g}\right) \tag{4.12}$$

where, the rates $R_2 = 0.24N_f\alpha_s^2\lambda_g T\ln(5.5/\lambda_g)$ and $R_3 = 2.1\alpha_s^2 T(2\lambda_g - \lambda_g^2)^{1/2}$ are defined as in Ref. [210, 211]. We would like to note that our gluon fugacity Eq. (4.11) differs from that given in Ref. [210, 211] by a factor of two in second term in the right hand side. We believe this is a typographical error. In Eq. (4.9) the first term on left hand side is due to expansion of the plasma, while on the right hand side the first term describes effect of chemical non-equilibrium and second term is due to the presence of (causal) viscosity. The last term in parenthesis of Eq. (4.10) arises because of the chemical non-equilibrium process. It should be noted that Eq. (4.9) differ from that considered in Ref. [212]. In their treatment first order viscous hydrodynamics is used which does not require time evolution of Φ. However such treatment give unphysical results like reheating artifact [107, 138] as mentioned before.

Elastic ($gg \leftrightarrow gg$) as well as non-elastic processes like $gg \leftrightarrow ggg$ can contribute to the shear viscosity. Shear viscosity coefficient was recently calculated for the inelastic process in the presence of chemical non-equilibrium in Ref. [213]. It was

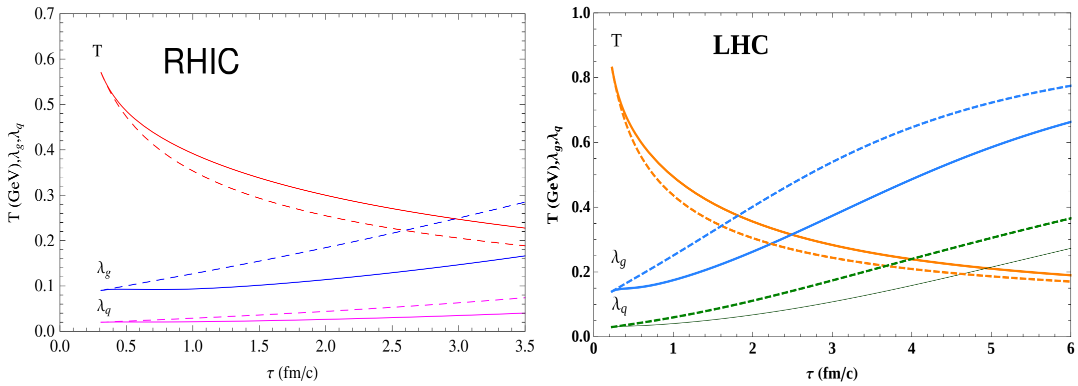

Figure 4.11: *Temperature, gluon fugacity and quark fugacity for RHIC and LHC. Solid lines indicate the case with the shear viscosity, while the dashed lines correspond to the case without viscosity.*

shown that $\eta/T^3 \simeq n_g/T^3 \simeq \lambda_g$. From this one can write [129],

$$\tau_\pi = \frac{9}{2\varepsilon}\lambda_g T^3. \tag{4.13}$$

It ought to be mentioned that this viscosity prescription was not considered in Ref. [212]. Kinetic theory without invoking non-equilibrium process gives $\tau_\pi = 3/2\pi T$.

We have solved the Eqs. (4.9 - 4.12) together with the initial conditions at τ_{iso} from HIJING Monte Carlo model [214]. Which are $\lambda_g^0 = 0.09$, $\lambda_q^0 = 0.02$ and $T_o = 0.57$ GeV for RHIC with $\tau_{iso} = 0.31$ fm/c and $\lambda_g^0 = 0.14$, $\lambda_q^0 = 0.03$ and $T_o = 0.83$ GeV for LHC with $\tau_{iso} = 0.23$ fm/c.

In Fig. [4.11] we have shown T, λ_g and λ_q as function of time. Presence of the causal viscosity decreases the fall of temperature due to expansion and the chemical non-equilibrium. However if one considers the first order theory, there can be unphysical instability. Fugacity of gluons and quarks increase more slowly due to the presence of the viscosity compared to the cases when no viscous effects were included. This is because the chemical equilibration is reached here with falling of the temperature. The temperature can decrease due to the expansion and chemical non-equilibration. The lowering of T can help in attaining chemical equilibrium and which in turn will increase the rate at which the fugacities reach their equilibrium values. Inclusion of the viscosity will slowdown the falling rate of the temperature. Consequently the fugacities will take more time to reach their equilibrium values. So we saw that the effect of viscosity to make system more away from chemical equilibrium compared with ideal case.

4.5 Conclusions

Using second order causal relativistic hydrodynamics we have analysed the role of shear viscosity, bulk viscosity and viscosity induced cavitation on the hydrodynamical evolution of QGP at RHIC and LHC energies. At RHIC energies, using a temperature dependent ζ/s which has a peak near T_c and minimal value of shear viscosity $\eta/s \approx 1/4\pi$ (as experiments suggest), we have seen that effective longitudinal pressure of the system can become negative due to the high values of bulk viscosity triggering cavitation [114, 115]. This will in turn make the hydrodynamic treatment invalid beyond cavitation time τ_c. We have studied the cavitation scenarios by changing width and height of the ζ/s curve, in order to account for the ambiguity regarding the exact values of the same. We have shown that bulk viscosity plays a dual role in heavy-ion collisions: On one hand it enhances the time by which the system attains the critical temperature, while on the other hand it can make the hydrodynamical treatment invalid much before it reaches T_c. Further, we found that at LHC energies bulk viscosity with a large value near T_c cannot drive system towards cavitation. We also note that minimal value value of shear viscosity alone is inadequate to trigger cavitation both at RHIC and LHC. However, we have shown by using various prescriptions for a temperature dependent η/s that at LHC energies the higher values of shear stresses can alone induce the cavitation. Based on the various prescriptions of η/s our results indicate that the hydrodynamical description is valid about $\tau_c \approx 2$ fm/c at LHC energies.

We have studied shear viscosity induced cavitation using one dimensional boost invariant causal dissipative hydrodynamics of Israel-Stewart type. One would of course like to do an analysis using a (3+1)-dimensional viscous hydrodynamics like e.g. in Ref. [215]. Since cavitation occurs during the early stages of the collision, we believe that the inclusion of transverse flow will not alter the result qualitatively. However, as a caveat, we would like to mention that the difference between the initial conditions for the "cavitation" and "no-cavitation" cases is rather small, see Table 4.1. It remains to be seen if the inclusion of transverse flow can alter the cavitation scenario in a qualitative way. It can also be argued that transverse flow is generated after the fragmentation [197]. It is worth noting here the negative pressure scenario may be circumvented by considering anisotropic corrections in the distribution functions [216]. Beyond τ_c, the fluid might fragment [197] or form inhomogeneous clusters. Let us note that one of the assumptions of the statistical hadronisation models lies in creation of extended clusters of quark matter which hadronise statistically [217]. Alternately, as has been attempted recently one can possibly use a hybrid approach for the description of fire ball expansion applying viscous hydrodynamics for the QGP stage and then coupling it to a microscopic kinetic evolution for the hadronic stage [218]. Mere integration of the equations of hydrodynamics may not tell us about cavitation. We therefore believe that the conditions for cavitation may be required to be incorporated in the hydrodynamical codes.

We have also studied the effect of finite shear viscosity on the chemical equilibration of the plasma. We found that system takes more time to reach equilibration in presence of even minimal value of shear viscosity. As expected, in presence of viscosity, we have seen that system temperature is falling more slowly compared to ideal case. Similarly quark and gluon fugacities also taking more time compared to the ideal case to reach equilibrated state.

Chapter 5

Electromagnetic probes of viscous QGP

Thermal photons and dileptons are among the most promising probes of the hot and dense matter created in relativistic heavy ion collisions. As their mean free path is larger than the transverse size of the fireball, they can escape from the system and there by provide information about the thermodynamic state and space-time history of the matter created in heavy ion collisions [12, 219, 220]. Production rates of these probes (particles) depend on the temperature of the system and by knowing the appropriate initial conditions, the time evolution of the temperature of the system can be obtained by using the equations of hydrodynamics. Once the temperature profile is obtained, the calculation of the thermal spectra can be done by evaluating the cross-section of the underlying scattering processes. We refer readers Refs. [221–225] for excellent reviews on the subject.

In this chapter we will study the following different scenarios:

- The effect of finite shear viscosity $\eta/s = 1/4\pi$ on thermal photon production from *chemically non-equilibrated* QGP, with $\varepsilon = 3P$ EoS, at RHIC/LHC energies.

- The effect of finite bulk and shear viscosity $\eta/s = 1/4\pi$ on thermal photon production from equilibrium QGP, with lQCD prescription for bulk viscosity and EoS, at RHIC energies.

- The effect of finite bulk and shear viscosity $\eta/s = 1/4\pi$ on thermal dilepton production from equilibrium QGP, with lQCD prescription for bulk viscosity and EoS, at RHIC energies.

5.1 Thermal photons

Thermal photon production from QGP have been studied under various conditions by several authors [199, 226–232] using ideal hydrodynamics. During QGP phase thermal photons are originated from various sources, like *Compton scattering* $q(\bar{q})g \to q(\bar{q})\gamma$, annihilation processes $q\bar{q} \to g\gamma$ etc. [226].

Recently Aurenche *et al.* showed that two-loop level *bremsstrahlung* process contribution to photon production is as important as *Compton* or *annihilation* contributions evaluated up to one-loop level [233]. They also discussed a new mechanism for hard photon production through the annihilation of an off-mass shell quark and an anti-quark, with the off-mass shell quark coming from scattering with another quark or gluon. These processes were also included in the calculation of total photon spectrum from heavy ion collisions in Refs. [199, 234]. Until recently only the processes of *Compton scattering* and *$q\bar{q}$-annihilation* were considered in studying the photon production rates.

5.1.1 Thermal photon production rates in QGP

In order to compute the photon production rates one needs to know the underlying amplitude $\mathcal{M}$ of the basic process involving the annihilation or Compton scattering process and the parton distribution functions given by [224]

$$\begin{aligned} \frac{dN}{d^4x d^3p} &= \frac{1}{(2\pi)^3 2E} \int \frac{d^3\mathbf{p}_1}{(2\pi)^3 2E_1} \frac{d^3\mathbf{p}_2}{(2\pi)^3 2E_2} \frac{d^3\mathbf{p}_3}{(2\pi)^3 2E_3} \times f_1(E_1) f_2(E_2)[1 \pm f_3(E_3)] \\ &\times \sum_i \langle |\mathcal{M}|^2 \rangle \, (2\pi)^4 \, \delta(p_1 + p_2 - p_3 - p). \end{aligned} \tag{5.1}$$

Here $p_1 = (E_1, \mathbf{p}_1)$ and p_2 are the 4-momenta of the incoming partons, p_3 of the outgoing parton, and p of the produced photon. In equilibrium, the distribution functions $f_i(E_i)$ are given by the Bose-Einstein distribution, $f_B(E_i) = 1/[\exp(E_i/T) - 1]$, for gluons and by the Fermi-Dirac distribution, $f_F(E_i) = 1/[\exp(E_i/T) + 1]$, for quarks, respectively. The factor $\langle|\mathcal{M}|^2\rangle$ is the matrix element of the basic process averaged over the initial states and summed over the final states. The $\sum_i$ indicates the sum over the initial parton states.

The production rate for hard ($E > T$) thermal photons from equilibrated QGP evaluated to the one-loop order using perturbative thermal QCD based on hard thermal loop (HTL) resummation to account medium effects. The *Compton scattering* and *$q\bar{q}$-annihilation* contribution to the photon production rate is [226, 228, 235],

$$E\frac{dN}{d^4xd^3p} = \frac{1}{2\pi^2}\alpha\alpha_s\left(\sum_f e_f^2\right) T^2\ e^{-E/T}\ \ln\left(\frac{\mathrm{cE}}{\alpha_\mathrm{s}\mathrm{T}}\right), \tag{5.2}$$

where the constant $c \approx 0.23$ and α and α_s are the electromagnetic and strong coupling constants respectively. In the summation f is over the flavors of the quarks and e_f is the electric charge of the quark in units of the charge of the electron.

The rate of photon production due to *Bremsstrahlung* processes is given by [233],

$$E\frac{dN}{d^4xd^3p} = \frac{8}{\pi^5}\alpha\alpha_s\left(\sum_f e_f^2\right)\frac{T^4}{E^2}\ e^{-E/T}\ (J_T - J_L)\ I(E,T), \tag{5.3}$$

where $J_T \approx 1.11$ and $J_L \approx 1.06$ for two flavors and three colors of quarks [234]. The expression for $I(E,T)$ is given by

$$\begin{aligned} I(E,T) &= (3\ \zeta(3) + \frac{\pi^2}{6}\frac{E}{T} + \left(\frac{E}{T}\right)^2 \ln(2) + 4\ \mathrm{Li}_3\left(-\mathrm{e}^{-|\mathrm{E}|/\mathrm{T}}\right) \\ &\quad +2\left(\frac{E}{T}\right)\mathrm{Li}_2\left(-\mathrm{e}^{-|\mathrm{E}|/\mathrm{T}}\right) - \left(\frac{\mathrm{E}}{\mathrm{T}}\right)^2\ \ln\left(1+\mathrm{e}^{-|\mathrm{E}|/\mathrm{T}}\right)), \end{aligned} \tag{5.4}$$

where Li are the polylogarithmic functions given by $\mathrm{Li_a(z)} = \sum_{\mathrm{n}=1}^{+\infty}\frac{\mathrm{z^n}}{\mathrm{n^a}}$.

Next, the rate due to *$q\bar{q}$-annihilation with an additional scattering in the medium* is given by [233],

$$E\frac{dN}{d^4xd^3p} = \frac{8}{3\pi^5}\alpha\alpha_s\left(\sum_f e_f^2\right)\ E\ T\ e^{-E/T}\ (J_T - J_L). \tag{5.5}$$

We use the parametrization $\alpha_s(T) = \frac{6\pi}{(33-2N_f)\ \ln(8\mathrm{T}/\mathrm{T_c})}$ by Karsch [236], in our rate calculations. Here N_f is the number of quark flavors in consideration. In Fig. [5.1], we plot the different photon rates for a fixed temperature $T =$

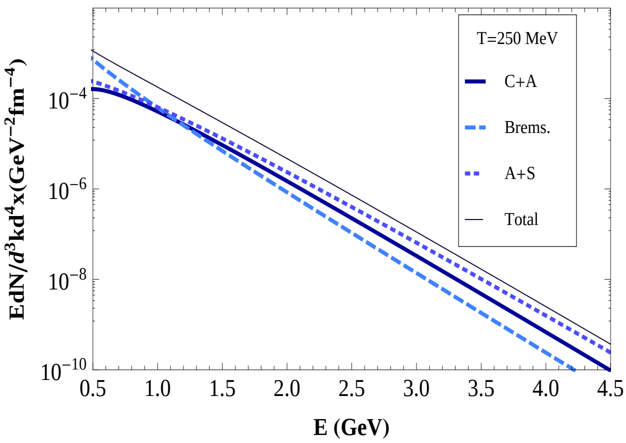

Figure 5.1: *Hard thermal photon rates in QGP as a function of energy for a fixed temperature T=250 MeV. Photon rates are plotted for different relevant processes.*

250 MeV. It shows the contributions from *Bremsstrahlung* (Brems), *annihilation with scattering* (A+S) and *Compton scattering* together with *$q\bar{q}$-annihilation* (C+A). *Bremsstrahlung* contributes to the photon production rate upto $E \sim 1$ GeV only, afterwards A+S and C+A processes become dominant. We might mention here that this observation is in agreement with Ref. [234].

5.1.2 Photon spectra in heavy-ion collision

Once the evolution of temperature is known from the hydrodynamical model, the *total photon spectrum* is obtained by integrating the *total rate* (obtained by adding different temperature depended photon rate expressions) over the space-time history of the collision,

$$\begin{aligned}\left(\frac{dN}{d^2p_T dy}\right)_{y,p_T} &= \int d^4x \left(E\frac{dN}{d^3pd^4x}\right) \\ &= Q\int_{\tau_0}^{\tau_1} d\tau\ \tau \int_{-y_{nuc}}^{y_{nuc}} d\eta_s \left(E\frac{dN}{d^3pd^4x}\right),\end{aligned} \tag{5.6}$$

where, we have used the fact that four-dimensional volume element in Björken model is given by $d^4x = d^2x_T d\eta_s \tau d\tau = Q\, d\eta_s \tau d\tau$, with Q being transverse cross-section of the colliding nuclei. Here τ_0 and τ_1 are the initial and final values of time we are interested. y_{nuc} is the rapidity of the nuclei. For a Au nucleus $Q \sim 180$ fm^2. p_T is the photon momentum in direction perpendicular to the collision axis. The quantity $\left(E\frac{dN}{d^3pd^4x}\right)$ is Lorentz invariant and it is evaluated in the local rest frame in Eq. (5.6), whereas the photon rates calculated in Section 5.1.1 are in rest frame. With the parametrisation of the 4-momentum of the photon as $p^\alpha = (p_T coshy, p_T cos\phi_p, p_T sin\phi_p, p_T sinhy)$ and 4-velocity given by Eq. (1.40): $u^\mu = (\cosh\eta_s, 0, 0, \sinh\eta_s)$, photon energy in frame co-moving with the plasma is given as $p_T cosh(y-\eta_s)$. So we will replace E in the photon rates with $p_T cosh(y-\eta_s)$ while calculating the photon spectrum. Having done this, from Eq. (5.6) we get the photon spectrum as a function of rapidity y and transverse momentum p_T of the photon.

5.1.3 Photon production from chemically non-equilibrated plasma

The plasma created in the heavy-ion collisions is expected to be in a state of chemical non-equilibrium. The photon emission from such a plasma has been studied earlier within the framework of ideal hydrodynamics [237–240]. It would be interesting to study the role that viscosity can play on the plasma signals.

We have already seen from Section 4.4 using $\varepsilon = 3P$ EoS, the effect of shear viscosity (with $\eta/s = 1/4\pi$) is to decrease the cooling rate of plasma and fugacities of quark and gluon increase more slowly compared to the ideal hydrodynamic case (Fig. [4.11]) [241]. In this analysis, we employ second order Israel-Stewart hydrodynamics to study time evolution of temperature and fugacities. The fugacity factors can enter Eq. (5.1) when Eq. (4.4) is considered:

$$f_1\, f_2\, (1 \pm\, f_3) \;\mapsto\; \lambda_1\, f_1\, \lambda_2\, f_2\, (1 \pm\, \lambda_3\, f_3).$$

This is can be rewritten as

$$\lambda_1\, f_1\, \lambda_2\, f_2\, (1 \pm\, \lambda_3\, f_3) = \lambda_1\, \lambda_2\, \lambda_3\, f_1\, f_2\, (1 \pm\, f_3) + \lambda_1\, \lambda_2\, (1 - \lambda_3)\, f_1\, f_2. \tag{5.7}$$

The first term on the right hand side of the above equation when inserted in Eq. (5.1) lead to the following photon rate using the Boltzmann distribution functions instead of a quantum mechanical ones [226, 237]:

$$\left(2E\frac{dN}{d^3pd^4x}\right)_1 = \frac{5\alpha\alpha_s\lambda_q^2\lambda_g}{9\pi^2}T^2e^{-E/T}\left[ln\left(\frac{4ET}{k_c^2}\right) - 1.42\right]. \tag{5.8}$$

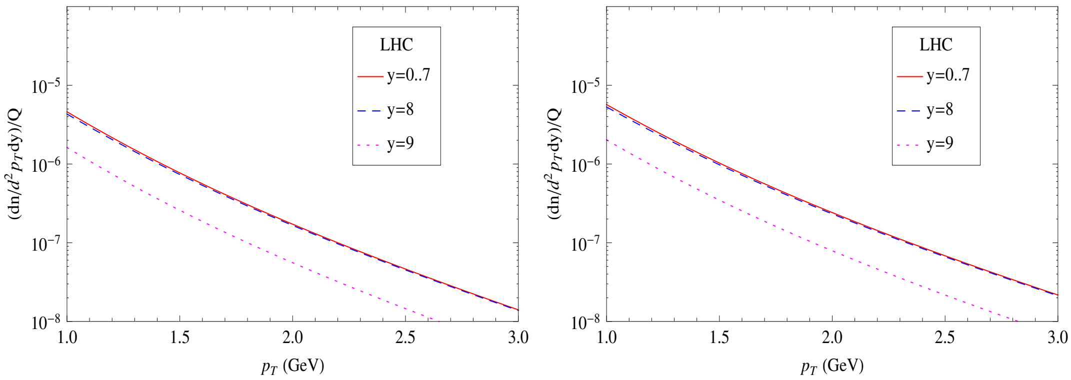

Figure 5.2: *(Left panel)Photon rate for different rapidities in LHC (y_{nuc} = 8.8). (Right panel) Same with the inclusion of viscosity.*

The second term in Eq. (5.7) will give, under the Boltzmann approximation, the following contribution to the photon rate [237]:

$$\left(2E\frac{dN}{d^3pd^4x}\right)_2 = \frac{10\alpha\alpha_s}{9\pi^4}T^2e^{-E/T}\times\mathcal{B} \tag{5.9}$$

where,

$$\begin{aligned}\mathcal{B} &= \lambda_q\lambda_g\left(1-\lambda_q\right)\left[1-2\gamma+2ln\left(4ET/k_c^2\right)\right] \\ &+ \lambda_q\lambda_q\left(1-\lambda_g\right)\left[-2-2\gamma+2ln\left(4ET/k_c^2\right)\right],\end{aligned} \tag{5.10}$$

with $k_c^2 = 2m_q^2 = 0.22g^2T^2\left(\lambda_g+\lambda_q/2\right)$.

The total photon production rate $2E\frac{dN}{d^3pd^4x}$ can be obtained by adding Eq. (5.8) and Eq. (5.9) and is required to be convoluted with the space-time evolution of the heavy-ion collision: Eq. (5.6).

We plot photon spectra by using Eq. (4.13) for τ_π in solving Eqs. (4.9–4.12). The Figs. [5.2 - 5.3] compare the case without viscosity with the case of finite shear viscosity.

Fig. [5.2] shows the photon spectra emitted at fixed rapidities as a function of transverse momenta p_T. The photon flux is normalized with the transverse size of the colliding nuclei (Q). For LHC we take: τ_0 = 0.5 fm/c, τ_1 = 6.25 fm/c and y_{nuc} = 8.8 [237]. The figure compares the case without viscosity with the case of finite shear viscosity.

Fig. [5.3] shows the comparison similar to that of Fig. [5.2] but with a set of initial conditions for RHIC: τ_0 = 0.7 fm/c, τ_1 = 4 fm/c and y_{nuc} = 6.0 [237].

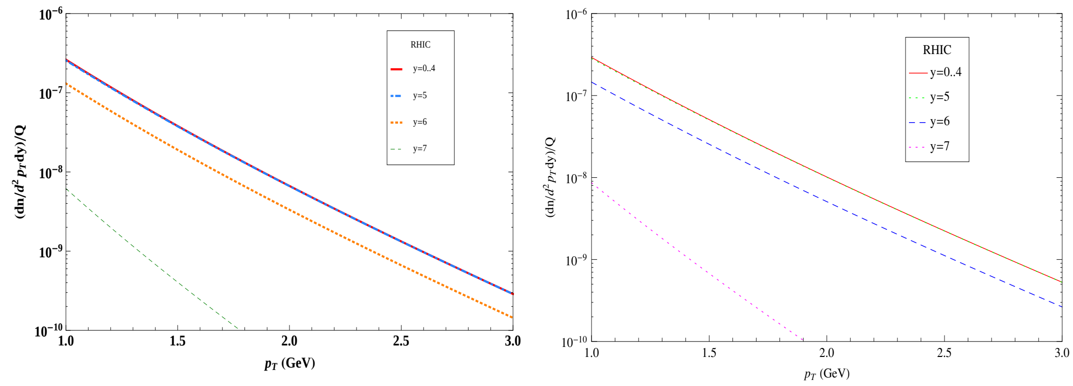

Figure 5.3: *(Left panel)Photon rate for different rapidities in RHIC (y_{nuc}=6.0). (Right panel) Same with the inclusion of viscosity.*

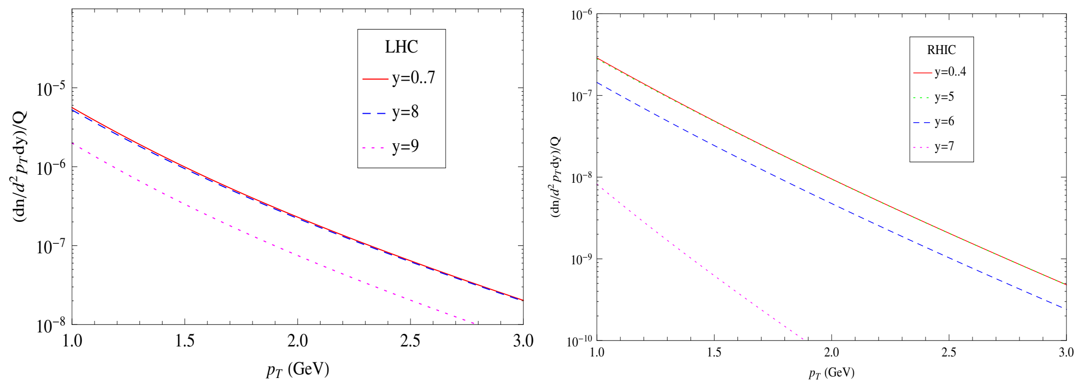

Figure 5.4: *Photon rate for different rapidities in RHIC (y_{nuc}=6.0) and LHC (y_{nuc}=8.8) with kinetic viscosity.*

For $\alpha_s = 0.3$, shear viscosity to entropy density ratio $\eta/s \sim 0.29$. Figs. [5.2 - 5.3] show that viscous effects enhance the photon flux by a factor (1.5-2).

Finally in Fig. [5.4], we compare the photon fluxes calculated using Eq. (4.13) with the fluxes calculated using the kinetic viscosity ($\tau_\pi = 3/2\pi T$). Fig. [5.4] shows the photon flux calculated using the kinetic viscosity prescription for LHC and RHIC. However, we do not find any significant change in the flux for the results obtained using Eq. (4.13).

5.1.4 Non-ideal effects on thermal photons

Thermal photons from QGP in the presence of shear viscosity was studied recently in Refs. [241–243] and they were proposed as a tool to measure the shear viscosity of the matter formed in the heavy ion collisions [241, 242]. We have already seen from Section 3.3 that near phase transition QCD matter is more and more non-conformal and follows $\varepsilon \neq 3P$ EoS and the effect of bulk viscosity becomes prominent compared to shear viscosity ($\sim 1/4\pi$ as RHIC experiments suggest) and cannot be ignored. Inclusion of bulk viscosity can lead to the phenomenon of cavitation, which in turn can significantly reduce the hydrodynamical evolution time. So in this study we would like to explore how these effects affect the thermal photon production from QGP at RHIC energies.

We use the hydrodynamical equations: Eqs. (4.1 - 4.3) and initial conditions relevant for RHIC [199]: $\tau_0 = 0.5$ fm/c, $T_0 = 0.310$ GeV and $y_{nuc} = 5.3$; discussed in Section 4.2, in our analysis. From Section 4.2, we know the temperature profiles $T(\tau)$ of the system under various conditions. Once we get the temperature profile we calculate the photon production rates. Total photon spectrum $E\frac{dN}{d^3pd^4x}$ (as a function of rapidity, y and transverse momentum of photon, p_T) is obtained by adding different photon rates using Eqs. (5.2, 5.3, 5.5) and convoluting with the space time evolution of the heavy-ion collision with Eq. (5.6). The final value of time τ_1 is the time at which temperature evolves to critical value τ_f, i.e.; $T(\tau_1) = T_c$. In all calculations we shall consider the photon production in mid-rapidity region ($y = 0$) only.

We have already seen that the calculation of photon production rates require the initial time τ_0, final time τ_1 and $T(\tau)$. τ_1 and $T(\tau)$ are determined from the hydrodynamics. Normally τ_1 is taken as the time taken by the system to reach T_c, i.e.; τ_f. Since hydrodynamics ceases to be valid beyond the cavitation time, we must set $\tau_1 = \tau_c$. Thus photon production from QGP will be influenced by the onset cavitation and temperature profile.

We emphasize that the production rates should only be integrated up to the cavitation time τ_c. Fig. [5.5] shows the case when there is no viscous correction to the distribution function. In the dashed curve the effect of cavitation is taken into account and $\tau_1 = \tau_c = 2.5$ fm/c. The solid line represents the same case but without the effect of the cavitation and $\tau_1 = \tau_f = 5.5$ fm/c. It can be seen from the curve that ignoring cavitation leads to an over-estimation of the rate by about 200% at $p_T = 0.5$ GeV and about 50% at $p_T = 2$ GeV. It is thus clear that the information about the cavitation time is crucial for correctly estimating thermal

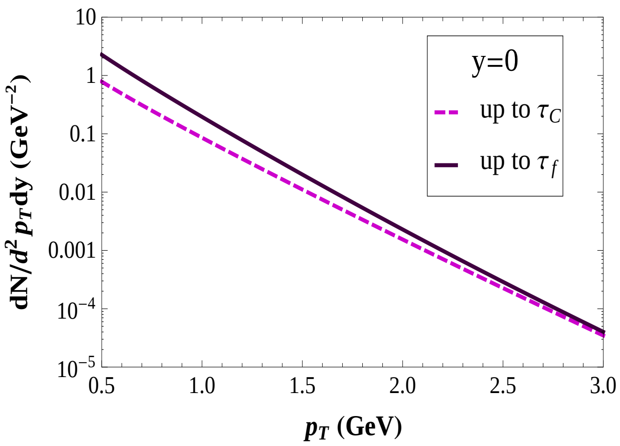

Figure 5.5: *Photon spectrum obtained by considering the effect of cavitation (dashed line). For a comparison we plot the spectrum without incorporating the effect of cavitation (solid line).*

photon production rate.

In Fig. [5.6] we plot photon production rates for various cavitation times obtained by varying ΔT (with $a = 0.901$ is fixed). Here the enhancement in the photon production when ΔT is reduced to half of its base value is about 75% at $p_T = 0.5$ GeV and about 55% at $p_T = 1$ GeV. A further reduction of the parameter value to $\Delta T/4$ is enhancing the photon production by about 110% at $p_T = 0.5$ GeV and about 80% at $p_T = 1$ GeV. The reason is, a reduction in ΔT amounts to increase in the cavitation time (see e.g., Fig. [4.3]), which in turn increases the time interval over which photon production is calculated. Therefore this increases the photon flux.

5.2 Thermal dileptons

Thermal dilepton production using the equations of *ideal* hydrodynamics is well studied by many authors [244–246]. The main source of thermal dileptons is from the quark-anti-quark annihilations: $q\bar{q} \to \gamma^* \to l^+l^-$. The cross-section of this lowest order α^2 process is well known [247]. There are other higher order processes which may also contribute in thermal dilepton production [248, 249]. However, we are not considering them in this present analysis. It may be noted that the thermal

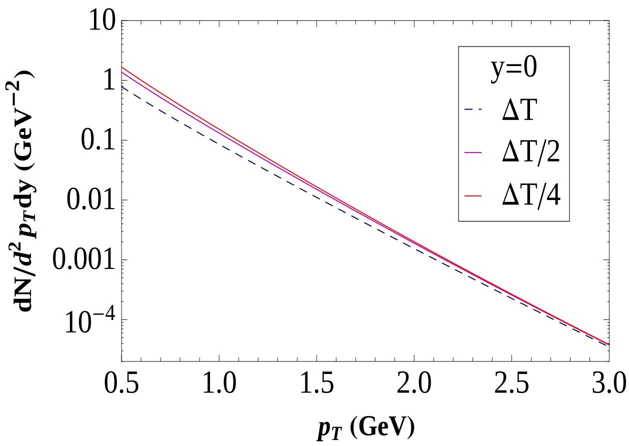

Figure 5.6: *Photon production rates showing the effect of different cavitation time.*

dileptons from the annihilation process is dominant in the window of intermediate invariant mass $1 < M < 3$ GeV and transverse momentum of the lepton pair p_T in the same range [250, 251].

Recently the thermal dilepton production from QGP in the presence of shear viscosity was studied [252]. However, we note that in this work authors had used an *ideal* EoS for the calculation and the effect of bulk viscosity was naturally not considered. We would like investigate the effects of finite bulk viscosity on the thermal dilepton production from QGP. We have seen from our previous studies that bulk viscosity plays a significant role in the hydrodynamics as well as in particle production [200]. In addition, the viscous effects can modify the temperature profile and thereby it can change the particle distribution functions of the plasma [128]. Using kinetic theory methods one can include these corrections in the distribution functions and this may have observable consequences. [150, 253]. We include these corrections by taking the viscosity modified distribution functions using the 14-moment Grad's method results, we calculate the first order correction due to both bulk and shear viscosities in the dilepton production rate.

In this section we present the results for the correction in distribution function and its role on thermal dilepton production rate in presence of finite bulk viscosity.

5.2.1 Thermal Dilepton production rates in QGP

In QGP the dominant mechanism for the production of thermal dileptons comes from $q\bar{q}$ annihilation process $q\bar{q} \to \gamma^* \to l^+l^-$. From kinetic theory rate of dilepton production (number of dileptons produced per unit volume per unit time) for this process is given by

$$\frac{dN}{d^4x} = \int \frac{d^3\mathbf{p}_1}{(2\pi)^3}\frac{d^3\mathbf{p}_2}{(2\pi)^3} f(E_1,T)f(E_2,T)v_{rel}\; g^2\sigma(M^2), \tag{5.11}$$

where $p_{1,2} = (E_{1,2}, \mathbf{p}_{1,2})$ is the four momentum of quark or anti-quark with $E_{1,2} = \sqrt{\mathbf{p}_{1,2}^2 + m_q^2} \simeq |\mathbf{p}_{1,2}|$ neglecting the quark masses. Here $M^2 = (E_1+E_2)^2 - (\mathbf{p}_1+\mathbf{p}_2)^2$ is the invariant mass of the virtual photon. The function $f(E,T) = 1/(1+e^{E/T})$ is the quark (anti-quark) distribution function in thermal equilibrium and g is the degeneracy factor. Further, in the above, $v_{rel} = \sqrt{\frac{M^2(M^2-4m_q^2)}{4E_1^2E_2^2}} \sim \frac{M^2}{2E_1E_2}$ is the relative velocity of the quark-anti-quark pair and $\sigma(M^2)$ is the thermal dilepton production cross section. The cross-section $\sigma(M^2)$ in the Born approximation is well known: $g^2\sigma(M^2) = \frac{16\pi\alpha^2\left(\sum_f e_f^2\right)N_c}{3M^2}$ and with N_f=2 and $N_c = 3$, we have $M^2g^2\sigma(M^2) = \frac{80\pi}{9}\alpha^2$ [221]. Since we are interested in the rate for a given dilepton mass and momentum, we write

$$\frac{dN}{d^4xd^4p} = \int \frac{d^3\mathbf{p}_1}{(2\pi)^3}\frac{d^3\mathbf{p}_2}{(2\pi)^3} f(E_1,T)f(E_2,T)\;\frac{M^2g^2\sigma(M^2)}{2E_1E_2}\delta^4(p-p_1-p_2) \tag{5.12}$$

where $p = (p_0 = E_1+E_2, \mathbf{p} = \mathbf{p}_1+\mathbf{p}_2)$ is the four momentum of the dileptons. At the present case we are interested in the invariant masses larger compared to the temperature i.e.; $M \gg T$, in this limit we can replace Fermi-Dirac distribution with classical Maxwell-Boltzmann distribution,

$$f(E,T) \to f_0 = e^{-E/T}. \tag{5.13}$$

5.2.2 Viscous corrections to distribution functions

Viscous effects contribute in two ways in kinetic theory: Firstly, it can change the width (temperature) of the distribution function. Secondly, it can modify the momentum dependence of the distribution function. The first effect is incorporated when we calculate the temperature as a function of time using dissipative hydrodynamics. To include the second effect one needs to compute the change in the distribution function as a function of momentum using the techniques of relativistic kinetic theory [128].

Let us write the modified distribution function as $f = f_0 + \delta f$, with viscous correction $\delta f = \delta f_\eta + \delta f_\zeta$, where δf_η and δf_ζ represent change in the distribution function due to shear and bulk viscosity respectively. We calculate δf using 14-moment Grad's method. It ought to be mentioned that recent results show that calculation of δf using this method fails near freeze-out region by making δf even larger than f_0 and $f < 0$ [253]. It is therefore important to note here that we are applying these corrections to calculate the photon production rate of hard thermal photons in the regime $T > T_c$. We have found that for p_T below 3 GeV, this approximation is reasonable but beyond it, this approximation breaks down as the contribution arising from the viscous correction δf to the distribution function becomes larger than f_0 [254]. We also note that in Ref. [253] it has been shown that the form of δf_ζ used in this calculation miss terms which are necessary for the Landau matching conditions. However, we note that basic qualitative features of the complete form of δf_ζ is obtained using our δf_ζ also. We still don't have a clear picture how to calculate the bulk viscosity corrections to the distribution functions and attempts in this direction are going on [255, 256]. With this caveats we proceed to calculate δf applying the techniques used in Refs. [150, 257].

We write the viscous correction to the (Boltzmann) distribution function as

$$\begin{aligned} f(p) &= f_0 + \delta f = f_0 + \delta f_\eta + \delta f_\zeta \\ &= f_0 \left(1 + \frac{C}{2T^3} p^\alpha p^\beta \nabla_{\langle\alpha} u_{\beta\rangle} + \frac{A}{2T^3} p^\alpha p^\beta \Delta_{\alpha\beta} \Theta \right) \end{aligned} \tag{5.14}$$

where we restrict the corrections to f upto quadratic order in momentum. In order to find coefficients A and C we first express the energy momentum tensor using f,

$$\begin{aligned} T^{\mu\nu} &= \int \frac{d^3p}{(2\pi)^3 E} p^\mu p^\nu f \\ &= T_o^{\mu\nu} + \eta \nabla^{\langle\mu} u^{\nu\rangle} + \zeta \Delta^{\mu\nu}\, \Theta, \end{aligned} \tag{5.15}$$

so that we have

$$\eta\nabla^{\langle\mu}u^{\nu\rangle} = \frac{C}{2T^3}\left[\int\frac{d^3p}{(2\pi)^3E}p^\mu p^\nu p^\alpha p^\beta f_o\right]\nabla_{\langle\alpha}u_{\beta\rangle}, \tag{5.16}$$

$$\zeta\Delta^{\mu\nu}\,\Theta = \frac{A}{2T^3}\left[\int\frac{d^3p}{(2\pi)^3E}p^\mu p^\nu p^\alpha p^\beta f_o\right]\Delta_{\alpha\beta}\Theta. \tag{5.17}$$

Now from Eq. (5.16) we get the correction δf_η due to the shear viscosity as given in Ref. [150] by finding out C and we will not repeat that calculation here. Next we will find out the coefficient A by constructing a fourth rank symmetric tensor out of $\Delta^{\mu\nu}$ and u^μ representing the term in square brackets in Eq. (5.17),

$$\begin{aligned}\frac{A}{2T^3}\left[\int\frac{d^3p}{(2\pi)^3E}p^\mu p^\nu p^\alpha p^\beta f_o\right] &= a_o\left(u^\mu u^\nu u^\alpha u^\beta\right)+a_1\left(\Delta^{\mu\nu}u^\alpha u^\beta+\text{permutations}\right)\\ &\quad +a_2\left(\Delta^{\mu\nu}\Delta^{\alpha\beta}+\Delta^{\mu\alpha}\Delta^{\nu\beta}+\Delta^{\mu\beta}\Delta^{\nu\alpha}\right)\ . \end{aligned}\tag{5.18}$$

Substituting this expression in Eq. (5.17) and by noting $\Delta_{\mu\nu}\,u^\nu=0\ ,\ \Delta_{\mu\nu}\Delta^{\mu\nu}=3$ and $\Delta^{\mu\nu}\Delta_{\mu\alpha}=\Delta^\nu_\alpha$; we get $\zeta=5a_2$. By contracting both sides of Eq. (5.18) with $\frac{1}{45}\left(\Delta_{\mu\nu}\Delta_{\alpha\beta}+\Delta_{\mu\alpha}\Delta_{\nu\beta}+\Delta_{\mu\beta}\Delta_{\nu\alpha}\right)$ we get,

$$\frac{A}{2T^3}\int\frac{d^3p}{(2\pi)^3E}f_o\frac{3}{45}\left[p^2-(u.p)^2\right]^2=a_2=\zeta/5. \tag{5.19}$$

Evaluating this expression in the local rest frame of the fluid $u^\mu=(1,\vec{0})$ we get,

$$\zeta=\frac{1}{3}\frac{A}{2T^3}\int\frac{d^3p}{(2\pi)^3E}f_o\left|\mathbf{p}\right|^4 . \tag{5.20}$$

Now for a Boltzmann gas with $f_0 = e^{-pu/T}$ we can calculate the integral and comparing the result with that of the entropy density s of an ideal boson gas [150]; we find, $A=\frac{2}{5}\,\zeta/s$. Therefore the bulk viscosity correction is given by [200]

$$\delta f_\zeta = f_0\left(\frac{2}{5}\frac{\zeta/s}{2T^3}p^\alpha p^\beta\Delta_{\alpha\beta}\Theta\right). \tag{5.21}$$

So the viscous correction to the distribution function due to both shear and bulk viscosities, up to quadratic order of momentum are given as [200],

$$f(p)=f_0(p)\left(1+\frac{\eta/s}{2T^3}p^\alpha p^\beta\nabla_{\langle\alpha}u_{\beta\rangle}+\frac{2}{5}\frac{\zeta/s}{2T^3}p^\alpha p^\beta\Delta_{\alpha\beta}\Theta\right). \tag{5.22}$$

5.2.3 Viscous modified dilepton production rates

In order to compute the effect of viscosity on the production rate, we substitute Eq. (5.22), representing the viscous corrections to the distribution function in dilepton rate Eq. (5.12). Thus keeping terms up to the second order in η/s and ζ/s, the dilepton production rates can be written as,

$$\frac{dN}{d^4xd^4p} = \frac{dN^{(0)}}{d^4xd^4p} + \frac{dN^{(\eta)}}{d^4xd^4p} + \frac{dN^{(\zeta)}}{d^4xd^4p}, \tag{5.23}$$

with

$$\frac{dN^{(0)}}{d^4xd^4p} = \int \frac{d^3\mathbf{p}_1}{(2\pi)^3}\frac{d^3\mathbf{p}_2}{(2\pi)^3}\; e^{-(E_1+E_2)/T}\frac{M^2g^2\sigma(M^2)}{2E_1E_2}\,\delta^4(p-p_1-p_2) \tag{5.24}$$

$$\frac{dN^{(\eta)}}{d^4xd^4p} = \int \frac{d^3\mathbf{p}_1}{(2\pi)^3}\frac{d^3\mathbf{p}_2}{(2\pi)^3}\; e^{-(E_1+E_2)/T}\left[\frac{\eta/s}{T^3}p_1^\alpha p_1^\beta \nabla_{\langle\alpha}u_{\beta\rangle}\right] \times \frac{M^2g^2\sigma(M^2)}{2E_1E_2}\,\delta^4(p-p_1-p_2) \tag{5.25}$$

$$\frac{dN^{(\zeta)}}{d^4xd^4p} = \int \frac{d^3\mathbf{p}_1}{(2\pi)^3}\frac{d^3\mathbf{p}_2}{(2\pi)^3}\; e^{-(E_1+E_2)/T}\left[\frac{2}{5}\frac{\zeta/s}{T^3}p_1^\alpha p_1^\beta \Delta_{\alpha\beta}\Theta\right] \times \frac{M^2g^2\sigma(M^2)}{2E_1E_2}\,\delta^4(p-p_1-p_2). \tag{5.26}$$

The first term (given by Eq. (5.24)) is the one without any viscous corrections (*ideal* part) and is well known [247]:

$$\frac{dN^{(0)}}{d^4xd^4p} = \frac{1}{2}\,\frac{M^2g^2\sigma(M^2)}{(2\pi)^5}\; e^{-p_0/T}. \tag{5.27}$$

The first order correction to the rate due to shear viscosity- given by Eq. (5.25), is calculated in Ref. [252] and the final expression is

$$\frac{dN^{(\eta)}}{d^4xd^4p} = \frac{1}{2}\,\frac{M^2g^2\sigma(M^2)}{(2\pi)^5}\; e^{-p_0/T}\;\frac{2}{3}\left[\frac{\eta/s}{2T^3}p^\alpha p^\beta \nabla_{\langle\alpha}u_{\beta\rangle}\right]. \tag{5.28}$$

Let us next proceed to estimate the correction to the rate due to bulk viscosity from Eq. (5.26). We can write

$$\begin{aligned}\frac{dN^{(\zeta)}}{d^4xd^4p} &= \int \frac{d^3\mathbf{p}_1}{(2\pi)^6}\; e^{-(E_1+E_2)/T}\left[\frac{2}{5}\frac{\zeta/s}{T^3}p_1^\alpha p_1^\beta \Delta_{\alpha\beta}\Theta\right]\frac{M^2g^2\sigma(M^2)}{2E_1E_2}\,\delta(p_0-E_1-E_2)\\ &= \frac{2}{5}\frac{\zeta/s}{T^3}I^{\alpha\beta}(p)\Delta_{\alpha\beta}\Theta,\end{aligned} \tag{5.29}$$

where we have represented

$$I^{\alpha\beta} = \int \frac{d^3\mathbf{p}_1}{(2\pi)^6}\; e^{-(E_1+E_2)/T}p_1^\alpha p_1^\beta\frac{M^2g^2\sigma(M^2)}{2E_1E_2}\delta(p_0-E_1-E_2) \tag{5.30}$$

Now we write the second rank tensor $I^{\alpha\beta}$ in the most general form constructed out of u^α and p^α:

$$I^{\alpha\beta} = a_0 g^{\alpha\beta} + a_1 u^\alpha u^\beta + a_2 p^\alpha p^\beta + a_3(u^\alpha p^\beta + u^\beta p^\alpha)\,. \tag{5.31}$$

Note that because of the identity $u^\alpha \Delta_{\alpha\beta} = 0$, the coefficients of $I^{\alpha\beta}$ which are going to survive after contraction with $\Delta_{\alpha\beta}$ are a_0 and a_2. We construct two projection operators to get these coefficients, i.e.; $Q^1_{\alpha\beta} I^{\alpha\beta} = a_0$ and $Q^2_{\alpha\beta} I^{\alpha\beta} = a_2$, so that

$$\frac{dN^{(\zeta)}}{d^4x d^4p} = \frac{2}{5}\frac{\zeta/s}{T^3}\left[\left(Q^1_{\mu\nu} I^{\mu\nu}\right) g^{\alpha\beta} + \left(Q^2_{\mu\nu} I^{\mu\nu}\right) p^\alpha p^\beta\right] \Delta_{\alpha\beta}\Theta. \tag{5.32}$$

The expressions for the projection operators in the local rest frame of the the medium ($u^\alpha = (1, \bar{0})$) are

$$Q^1_{\alpha\beta} = \frac{1}{2|\mathbf{p}|^2}\left[|\mathbf{p}|^2 g_{\alpha\beta} + M^2 u_\alpha u_\beta + p_\alpha p_\beta - 2p_0 u_\alpha p_\beta\right], \tag{5.33}$$

$$Q^2_{\alpha\beta} = \frac{1}{2|\mathbf{p}|^4}\left[|\mathbf{p}|^2 g_{\alpha\beta} + (3p_0^2 - |\mathbf{p}|^2) u_\alpha u_\beta + 3p_\alpha p_\beta - 6p_0 u_\alpha p_\beta\right]. \tag{5.34}$$

With the help of definition of $I^{\alpha\beta}$ i.e.; Eq. (5.30), we can calculate $\left(Q^1_{\mu\nu} I^{\mu\nu}\right)$ and $\left(Q^2_{\mu\nu} I^{\mu\nu}\right)$. Using these, the final expression for the first order correction due to bulk viscosity in dilepton rate is given as [201],

$$\frac{dN^{(\zeta)}}{d^4x d^4p} = \frac{1}{2}\frac{M^2 g^2 \sigma(M^2)}{(2\pi)^5}\, e^{-p_0/T}\left[\frac{2}{3}\left(\frac{2}{5}\frac{\zeta/s}{2T^3} p^\alpha p^\beta \Delta_{\alpha\beta}\Theta\right) - \frac{2}{5}\frac{\zeta/s}{4T^3} M^2\Theta\right]. \tag{5.35}$$

The *total* dilepton rate, including the first order viscous corrections due to both shear and bulk viscosity is obtained by adding Eqs. (5.27), (5.28) and (5.35).

Apart from rates as function of four momentum of the dileptons we will be interested in particle production as a function of invariant mass (M), transverse momentum (p_T) and rapidity (y) of the dilepton pair. This can be obtained from Eq. (5.23) by changing the variables appropriately [221] and leads to [201],

$$\begin{aligned}\frac{dN}{d^4x dM^2 d^2p_T dy} &= \frac{1}{2}\frac{dN}{d^4x d^4p} = \frac{1}{2^3}\frac{5\alpha^2}{9\pi^4}\, e^{-p_0/T} \\ &\times\left[1 + \frac{2}{3}\left(\frac{\eta/s}{2T^3} p^\alpha p^\beta \nabla_{\langle\alpha} u_{\beta\rangle} + \frac{2}{5}\frac{\zeta/s}{2T^3} p^\alpha p^\beta \Delta_{\alpha\beta}\Theta\right) - \frac{2}{5}\frac{\zeta/s}{4T^3} M^2\Theta\right].\end{aligned} \tag{5.36}$$

5.2.4 Dilepton spectra in heavy-ion collision

The total dilepton spectrum is obtained by convoluting the dilepton rate with the space-time evolution of the heavy-ion collision. Dilepton rates are temperature dependent and temperature profile is obtained after hydrodynamically evolving the system. In Bjorken model we have $d^4x == \pi R_A^2 d\eta_s \tau d\tau$, where $R_A = 1.2A^{1/3}$ is the radius of the nucleus used for the collision (for $Au,\ A = 197$). We can calculate different differential rates as functions of M, p_T and y. In this work we will be calculating the rates $dN/(p_T dp_T dM dy)$ and $dN/dMdy$; and these dilepton yields are obtained from,

$$\left(\frac{dN}{dM^2 d^2p_T dy}\right)_{M,p_T,y} = \pi R_A^2 \int_{\tau_0}^{\tau_1} d\tau \ \tau \int_{-y_{nuc}}^{y_{nuc}} d\eta_s \left(\frac{1}{2}\frac{dN}{d^4x d^4p}\right)$$

and are given by

$$\left(\frac{dN}{p_T dp_T dM dy}\right)_{M,p_T,y} = (4\pi M)\pi R_A^2 \int_{\tau_0}^{\tau_1} d\tau \ \tau \int_{-y_{nuc}}^{y_{nuc}} d\eta_s \left(\frac{1}{2}\frac{dN}{d^4x d^4p}\right), \tag{5.37}$$

$$\left(\frac{dN}{dMdy}\right)_{M,y} = (4\pi M)\pi R_A^2 \int_{\tau_0}^{\tau_1} d\tau \ \tau \int_{-y_{nuc}}^{y_{nuc}} d\eta_s \int_{p_{T_{min}}}^{p_{T_{max}}} p_T dp_T \left(\frac{1}{2}\frac{dN}{d^4x d^4p}\right). \tag{5.38}$$

Where the expression for $dN/(d^4xd^4p)$ is obtained from Eq. (5.37). Here τ_0 and τ_1 are the initial and final values of time that we are interested. Generally τ_1 is taken as the time taken by the system to reach T_c, i.e.; τ_f, but in the case of occurrence of cavitation we must set $\tau_1 = \tau_c$, the cavitation time, in order to avoid erroneous estimation of rates [200], as we have seen in the case of photons from Section 5.1.4. Here we note that the dilepton production rates calculated in Section 5.2.3 correspond to the rest frame of the system. So in a longitudinally expanding system, we must replace f_0 of Eq. (5.13) with $f_0 = e^{-u.p/T}$ in Eqs. (5.37 - 5.38). With 4-momentum of the dilepton parametrised as $p^\alpha = (m_T coshy, p_T cos\phi_p, p_T sin\phi_p, m_T sinhy)$, where $m_T^2 = p_T^2 + M^2$ [150] and the four velocity of the medium given by Eq. (1.40) we get, $u.p = m_T cosh(y - \eta_s)$. Thus using the 1D boost invariant flow, the factors appearing in the modified rate Eq. (5.37) can be calculated as [201]:

$$p^\alpha p^\beta \nabla_{\langle\alpha}u_{\beta\rangle} = \frac{2}{3\tau}p_T^2 - \frac{4}{3\tau}m_T^2 sinh^2(y-\eta_s), \tag{5.39}$$

$$p^\alpha p^\beta \Delta_{\alpha\beta}\Theta = -\frac{p_T^2}{\tau} - \frac{m_T^2}{\tau} sinh^2(y-\eta_s). \tag{5.40}$$

5.2.5 Non-ideal effects on thermal dileptons

By numerically solving the hydrodynamical equations describing the longitudinal expansion of the plasma Eqs. (4.1 - 4.3), we get the temporal evolution profile for $T(\tau)$, $\Phi(\tau)$ and $\Pi(\tau)$. We can evolve the hydrodynamics till the temperature of the system reaches critical temperature, i.e.; τ_f. We use the same set of equations for hydrodynamics, second order coefficients and viscosity prescriptions used as in Section 4.2.

Now we calculate the initial conditions as follows. We relate the observed emitted charged particle number per unit rapidity $\frac{dN}{dy}$ to the initial entropy density s_0, in order to estimate the initial conditions for hydrodynamics. In the case of viscous evolution, we need to consider the entropy produced due to viscous heating also [258]. However, these additional sources of entropy due to both bulk and shear viscosity are shown to be not significant [114, 259, 260] and their influence on final multiplicity can be neglected [161]. Assuming a linear relation between entropy density and particle number density $s = \xi n$, we can relate the entropy density to the total charged hadron multiplicity $\frac{dN_{ch}}{dy}$ with a proportionality factor given as, $s_0 \backsimeq \frac{7.85}{\pi R_A^2 \tau_0} \frac{dN_{ch}}{dy}$ [261], where πR_A^2 is the transverse size of the nucleus. Next, using the EoS and the thermodynamics relation $s = (\varepsilon + P)/T$ we can convert the initial entropy density to the initial energy density (or equivalently to the initial temperature T_0), assuming an initial time τ_0. This initial time can be fixed by the models like CGC which is used to estimate the early thermalisation time. Relevant for RHIC ($Au + Au$, $\sqrt{s} = 200$ GeV), we have $\frac{dN_{ch}}{dy} = 800$ [161] and we fix initial time from CGC models to be $\tau_0 = 0.5$ fm/c [262]. With these conditions we get our initial temperature as $T_0 = 330$ MeV. The rapidity of the nucleus is give by $y_{nuc} = 5.3$ [199]. The initial values of viscous terms are taken to be zero, i.e.; $\Phi(\tau_0) = 0$ and $\Pi(\tau_0) = 0$. We take critical temperature T_c to be 190 MeV.

From the study of thermal photons in Section 5.1.4, we know how cavitation affects the thermal spectra. Since we expect qualitatively same results (as shown in Figs. [5.5 & 5.6]) we are not repeating them here. So we will not be varying the height or width (controlled by the parameter a and ΔT respectively) of the ζ/s curve in this analysis. These parameters are kept to their base values: $a = 0.901$ and $\Delta T = T_c/14.5$ throughout this analysis.

Next we include the another *non-ideal* effect, viscosity in the calculations. Now we study the longitudinal pressure $P_z = P + \Pi - \Phi$ of the system. It is already seen from Section 4.1 that in such a scenario, the viscous contribution to the equilibrium pressure makes the effective longitudinal pressure of the system zero, triggering *cavitation*. Hydrodynamics is applicable only till τ_c in case of occurrence

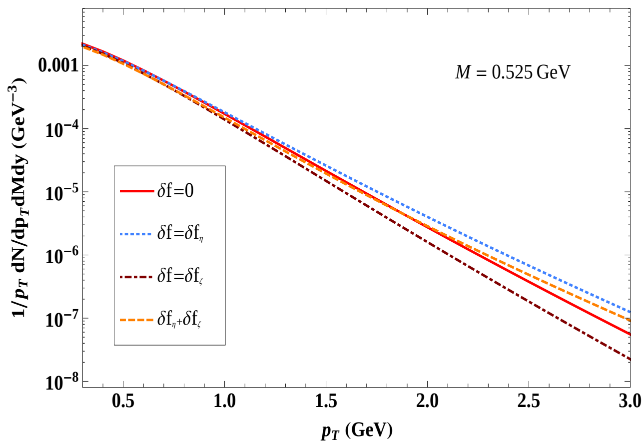

Figure 5.7: *Transverse momentum spectra of dileptons from a viscous QGP calculated at $M = 0.525$ GeV. The red line shows the dilepton production rate without considering the viscous corrections to the distribution functions. The effect of inclusion of viscous corrections due to shear and bulk is shown in separate curves.*

of cavitation instead of τ_f. This calculation is presented in Section 4.1 in detail and will not be repeated here. We quote the final results with the initial conditions $T_0 = 330$ MeV and $\tau_0 = 0.5$ fm/c here: Eventhough system reaches T_c at $\tau_f = 6.5$ fm/c only, much before that at $\tau_c = 3.7$ fm/c it undergoes cavitation at a temperature 204 MeV.

Once we get the temperature profile we can calculate the desired dilepton yields as discussed in Section 5.2.4. We again emphasise that we must be integrating the rates from τ_0 to $\tau_1 = \tau_c$ instead of $\tau_1 = \tau_f$ in the case of cavitation, to avoid overestimation of the yields [200]. From Eqs. (5.37 - 5.38) we can now calculate the dilepton yields as functions of invariant mass M, transverse momentum perpendicular to collision axis p_T and rapidity y of the dileptons. We present all our calculations at the mid rapidity region of the dileptons ($y = 0$).

It must be noted here that while calculating the particle spectra we use $\tau_1 = \tau_c$ as we have cavitation in the system. As we saw from Section 5.1.4, particle rates should be integrated upto τ_c and if we include τ_f instead of τ_c we will end up with a large overestimation [200]. In what follows we present the particle yields by taking into consideration of the effect of cavitation. In Fig. [5.7] we show the dilepton rate as a function of transverse momentum p_T for invariant mass $M = 0.525$ GeV.

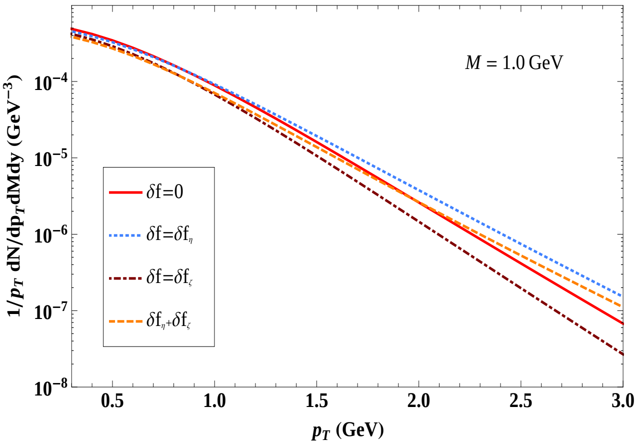

Figure 5.8: *Same as in Fig.[5.7], but for invariant mass $M = 1.0$ GeV.*

The solid curve shows the production rate without any viscous correction to the distribution function ($\delta f = 0$). The dotted curve represents the case when only the shear viscosity induced correction to the distribution function ($\delta f = \delta f_\eta$) is taken into account. In the "low p_T regime" ($p_T \leq 0.5$ GeV), inclusion of shear viscosity corrections marginally decreases the dilepton production rate as compared to $\delta f = 0$ case. However, for $p_T > 0.5$ GeV shear viscosity corrections can significantly enhance the dilepton production rate. The 'dot-dashed' curve shows the case when only bulk viscosity induced correction in f is taken into account. The general effect of the bulk viscosity is to deplete the dilepton production as also seen in the case of particle spectra in Refs. [200, 254]. Finally, the dashed curve shows the combined effects of bulk and shear viscosity corrections on the dilepton production rate. In the regime of $p_T < 2$ GeV, the production rate is depleted due to the viscous effects. For $p_T > 2$GeV the shear viscosity corrections dominates over the corrections due to the bulk viscosity and enhances the dilepton production rate. *It ought to be noted here that the only shear viscosity induced enhancement of dilepton production rate [252] gets significantly reduced when bulk viscosity effects are included.*

Fig. [5.8] shows the case similar to Fig. [5.7] but with a larger invariant mass $M = 1$ GeV. The viscosity induced corrections are consistently larger as compared to M=0.525 GeV case. Here our results show that as the invariant mass M increases the viscous corrections to distribution function become larger and can violate the condition $f_0 > \delta f$ thereby violating the applicability of the Grad's method.

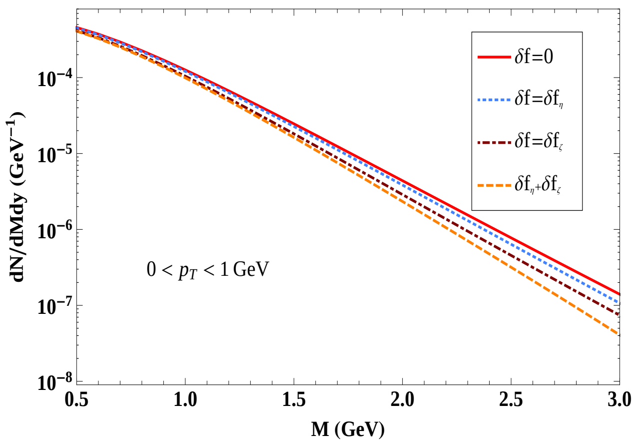

Figure 5.9: *p_T integrated emission rate as a function of invariant mass. Here $p_{T_{min}} = 0$ and $p_{T_{max}} = 1$ GeV.*

In Fig. [5.9] we plot the dilepton rate $dN/dMdy$ as a function of invariant mass. Here, we have used $p_{T_{min}} = 0$ GeV and $p_{T_{max}} = 1$ GeV in the integral in Eq. (5.38) while calculating the spectra. The shear viscosity contribution is negative in this p_T regime as may be seen in Figs.[5.7 - 5.8] and this can also be inferred from Eqs. (5.39 & 5.40).

In order to analyse the applicability of Grad's method quantitatively, we define the following ratios:

$$R_M = \left(\frac{dN}{dMdy}\,[f_0 + \delta f]\right) / \left(\frac{dN}{dMdy}\,[f_0]\right), \tag{5.41}$$

$$R_{p_T} = \left(\frac{dN}{p_T dp_T dMdy}\,[f_0 + \delta f]\right) / \left(\frac{dN}{p_T dp_T dMdy}\,[f_0]\right). \tag{5.42}$$

In both the equations above, the numerators are evaluated with distribution functions with viscous correction arising due to both bulk as well as shear contributions. The denominators are evaluated using distribution functions without any viscous corrections. One may expect $0 < R_M,\, R_{p_T} < 2$ for the validity of Grad's method. The plots of R_M and R_{p_T} for the cases considered in Figs. [5.7 - 5.9] are shown in Fig. [5.10]. If viscous corrections are about 60% i.e. $R_{p_T} \sim 1.6$, then the allowed range of p_T is between $0 - 3$ GeV. On the other hand for a similar magnitude of viscous correction in $R_M(\sim 0.4)$, the maximum allowed value of $M \sim 2.6$ GeV.

Finally, we comment on the use of one dimensional (1D) evolution analysis as compared to the three dimensional (3D) simulation results where the effect of

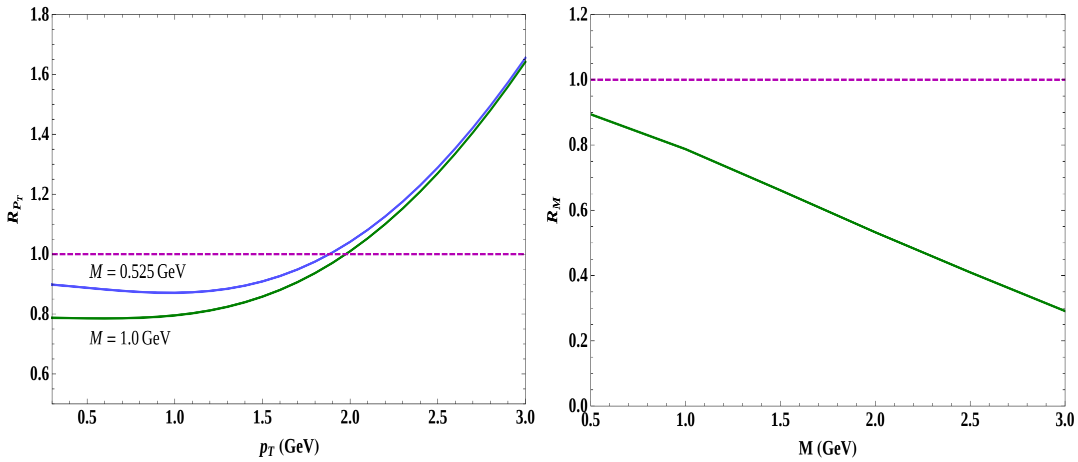

Figure 5.10: *Applicability of Grad's method.*

transverse flow is taken into account. We compare the dilepton yield calculated in our 1D hydrodynamical model with that of 3D simulation of Dusling and Lin [252]. They calculated the yield using ideal hydrodynamics for the evolution and shear viscosity modified dilepton production rate. In order to compare the results we also take only shear viscosity correction to the production rate and ideal hydrodynamical evolution of the system, while calculating the dilepton yield. Initial conditions and value of shear viscosity are also adjusted to that of [252] ($\eta/s = 0.2$). In Fig. [5.10] we plot our results with $M = 0.525$ GeV versus the results shown in Fig.[3] of Ref. [252]. As may be observed, broadly, the viscous corrections always enhance the dilepton production rate for $p_T > 0.5$ GeV, for both 1D as well as 3D simulations. Next, let us compare the results of the ideal hydrodynamics for 3D vis a vis 1D simulations. For ideal hydrodynamics, the 3D code gives systematically higher production rate as compared to the 1D code for $p_T \geq 0.7$ GeV. However, in the low momentum regime i.e. $p_T < 0.7$ GeV, 1D simulations leads to a marginal overestimation of the dilepton production rate. On the other hand, when viscous effects are included the situation is changed resulting in an *underestimation* of the production rate for 1D code upto $p_T \leq 3$ GeV. It must be noted here that in order to have a proper comparison of the 3D results of Ref. [252], the effect of cavitation and bulk viscosity are not included in the 1D results shown in Fig. [5.11]. However, we expect that the results with inclusion of bulk viscosity will also show a similar trend. Secondly, inclusion of cavitation effects can further reduce the production

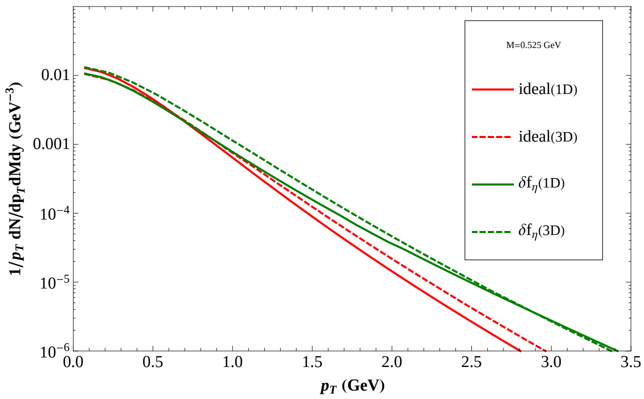

Figure 5.11: *Comparison of the dilepton production rate between 1D and 3D simulations. The 3D simulations are from Ref. [252]. The dotted lines are the 3D simulation results while solid lines are the results with our 1D simulations. The effects of bulk viscosity as well as cavitation are not included in the 1D simulations for a proper comparison with the 3D results given in Ref. [252].*

rate as the total time available for evolution reduces [200]. Moreover, in the calculation related to cavitation / fragmentation, the transverse flow is neglected as the hydrodynamic becomes invalid after τ_c. In this scenario it is assumed that the observed transverse flow can be due to some different physical effect unrelated to hydrodynamics [197].

5.3 Conclusions

In this chapter we studied the role of shear and bulk viscosities on thermal particle production from QGP at RHIC and LHC energies using the boost-invariant second order Israel-Stewart hydrodynamics formalism.

Firstly, we have studied the thermal photon production from chemically non-equilibrated plasma with minimal shear viscosity $\eta/s \approx 1/4\pi$ using $\varepsilon = 3P$ EoS. We find that the effect of viscosity enhancing the photon flux by a factor ranging between 1.5-2 for the parameter space relevant for LHC and RHIC. We propose that these direct photons can be used to estimate the viscosity of QGP. Our results are in a broad qualitative agreement with the results obtained in Ref. [212] using the first order theory. We also find that the two viscosity prescriptions with inelastic scattering [213] and the one involving elastic collisions only using kinetic theory give similar results for the photon production rate.

We have studied the effect of bulk viscosity, shear viscosity and bulk viscosity induced cavitation on the thermal photon production from QGP at RHIC energies. Effect of bulk viscosity was not considered in earlier studies. We have used recent lattice QCD results for temperature depended bulk viscosity and EoS. We take the value of shear viscosity to be the minimal $\eta/s = 1/4\pi$ as RHIC experiments suggest. As we have already seen, in such scenarios, large values of bulk viscosity near T_c can induce cavitation. Onset condition for the cavitation for the hydrodynamics has been implemented by stopping the integration of the hydrodynamic code when the effective longitudinal pressure become negative at cavitation time τ_c. In addition, while calculating the thermal particle emission rate it is required to cut off the temporal integral at τ_c. We find that the novel phenomenon of bulk viscosity driven cavitation can have a significant effect on the thermal photon production. We have shown that if the phenomenon of cavitation is ignored, one can have erroneous estimates of the photon production. Another result we would like to emphasize is that reduction in cavitation time can lead to significant reduction in the photon production.

Next, we have studied the effect of both the bulk and the shear viscosities on thermal dilepton production rates for the initial conditions relevant for QGP at RHIC. The role of a finite bulk viscosity on the dilepton rates was not analyzed in the earlier studies. In addition we have also studied the role of the onset-condition for the cavitation in influencing the emission rates of the thermal dileptons. The viscous corrections to the distribution functions are calculated using the 14-point Grad's method. We find that the validity condition for the Grad's method is altered due to finite mass of the dileptons unlike case for the thermal photon production. Overall effect of the bulk viscosity induced corrections in the distribution function is negative and thereby it can decrease the thermal dilepton production rate. A similar effect on particle production rate were also seen in Ref. [254]. We find that even though the finite bulk viscosity corrections and the onset of the cavitation reduce the production rates, the effect of the minimal $\eta/s = 1/4\pi$ can enhance the dilepton production rates significantly in the regime $p_T \geq 2$ GeV.

In this study we have analysed the thermal particle production till cavitation, if it occurs. It ought to be mentioned that one may expect radiation from the cavitating phase of the fluid, as this kind of radiation is already observed in some other systems and is known as sonoluminescence [263]. But this kind of analysis is beyond the scope of the hydrodynamics model considered in this study.

Chapter 6

Summary

In this thesis we studied the dissipative effects of the matter under extreme conditions like high density and temperature. In Chapter 1, we gave a brief introduction to the phase diagram of QCD and we discussed the regimes that we will be interested in the study of this thesis, namely a) neutron star matter (high baryon density and low temperature) and b) quark-gluon plasma (high temperature and almost zero baryon density) produced in relativistic heavy ion collision experiments. Here we briefly discussed Walecka's mean field model that is used to model the high density nuclear matter. We also discussed about the different possibilities regarding the matter that can be conceived inside a neutron star and discussed the r-mode instability, which can shed some light into the internal neutron star constituent structure. While discussing the QGP produced in heavy ion collisions, we analysed the relativistic ideal fluid hydrodynamics as well as boost invariant *Björken flow*, which is used to prescribe the longitudinal expansion of the plasma.

A rotating neutron star is various pulsating modes, and particularly interesting is the unstable r-mode, which can couple with gravitational radiation and reduce the angular momentum of the star through the emission of gravitational waves, unless these modes are effectively damped by the viscosity of the stellar matter. In Chapter 2, we considered a neutron star with a hyperonic core and the effect of r-mode instability. We used a chiral lagrangian to include the lowest lying octet of baryons within mean field approximation to extract the equation of state (EoS) of the hyperonic matter. We estimated the hyperonic bulk viscosity due to the dominant non-leptonic weak interactions. By calculating the time scales associated with various dissipative mechanisms, i.e.; bulk viscosity due to *Urca* processes and shear shear viscosity, together with that of dominant hyperon bulk viscosity, we analysed the role of these dissipative processes in the damping of the r-mode. We found that below 10^8 K, hyperon bulk viscosity is effectively damping the r-mode instability and beyond 10^10 bulk viscosity due to *Urca* processes suppresses the instability. However, we found that there exists a window $10^8 - 10^{10}$ K where r-mode instability is rather strong and it can reduce the star's angular momentum upto $\sim 0.04\Omega_K$, with Ω_K being Kepler velocity of the star. We also note that in our scenario the observed LMXB stars are placed in the stable region. However, we note here that effect of superfluidity was not considered in our analysis and it can change our results and conclusions. Although we have considered a star with hyperonic core in the context of r-mode instability, it will be interesting to see how prominent the instabilities can become in presence of phase transition to quark matter, perhaps be in a color-superconducting phase. It would also be interesting to study this r-mode instabilities in presence of strong magnetic fields.

In Chapter 3, we reviewed the relativistic dissipative hydrodynamics formalisms, both *first order* (Navier-Stokes) and *second order* (Israel-Stewart type). We discussed the inherent problems associated with the Navier-Stokes theory and the need for second order theories for a causal description. We also discussed boost invariant viscous flow with Navier-Stokes and second order theories in the context of heavy ion collisions. By obtaining the governing equations, we analysed the unphysical reheating of the fireball when one considers first order theory and how this problem can be avoided using second order theories. We saw that results from new studies with various techniques like lattice QCD (lQCD) and AdS/CFT correspondence, indicate a deviation in EoS from *ideal* $\varepsilon = 3P$ case near critical temperature T_c and at this region bulk viscosity can become much more prominent than the experimentally observed low value of shear viscosity. More experiments like RHIC beam energy scan and FAIR are aiming to study the matter produced in the heavy-ion collisions. However, in the regime where they expect to produce QGP (with non-zero baryon chemical potential), we may need to use *Landau flow*. It will be interesting to study the effect of viscosities in this context.

In Chapter 4, we considered the effect of both bulk and shear viscosity in the hydrodynamical evolution of QGP at both RHIC and LHC energies. Using a lQCD $\varepsilon \neq 3P$ EoS, lQCD prescription for the bulk viscosity and minimal value for shear viscosity, we found that the high value of temperature dependent bulk viscosity near T_c can make the effective longitudinal pressure of the system zero, in RHIC energies. Such a situation is known as *cavitation* and beyond which the hydrodynamic description becomes invalid. We studied the hydrodynamical evolution in this scenario and found that bulk viscosity plays a dual role: On one hand it enhances the time by which the system attains the critical temperature, while on the other hand it can make the hydrodynamical treatment invalid much before it reaches T_c. These results are indicative of the fact that effect of bulk viscosity cannot be ignored if it is strong enough to drive the cavitation at RHIC energy. We also have found that at LHC energies large values of bulk viscosity near T_c alone is not triggering cavitation. Further, at LHC energies, using various temperature dependent η/s prescriptions available, we showed that shear viscosity alone can drive the system to cavitation. We also demonstrate that the conformal terms used in equations of the relativistic dissipative hydrodynamic can influence the cavitation time. Our result indicate that hydrodynamical description in this context is valid about 2 fm/c only. These results show the need for consistently checking the cavitation conditions in hydrodynamical codes calculating the flow properties. We note here that all these studies were done ignoring the transverse flow in the hydrodynamics. Since cavitations are setting in very early stages of the evolution, we believe our result may not change very much qualitatively, with the inclusion of transverse flow. We also studied the effect of finite minimal shear viscosity $\eta/s = 1/4\pi$ on the chemical equilibration of the plasma using $\varepsilon = 3P$ EoS. Our results indicate that the minimal value of shear viscosity alone is making the system take more time to reach the chemical equilibrium compared to the ideal case. It will be interesting to study the effect of finite bulk viscosity on the chemical equilibration. One can further study the effect of *non-ideal* EoS and temperature dependent η/s on equilibration.

Finally in Chapter 5, we studied the effect of viscosity, both bulk and shear; using causal second order Israel-Stewart hydrodynamics on the thermal particle production from the QGP phase in heavy ion collisions. We have considered thermal photons and dileptons in this context. By studying the thermal photon production from dissipative chemically non-equilibrated plasma with minimal $\eta/s = 1/4\pi$ using $\varepsilon = 3P$ EoS, we found that photon production is enhanced several times at RHIC and LHC energies. We propose that these additional radiation due to viscosity can be used to measure the viscosity of QGP. Using an *non-ideal* EoS from lQCD, we studied the effect of bulk viscosity and shear viscosity on the thermal photon production from the equilibrium plasma at RHIC energies. We took lQCD inspired result for the bulk viscosity which has a peak around T_c and for shear viscosity we took the minimal value as experiments suggest. We found that that the novel phenomenon of cavitation can have significant effect on thermal photon production. The effect of cavitation is incorporated in the particle spectrum by terminating the integration of the particle rates at the cavitation time. We saw that that reduction in cavitation time can lead to significant reduction in the photon production. Our studies indicate that if the phenomenon of cavitation is ignored one can have erroneous estimates of the particle production. We also studied the effect of bulk viscosity and shear viscosity in the thermal dilepton production in a similar manner. However, we have considered another viscous effect also into consideration- corrections to the distribution functions using Grad's method. We calculated the corrections due to both bulk and shear in the distribution function and used the modified distribution function in the dilepton rates to calculate the dilepton production rates. We found that the validity condition for the Grads method is altered due to finite mass of the dileptons unlike case for the thermal photon production. We also found that since the overall effect of the bulk viscosity induced corrections in the distribution function was negative, the thermal dilepton production rate can get decreased. We showed that, eventhough finite bulk viscosity corrections in the distribution function and the effect of cavitation reduce the particle production rates, the effect of minimal $\eta/s = 1/4\pi$ can enhance the the dilepton production rates in the high transverse momenta regime $p_T \geq 2$ GeV. We still don't have a correct theory to describe the bulk viscosity corrections to the distribution functions. Existing theories are highly non-reliable at large momenta. This problem is needed to be addressed in more detail.

Again in all these analysis we have used (1+1) dimensional analysis and transverse momenta was neglected. So it is desirable to make some progress with the incorporation of transverse flow. We also note that after cavitation, we expect radiation from the cavitating phase of the fluid, however such an analysis is beyond the scope of this thesis. However, it will be interesting to study the dynamics of cavitating phase and its evolution.

Thus we have studied certain aspects of nuclear matter under extreme conditions like density and temperature. As we discussed above, there are many interesting avenues that need further examination.

Appendix A

EoS for a relativistic non-interacting massless gas ($\varepsilon = 3P$)

Here we calculate the equation of state (EoS) associated with a realativistic non-interacting massless gas of quarks and gluons. In order to calculate thermodynamic quanities at a temperature T of the system, we use the partition function $\mathcal{Z}$ given by

$$ln\, \mathcal{Z} = V \int \frac{d^3p}{(2\pi)^3}\, ln \left[1 \pm e^{-\beta\,(\omega - \mu)}\right]^{\pm 1}, \tag{A.1}$$

where '+' refers to the case of fermions and '$-$' refers to that of bosons. Here $\beta = T^{-1}$, μ is the chemical potential, V is the volume and for the relativitic particle with momentum $\vec{p}$ and mass m, $\omega = \sqrt{|\vec{p}|^2 + m^2}$. Now the thermodynamic quanities, like pressure P, particle number N_i, entropy S and energy E are obtained from,

$$\begin{aligned} P &= \frac{\partial T\, ln\, \mathcal{Z}}{\partial V} \\ N_i &= \frac{\partial T\, ln\, \mathcal{Z}}{\partial \mu_i} \\ S &= \frac{\partial T\, ln\, \mathcal{Z}}{\partial T} \\ E &= -PV + TS + \sum_i \mu_i N_i, \end{aligned} \tag{A.2}$$

where i denotes quarks and gluons. Now using the expression for $\mathcal{Z}$ it is straight forward to see that pressure, particle number density n and energy density ε are given by,

$$
\begin{aligned}
P &= \frac{T}{V}\, ln\, \mathcal{Z} && \text{(A.3)}\\
n &= \frac{N}{V} = \int \frac{d^3p}{(2\pi)^3}\, \frac{1}{e^{\beta\,(\omega-\mu)}\ \pm 1} && \text{(A.4)}\\
\varepsilon &= \frac{E}{V} = \int \frac{d^3p}{(2\pi)^3}\, \frac{\omega}{e^{\beta\,(\omega-\mu_i)}\ \pm 1}, && \text{(A.5)}
\end{aligned}
$$

again '+' refers to the case of quarks and '−' refers to that of gluons.

Let us first consider the case of massless quarks (fermions) with zero chemical potential, i.e.; $m = 0$ and $\mu = 0$, then $\omega = |\vec{p}|$. Now energy density of quarks is given by

$$
\varepsilon_q = \gamma_q \int \frac{d^3p}{(2\pi)^3}\, \frac{p}{e^{\beta|\vec{p}|}\ + 1} = \frac{\gamma_q}{2\pi^2}\, \frac{1}{\beta^4} \int_0^\infty du\, \frac{u^3}{e^u\ + 1},
$$

where $u = \beta|\vec{p}|$ and γ_q is the degenaracy factor for quarks. The integral in this expression can be calculated using the formulae

$$
\int_0^\infty du\, \frac{u^{n-1}}{e^u\ \pm 1} = \Gamma(n)\,\zeta(n)\,a_n^{\pm}; \quad n \geq 2, \tag{A.6}
$$

where $a_n^+ = [1 - 2^{1-n}]$, $a_n^- = 1$, $\Gamma(n) = n!$ is the gamma function and $\zeta(n)$ is the Riemann zeta function. Noting that $\zeta(4) = \pi^4/90$, now we have

$$
\varepsilon_q = \gamma_q\, \frac{21}{8}\, \frac{\pi^2}{90}\, T^4. \tag{A.7}
$$

Now let us calculate the pressure due to quarks P_q using Eq. (A.3),

$$
P_q = \frac{\gamma_q}{2\pi^2}\, \frac{1}{\beta} \int_o^\infty |\vec{p}|^2 d|\vec{p}|\ ln\left[1 + \ e^{-\beta\,|\vec{p}|}\right]. \tag{A.8}
$$

After integration by parts, it is straightforward to see that

$$
P_q = \frac{\gamma_q}{2\pi^2}\, \frac{1}{3\beta^4} \int_0^\infty du\, \frac{u^3}{e^u\ + 1}. \tag{A.9}
$$

clearly,

$$
P_q = \frac{1}{3}\,\varepsilon_q = \gamma_q\, \frac{7}{8}\, \frac{\pi^2}{90}\, T^4. \tag{A.10}
$$

In a similar way it is easy to see that energy density and pressure corresponding to gluons are given by,

$$
P_g = \frac{1}{3}\,\varepsilon_g = \gamma_g\, \frac{\pi^2}{90}\, T^4, \tag{A.11}
$$

where γ_g is the gluon degenaracy factor. Now the *total* pressure $P = P_g + P_q$ and $\varepsilon = \varepsilon_g + \varepsilon_q$ of the system is given by,

$$P = \frac{1}{3}\,\varepsilon \, = \left(\gamma_g + \frac{7}{8}\gamma_q\right)\, \frac{\pi^2}{90}, \tag{A.12}$$

and this equation defines the EoS for *ideal* non-interacting massless quarks and gluons. Now in QGP the degenaracy factors are given as,

$$\gamma_q \;=\; N_s \times N_{q\bar{q}} \times N_C \times N_f = 2 \times 2 \times 3 \times N_f = 12 N_f, \tag{A.13}$$

$$\gamma_g \;=\; N_s \times (N_C^2 - 1) = 2 \times 8 = 16, \tag{A.14}$$

where N_f is the number of flavours and $N_C = 3$ is the number of colours. $N_s = 2$ corresponds to spin and $N_{q\bar{q}} = 2$ to quark and antiquark. Now in this case *ideal* EoS becomes,

$$P = \frac{1}{3}\varepsilon = a\,T^4\,; \quad a = \left(16 + \frac{21}{2}N_f\right)\, \frac{\pi^2}{90}. \tag{A.15}$$

Bibliography

[1] E. V. Shuryak, *The QCD vacuum, hadrons, and the superdense matter*, World Scientific, Singapore (2004).

[2] D. J. Gross and F. Wilczek, Phys. Rev. Lett. **30** (1973) 1343.

[3] H. D. Politzer, Phys. Rev. Lett. **30** (1973) 1346.

[4] K. G. Wilson, Phys. Rev. **D10** (1974) 2445-2459.

[5] picture is taken from http : //www.bnl.gov

[6] Y. Aoki, G. Endrodi, Z. Fodor, S. D. Katz and K. K. Szabo, Nature **443** (2006) 675 [arXiv:hep-lat/0611014].

[7] A. Bazavov *et al.*, Phys. Rev. D **80** (2009) 014504 [arXiv:0903.4379 [hep-lat]].

[8] H. Satz, Nature **336** (1988) 425.

[9] S. Hands, Contemp. Phys. **42** (2001) 209 [physics/0105022 [physics.ed-ph]].

[10] T. Schafer, hep-ph/0304281.

[11] D. H. Rischke, Prog. Part. Nucl. Phys. **52** (2004) 197-296. [nucl-th/0305030].

[12] J. Kapusta and C. Gale, *Finite Temperature Field Theory*, Cambridge University Press, (2006).

[13] N. K. Glendenning, *Compact Stars: Nuclear Physics, Particle Physics and General Relativity*, Springer, (2000).

[14] K. Yagi, T. Hatsuda, Y. Miake, *Quark-Gluon Plasma*, Cambridge University Press, (2008).

[15] N. K. Glendenning, S. A. Moszkowski, Phys. Rev. Lett. **67** (1991) 2414-2417.

[16] J. Schaffner, I. N. Mishustin, Phys. Rev. **C53** (1996) 1416-1429. [nucl-th/9506011].

[17] M. Prakash, I. Bombaci, M. Prakash, P. J. Ellis, J. M. Lattimer, R. Knorren, Phys. Rept. **280** (1997) 1-77. [nucl-th/9603042].

[18] F. Weber, Prog. Part. Nucl. Phys. **54** (2005) 193-288. [astro-ph/0407155].

[19] N. Itoh, Prog. Theor. Phys. **44** (1970) 291.

[20] J. C. Collins, M. J. Perry, Phys. Rev. Lett. **34** (1975) 1353.

[21] K. Rajagopal, F. Wilczek, In *Shifman, M. (ed.): At the frontier of particle physics, vol. 3* 2061-2151. [hep-ph/0011333].

[22] D. K. Hong, Acta Phys. Polon. **B32** (2001) 1253-1276. [hep-ph/0101025].

[23] M. G. Alford, Ann. Rev. Nucl. Part. Sci. **51** (2001) 131-160. [hep-ph/0102047].

[24] G. Nardulli, Riv. Nuovo Cim. **25N3** (2002) 1-80. [arXiv:hep-ph/0202037 [hep-ph]].

[25] S. Reddy, Acta Phys. Polon. **B33** (2002) 4101-4140. [nucl-th/0211045].

[26] H. -c. Ren, [hep-ph/0404074].

[27] M. Huang, Int. J. Mod. Phys. **E14** (2005) 675. [hep-ph/0409167].

[28] I. A. Shovkovy, Found. Phys. **35** (2005) 1309-1358. [nucl-th/0410091].

[29] M. G. Alford, A. Schmitt, K. Rajagopal, T. Schafer, Rev. Mod. Phys. **80** (2008) 1455-1515. [arXiv:0709.4635 [hep-ph]].

[30] E. Witten, Phys. Rev. **D30** (1984) 272-285.

[31] F. Neumann, M. Buballa, M. Oertel, Nucl. Phys. **A714** (2003) 481-501. [hep-ph/0210078].

[32] I. A. Shovkovy, S. B. Ruester, D. H. Rischke, J. Phys. G **G31** (2005) S849-S856. [nucl-th/0411040].

[33] K. Rajagopal, R. Sharma, Phys. Rev. **D74** (2006) 094019. [hep-ph/0605316].

[34] M. Buballa, M. Oertel, Nucl. Phys. **A703** (2002) 770-784. [hep-ph/0109095].

[35] A. W. Steiner, S. Reddy, M. Prakash, Phys. Rev. **D66** (2002) 094007. [hep-ph/0205201].

[36] A. Mishra, H. Mishra, Phys. Rev. **D69** (2004) 014014. [hep-ph/0306105].

[37] S. B. Ruester, I. A. Shovkovy, D. H. Rischke, Nucl. Phys. **A743** (2004) 127-146. [hep-ph/0405170].

[38] A. Mishra, H. Mishra, Phys. Rev. **D71** (2005) 074023. [hep-ph/0412213].

[39] A. Mishra, H. Mishra, Phys. Rev. **D74** (2006) 054024. [hep-ph/0605223].

[40] M. Alford, D. Blaschke, A. Drago, T. Klahn, G. Pagliara, J. Schaffner-Bielich, Nature **445** (2007) E7-E8. [astro-ph/0606524].

[41] J. D. Walecka, Annals Phys. **83** (1974) 491-529.

[42] S. A. Chin, J. D. Walecka, Phys. Lett. **B52** (1974) 24.

[43] F. E. Serr, J. D. Walecka, Phys. Lett. **B79** (1978) 10.

[44] C. J. Horowitz, B. D. Serot, Nucl. Phys. **A399** (1983) 529.

[45] B. D. Serot, J. D. Walecka, Adv. Nucl. Phys. **16** (1986) 1-327.

[46] S. Weinberg, *Gravitation and Cosmology*, John Wiley & Sons, (1972).

[47] P. Papazoglou, J. Schaffner, S. Schramm, D. Zschiesche, H. Stoecker, W. Greiner, Phys. Rev. **C55** (1997) 1499-1508. [nucl-th/9609035].

[48] P. Papazoglou, S. Schramm, J. Schaffner-Bielich, H. Stoecker, W. Greiner, Phys. Rev. **C57** (1998) 2576-2588. [nucl-th/9706024].

[49] V. Dexheimer, S. Schramm, D. Zschiesche, Phys. Rev. **C77** (2008) 025803. [arXiv:0710.4192 [nucl-th]].

[50] A. Mishra, A. Kumar, S. Sanyal, V. Dexheimer, S. Schramm, Eur. Phys. J. **A45** (2010) 169-177. [arXiv:0905.3518 [nucl-th]].

[51] D. Zschiesche, L. Tolos, J. Schaffner-Bielich, R. D. Pisarski, Phys. Rev. **C75** (2007) 055202. [nucl-th/0608044].

[52] M. Prakash, T. L. Ainsworth, Phys. Rev. **C36** (1987) 346-353.

[53] N. K. Glendenning, Nucl. Phys. **A480** (1988) 597-614.

[54] P. K. Sahu, R. Basu, B. Datta, Astrophys. J. **416** (1993) 267-275.

[55] P. K. Sahu, A. Ohnishi, Prog. Theor. Phys. **104** (2000) 1163-1171. [nucl-th/0007068].

[56] P. K. Sahu, T. K. Jha, K. C. Panda, S. K. Patra, Nucl. Phys. **A733** (2004) 169-184. [nucl-th/0312128].

[57] T. K. Jha, P. K. Raina, P. K. Panda, S. K. Patra, Phys. Rev. **C74** (2006) 055803. [nucl-th/0608013].

[58] J. R. Oppenheimer, G. M. Volkoff, Phys. Rev. **55** (1939) 374-381.

[59] R. C. Tolman, Phys. Rev. **55** (1939) 364-373.

[60] H. Komatsu, Y. Eriguchi, I. Hachisu, Mon. Not. Roy. Astron. Soc. **237** (1989) 355-379.

[61] N. Andersson, Astrophys. J. **502** (1998) 708-713. [gr-qc/9706075].

[62] J. L. Friedman, S. M. Morsink, Astrophys. J. **502** (1998) 714-720. [gr-qc/9706073].

[63] L. Lindblom, B. J. Owen, S. M. Morsink, Phys. Rev. Lett. **80** (1998) 4843-4846. [gr-qc/9803053].

[64] N. Andersson, K. D. Kokkotas, Int. J. Mod. Phys. **D10** (2001) 381-442. [gr-qc/0010102].

[65] L. Lindblom, [astro-ph/0101136].

[66] N. Andersson, Class. Quant. Grav. **20** (2003) R105. [astro-ph/0211057].

[67] J. Papaloizou, J. E. Pringle, Mon. Not. Roy. Astron. Soc. **182** (1978) 423-442.

[68] H. Saio, Astrophys. J. **256** (1982) 717.

[69] J. Provost, G. Berthomeiu, A. Rocca, Astron. Astrophys. **94** (1981) 126.

[70] S. Chandrasekhar, Phys. Rev. Lett. **24** (1970) 611-615.

[71] J. L. Friedman, B. F. Schutz, Astrophys. J. **222** (1978) 281.

[72] P. Arras, E. E. Flanagan, S. M. Morsink, A. K. Schenk, S. A. Teukolsky, I. Wasserman, Astrophys. J. **591** (2003) 1129-1151. [astro-ph/0202345].

[73] D. R. Lorimer, Living Rev. Relativity **4**, (2001), 5. http://www.livingreviews.org/lrr-2001-5

[74] E. Flowers, N. Itoh, Astrophys. J. **230** (1979) 847.

[75] C. Cutler, L. Lindblom, Astrophys. J. **314** (1987) 234.

[76] P. B. Jones, Phys. Rev. **D64** (2001) 084003.

[77] P. B. Jones, Phys. Rev. Lett. **86** (2001) 1384.

[78] L. Lindblom, B. J. Owen, Phys. Rev. **D65** (2002) 063006. [astro-ph/0110558].

[79] P. Haensel, K. P. Levenfish, D. G. Yakovlev, Astron. Astrophys. **381** (2002) 1080-1089. [astro-ph/0110575].

[80] E. N. E. van Dalen, A. E. L. Dieperink, Phys. Rev. **C69** (2004) 025802. [nucl-th/0311103].

[81] A. Drago, A. Lavagno, G. Pagliara, Phys. Rev. **D71** (2005) 103004. [astro-ph/0312009].

[82] M. Nayyar, B. J. Owen, Phys. Rev. **D73** (2006) 084001. [astro-ph/0512041].

[83] D. Chatterjee, D. Bandyopadhyay, Phys. Rev. **D74** (2006) 023003. [astro-ph/0602538].

[84] D. Chatterjee, D. Bandyopadhyay, Phys. Rev. **D75** (2007) 123006. [astro-ph/0702259].

[85] J. Madsen, Phys. Rev. Lett. **85** (2000) 10-13. [astro-ph/9912418].

[86] B. A. Sa'd, I. A. Shovkovy, D. H. Rischke, Phys. Rev. **D75** (2007) 065016. [astro-ph/0607643].

[87] B. A. Sa'd, I. A. Shovkovy, D. H. Rischke, Phys. Rev. **D75** (2007) 125004. [astro-ph/0703016].

[88] P. Jaikumar, G. Rupak, A. W. Steiner, Phys. Rev. **D78** (2008) 123007. [arXiv:0806.1005 [nucl-th]].

[89] X. -G. Huang, M. Huang, D. H. Rischke, A. Sedrakian, Phys. Rev. **D81** (2010) 045015. [arXiv:0910.3633 [astro-ph.HE]].

[90] E. Iancu and R. Venugopalan, In *Hwa, R.C. (ed.) et al.: Quark gluon plasma* 249-3363 [hep-ph/0303204].

[91] F. Gelis, E. Iancu, J. Jalilian-Marian and R. Venugopalan, Ann. Rev. Nucl. Part. Sci. **60** (2010) 463 [arXiv:1002.0333 [hep-ph]].

[92] E. Fermi, Prog. Theor. Phys. **5** (1950) 570-583.

[93] L. D. Landau, Izv. Akad. Nauk Ser. Fiz. **17** (1953) 51-64

[94] S. Z. Belenkij, L. D. Landau, Nuovo Cim. Suppl. **3S10** (1956) 15.

[95] J. D. Bjorken, Phys. Rev. D **27** (1983) 140.

[96] L. D. Landau and E. M. Lifshitz, *Fluid Mechanics*, 2nd edition, Butterworth-Heinemann, Oxford, 1999.

[97] J. -Y. Ollitrault, Phys. Rev. D **46** (1992) 229.

[98] P. F. Kolb and U. W. Heinz, In *Hwa, R.C. (ed.) et al.: Quark gluon plasma* 634-714 [nucl-th/0305084].

[99] R. S. Bhalerao and S. Gupta, Phys. Rev. C **77** (2008) 014902 [arXiv:0706.3428 [nucl-th]].

[100] K. Kajantie, Nucl. Phys. **A418** (1984) 41C-55C.

[101] G. Baym, Nucl. Phys. **A418** (1984) 525C-537C.

[102] C. Cattaneo, C.R. Acad. Sci. (Paris) **247** (1958) 431.

[103] W. A. Hiscock, L. Lindblom, Phys. Rev. **D31** (1985) 725-733.

[104] W. Israel, Annals Phys. **100** (1976) 310-331.

[105] J.M. Stewart, Proc. Roy. Soc. A **357** (1977) 59;

[106] W. Israel, J. M. Stewart, Annals Phys. **118** (1979) 341-372.

[107] A. Muronga, Phys. Rev. Lett. **88** (2002) 062302. [nucl-th/0104064].

[108] I. Arsene *et al.*, Nucl. Phys. **A757**, 1 (2005); B. B. Back *et al.*, *ibid.,* p. 28; J. Adams *et al.*, *ibid.,* p. 102; K. Adcox *et al.*, *ibid.,* p. 184.

[109] P. Romatschke and U. Romatschke, Phys. Rev. Lett. **99** (2007) 172301 [arXiv:0706.1522 [nucl-th]].

[110] P. Kovtun, D. T. Son and A. O. Starinets, Phys. Rev. Lett. **94** (2005) 111601 [arXiv:hep-th/0405231].

[111] T. Hirano, M. Gyulassy, Nucl. Phys. **A769** (2006) 71-94. [nucl-th/0506049].

[112] T. Schafer and D. Teaney, Rept. Prog. Phys. **72** (2009) 126001 [arXiv:0904.3107 [hep-ph]].

[113] H. B. Meyer, Phys. Rev. Lett. **100** (2008) 162001 [arXiv:0710.3717 [hep-lat]].

[114] R. J. Fries, B. Muller and A. Schafer, Phys. Rev. C **78** (2008) 034913 [arXiv:0807.4333 [nucl-th]].

[115] K. Rajagopal and N. Tripuraneni, JHEP **1003** (2010) 018 [arXiv:0908.1785 [hep-ph]].

[116] T. K. Jha, H. Mishra, V. Sreekanth, Phys. Rev. **C77** (2008) 045801. [arXiv:0710.5392 [nucl-th]].

[117] T. K. Jha, H. Mishra, Phys. Rev. **C78** (2008) 065802. [arXiv:0811.4233 [nucl-th]].

[118] M. Prakash, M. Prakash, J. Lattimer, C. Pethick, Astrophys. J. **390** (1992) L77.

[119] W. D. Langer, A. G. W. Cameron, Astrophys. Space Sci. **5** (1969) 213.

[120] L. Lindblom, G. Mendell, B. J. Owen, Phys. Rev. **D60** (1999) 064006. [gr-qc/9902052].

[121] R. F. Sawyer, Phys. Rev. **D39** (1989) 3804-3806.

[122] J. R. Isper, L. Lindblom, Astrophys. J. **373** (1991) 213-221.

[123] N. Stergioulas, J. .L. Friedman, Astrophys. J. **444** (1995) 306. [astro-ph/9411032].

[124] J. B. Hartle, Astrophys. J. **150** (1967) 1005-1029.

[125] J. B. Hartle, K. S. Thorne, Astrophys. J. **153** (1968) 807.

[126] E. F. Brown, L. Bildsten, P. Chang, Astrophys. J. **574** (2002) 920.

[127] B. A. Sa'd, [arXiv:0806.3359 [astro-ph]].

[128] S. de Groot, W. van Leeuven, and Ch. van Veert, *Relativistic Kinetic Theory*, North-Holland, (1980).

[129] A. Muronga, Phys. Rev. **C69** (2004) 034903. [nucl-th/0309055].

[130] U. W. Heinz, arXiv:nucl-th/0512049.

[131] C. Eckart, Phys. Rev. **58** (1940) 919.

[132] I. Muller, Z. Phys. **198** (1967) 329-344.

[133] D. H. Rischke, arXiv:nucl-th/9809044.

[134] A. Muronga, D. H. Rischke, [nucl-th/0407114].

[135] A. Muronga, Phys. Rev. **C76** (2007) 014909. [nucl-th/0611090].

[136] A. Muronga, Phys. Rev. **C76** (2007) 014910. [nucl-th/0611091].

[137] P. Romatschke, Int. J. Mod. Phys. **E19** (2010) 1-53. [arXiv:0902.3663 [hep-ph]].

[138] R. Baier, P. Romatschke, U. A. Wiedemann, Phys. Rev. **C73** (2006) 064903. [hep-ph/0602249].

[139] B. Betz, D. Henkel and D. H. Rischke, Prog. Part. Nucl. Phys. **62** (2009) 556 [arXiv:0812.1440 [nucl-th]].

[140] R. Loganayagam, JHEP **0805** (2008) 087. [arXiv:0801.3701 [hep-th]].

[141] S. Bhattacharyya, V. E. Hubeny, R. Loganayagam, G. Mandal, S. Minwalla, T. Morita, M. Rangamani, H. S. Reall, JHEP **0806** (2008) 055. [arXiv:0803.2526 [hep-th]].

[142] P. Romatschke, Class. Quant. Grav. **27** (2010) 025006. [arXiv:0906.4787 [hep-th]].

[143] R. Baier, P. Romatschke, D. T. Son, A. O. Starinets, M. A. Stephanov, JHEP **0804** (2008) 100. [arXiv:0712.2451 [hep-th]].

[144] M. Natsuume and T. Okamura, Phys. Rev. D **77** (2008) 066014 [Erratum-ibid. D **78** (2008) 089902] [arXiv:0712.2916 [hep-th]].

[145] S. Bhattacharyya, V. E. Hubeny, S. Minwalla and M. Rangamani, JHEP **0802** (2008) 045 [arXiv:0712.2456 [hep-th]].

[146] A. Buchel and M. Paulos, Nucl. Phys. B **805** (2008) 59 [arXiv:0806.0788 [hep-th]].

[147] I. Kanitscheider and K. Skenderis, JHEP **0904** (2009) 062 [arXiv:0901.1487 [hep-th]].

[148] M. A. York, G. D. Moore, Phys. Rev. **D79** (2009) 054011. [arXiv:0811.0729 [hep-ph]].

[149] J. Casalderrey-Solana, H. Liu, D. Mateos, K. Rajagopal, U. A. Wiedemann, [arXiv:1101.0618 [hep-th]].

[150] D. Teaney, Phys. Rev. **C68** (2003) 034913. [nucl-th/0301099].

[151] A. Hosoya, K. Kajantie, Nucl. Phys. **B250** (1985) 666.

[152] P. Danielewicz, M. Gyulassy, Phys. Rev. **D31** (1985) 53-62.

[153] S. Gavin, Nucl. Phys. **A435** (1985) 826-843.

[154] H. Kouno, M. Maruyama, F. Takagi, K. Saito, Phys. Rev. **D41** (1990) 2903.

[155] U. W. Heinz, H. Song and A. K. Chaudhuri, Phys. Rev. C **73** (2006) 034904 [arXiv:nucl-th/0510014].

[156] R. Baier and P. Romatschke, Eur. Phys. J. C **51** (2007) 677 [arXiv:nucl-th/0610108].

[157] H. Song and U. W. Heinz, Phys. Rev. C **77** (2008) 064901 [arXiv:0712.3715 [nucl-th]].

[158] M. Luzum and P. Romatschke, Phys. Rev. C **78** (2008) 034915 [Erratum-ibid. C **79** (2009) 039903] [arXiv:0804.4015 [nucl-th]].

[159] D. Molnar and P. Huovinen, J. Phys. G **35** (2008) 104125 [arXiv:0806.1367 [nucl-th]].

[160] H. Song and U. W. Heinz, J. Phys. G **36** (2009) 064033 [arXiv:0812.4274 [nucl-th]].

[161] M. Luzum and P. Romatschke, Phys. Rev. Lett. **103** (2009) 262302 [arXiv:0901.4588 [nucl-th]].

[162] D. A. Teaney, [arXiv:0905.2433 [nucl-th]].

[163] P. Huovinen, D. Molnar, Phys. Rev. **C79** (2009) 014906. [arXiv:0808.0953 [nucl-th]].

[164] R. Gupta, [hep-lat/9807028].

[165] J. M. Maldacena, Adv. Theor. Math. Phys. **2** (1998) 231-252. [hep-th/9711200].

[166] S. S. Gubser, I. R. Klebanov, A. M. Polyakov, Phys. Lett. **B428** (1998) 105-114. [hep-th/9802109].

[167] E. Witten, Adv. Theor. Math. Phys. **2** (1998) 505-532. [hep-th/9803131].

[168] M. Cheng *et al.*, Phys. Rev. D **77** (2008) 014511 [arXiv:0710.0354 [hep-lat]].

[169] S. Borsanyi *et al.*, JHEP **1011** (2010) 077 [arXiv:1007.2580 [hep-lat]].

[170] Z. Fodor, PoS **LAT2007** (2007) 011 [arXiv:0711.0336 [hep-lat]].

[171] A. Hosoya, M. -a. Sakagami, M. Takao, Annals Phys. **154** (1984) 229.

[172] P. B. Arnold, G. D. Moore and L. G. Yaffe, JHEP **0011** (2000) 001 [arXiv:hep-ph/0010177].

[173] P. B. Arnold, G. D. Moore and L. G. Yaffe, JHEP **0305** (2003) 051 [arXiv:hep-ph/0302165].

[174] G. Policastro, D. T. Son and A. O. Starinets, Phys. Rev. Lett. **87** (2001) 081601 [arXiv:hep-th/0104066].

[175] A. Buchel, J. T. Liu and A. O. Starinets, Nucl. Phys. B **707** (2005) 56 [arXiv:hep-th/0406264].

[176] S. C. Huot, S. Jeon and G. D. Moore, Phys. Rev. Lett. **98** (2007) 172303 [arXiv:hep-ph/0608062].

[177] P. Kovtun, D. T. Son and A. O. Starinets, JHEP **0310** (2003) 064 [arXiv:hep-th/0309213].

[178] A. Buchel and J. T. Liu, Phys. Rev. Lett. **93** (2004) 090602 [arXiv:hep-th/0311175].

[179] L. P. Csernai, J. .I. Kapusta, L. D. McLerran, Phys. Rev. Lett. **97** (2006) 152303. [nucl-th/0604032].

[180] A. Buchel, R. C. Myers and A. Sinha, JHEP **0903** (2009) 084 [arXiv:0812.2521 [hep-th]].

[181] K. H. Ackermann et al. [STAR Collaboration], Phys. Rev. Lett. **86**, 402 (2001); C. Adler et al. [STAR Collaboration], ibid. **87** (2001) 182301; **89**, 132301 (2002); Phys. Rev. **C 66**, 034904 (2002); J. Adams et al. [STAR Collaboration], nucl-ex/0409033; J. Adams et al. [STAR Collaboration], Phys. Rev. Lett. **92**, 052302 (2004).

[182] K. Adcox et al. [PHENIX Collaboration], Phys. Rev. Lett. **89**, 212301 (2002); S. S. Adler et al. [PHENIX Collaboration], ibid. **91**, 182301(2003);

[183] B. B. Back et al. [PHOBOS Collaboration], Phys. Rev. Lett. **89**, 222301(2002), B. B. Back et al. [PHOBOS Collaboration], Phys. Rev. Lett. **94**, 122303 (2005), arXiv:nucl-ex/0406021, B. B. Back et al. Phys. Rev. **C 72**, 051901 (2005), arXiv:nucl-ex/0407012.

[184] A. Nakamura, S. Sakai, Phys. Rev. Lett. **94**, 072305 (2005). [hep-lat/0406009].

[185] H. B. Meyer, Phys. Rev. D **76** (2007) 101701 [arXiv:0704.1801 [hep-lat]].

[186] P. B. Arnold, C. Dogan and G. D. Moore, Phys. Rev. D **74** (2006) 085021 [arXiv:hep-ph/0608012].

[187] K. Paech and S. Pratt, Phys. Rev. C **74** (2006) 014901 [arXiv:nucl-th/0604008].

[188] F. Karsch, D. Kharzeev and K. Tuchin, Phys. Lett. B **663** (2008) 217 [arXiv:0711.0914 [hep-ph]].

[189] D. Kharzeev and K. Tuchin, JHEP **0809** (2008) 093 [arXiv:0705.4280 [hep-ph]].

[190] G. D. Moore and O. Saremi, JHEP **0809** (2008) 015 [arXiv:0805.4201 [hep-ph]].

[191] S. Caron-Huot, Phys. Rev. D **79** (2009) 125009 [arXiv:0903.3958 [hep-ph]].

[192] P. Romatschke and D. T. Son, Phys. Rev. D **80** (2009) 065021 [arXiv:0903.3946 [hep-ph]].

[193] A. Buchel, Phys. Rev. D **72** (2005) 106002 [arXiv:hep-th/0509083].

[194] P. Benincasa, A. Buchel and A. O. Starinets, Nucl. Phys. B **733** (2006) 160 [arXiv:hep-th/0507026].

[195] A. Buchel, Phys. Lett. B **663** (2008) 286 [arXiv:0708.3459 [hep-th]].

[196] J. K. Batchelor, *An Introduction to Fluid Dynamics*, Cambridge University Press, (2009).

[197] G. Torrieri, B. Tomasik and I. Mishustin, Phys. Rev. C **77** (2008) 034903 [arXiv:0707.4405 [nucl-th]].

[198] G. Torrieri and I. Mishustin, Phys. Rev. C **78** (2008) 021901 [arXiv:0805.0442 [hep-ph]].

[199] D. K. Srivastava, Eur. Phys. J. C **10** (1999) 487 [arXiv:nucl-th/0103023].

[200] J. R. Bhatt, H. Mishra and V. Sreekanth, JHEP **1011** (2010) 106 [arXiv:1011.1969 [hep-ph]].

[201] J. R. Bhatt, H. Mishra, V. Sreekanth, [[arXiv:1101.5597 [hep-ph]].

[202] H. Niemi, G. S. Denicol, P. Huovinen, E. Molnar, D. H. Rischke, [arXiv:1101.2442 [nucl-th]].

[203] S. Mattiello, W. Cassing, Eur. Phys. J. **C70** (2010) 243-249. [arXiv:0911.4647 [hep-ph]].

[204] C. Shen, U. W. Heinz, P. Huovinen, H. Song, [arXiv:1105.3226 [nucl-th]].

[205] O. Andreev, arXiv:1101.5481 [hep-ph].

[206] A. Klimek, L. Leblond and A. Sinha, Phys. Lett. B **701** (2011) 144 [arXiv:1103.3987 [hep-th]].

[207] G. S. Denicol, T. Kodama, T. Koide, J. Phys. G **G37** (2010) 094040. [arXiv:1002.2394 [nucl-th]].

[208] M. Martinez, M. Strickland, Phys. Rev. **C79** (2009) 044903. [arXiv:0902.3834 [hep-ph]].

[209] M. Asakawa, S. A. Bass, B. Muller, Phys. Rev. Lett. **96** (2006) 252301. [hep-ph/0603092].

[210] T. S. Biró, E. van Doorn, B. Müller and X. -N. Wang, Phys. Rev. **C48** (1993) 1275-1284. [nucl-th/9303004].

[211] P. Lévai, B. Müller, X. -N. Wang, Phys. Rev. **C51** (1995) 3326-3335. [hep-ph/9412352].

[212] A. K. Chaudhuri, J. Phys. G **G26** (2000) 1433. [nucl-th/9808074].

[213] A. El, A. Muronga, Z. Xu, C. Greiner, Phys. Rev. **C79** (2009) 044914. [arXiv:0812.2762 [hep-ph]].

[214] X. -N. Wang, M. Gyulassy, Phys. Rev. **D44** (1991) 3501-3516; Comput. Phys. Commun. **83**, 307 (1994).

[215] B. Schenke, S. Jeon and C. Gale, Phys. Rev. Lett. **106** (2011) 042301 [arXiv:1009.3244 [hep-ph]].

[216] M. Martinez and M. Strickland, Nucl. Phys. A **848** (2010) 183 [arXiv:1007.0889 [nucl-th]].

[217] F. Becattini, arXiv:0901.3643 [hep-ph].

[218] H. Song, S. A. Bass, U. Heinz, Phys. Rev. **C83** (2011) 024912. [arXiv:1012.0555 [nucl-th]].

[219] E. L. Feinberg, Nuovo Cim. A **34** (1976) 391.

[220] E. V. Shuryak, Phys. Lett. B **78** (1978) 150 [Sov. J. Nucl. Phys. **28** (1978) 408] [Yad. Fiz. **28** (1978) 796].

[221] J. Alam, B. Sinha and S. Raha, Phys. Rept. **273** (1996) 243.

[222] J. Alam, S. Sarkar, P. Roy, T. Hatsuda and B. Sinha, Annals Phys. **286** (2001) 159 [arXiv:hep-ph/9909267].

[223] C. Gale and K. L. Haglin, arXiv:hep-ph/0306098.

[224] T. Peitzmann and M. H. Thoma, Phys. Rept. **364** (2002) 175 [arXiv:hep-ph/0111114].

[225] H. van Hees and R. Rapp, Nucl. Phys. A **806** (2008) 339 [arXiv:0711.3444 [hep-ph]].

[226] J. I. Kapusta, P. Lichard and D. Seibert, Phys. Rev. D **44** (1991) 2774 [Erratum-ibid. D **47** (1993) 4171] [Phys. Rev. D **47** (1993) 4171].

[227] P. V. Ruuskanen, Nucl. Phys. A **544** (1992) 169.

[228] R. Baier, H. Nakkagawa, A. Niegawa and K. Redlich, Z. Phys. C **53** (1992) 433.

[229] M. H. Thoma, Phys. Rev. D **51** (1995) 862 [arXiv:hep-ph/9405309].

[230] P. B. Arnold, G. D. Moore and L. G. Yaffe, JHEP **0111** (2001) 057 [arXiv:hep-ph/0109064].

[231] D. K. Srivastava, J. Phys. G **35** (2008) 104026 [arXiv:0805.3401 [nucl-th]].

[232] F. M. Liu and K. Werner, J. Phys. G **36** (2009) 035101 [arXiv:0712.3619 [hep-ph]].

[233] P. Aurenche, F. Gelis, R. Kobes and H. Zaraket, Phys. Rev. D **58** (1998) 085003 [arXiv:hep-ph/9804224].

[234] F. D. Steffen and M. H. Thoma, Phys. Lett. B **510** (2001) 98 [Erratum-ibid. B **660** (2008) 604] [arXiv:hep-ph/0103044].

[235] C. T. Traxler, H. Vija, M. H. Thoma, Phys. Lett. **B346** (1995) 329-334. [hep-ph/9410309].

[236] F. Karsch, Z. Phys. C **38** (1988) 147.

[237] C. T. Traxler, M. H. Thoma, Phys. Rev. **C53** (1996) 1348-1352. [hep-ph/9507444].

[238] R. Baier, M. Dirks, K. Redlich, D. Schiff, Phys. Rev. **D56** (1997) 2548-2554. [hep-ph/9704262].

[239] D. Dutta, A. K. Mohanty, K. Kumar, R. K. Choudhury, Phys. Rev. **C61** (2000) 064911. [hep-ph/9912352].

[240] J. L. Long, Z. J. He, Y. G. Ma, B. Liu, Phys. Rev. **C72** (2005) 064907.

[241] J. R. Bhatt, V. Sreekanth, Int. J. Mod. Phys. **E19** (2010) 299-306. [arXiv:0901.1363 [hep-ph]].

[242] K. Dusling, Nucl. Phys. A **839** (2010) 70 [arXiv:0903.1764 [nucl-th]].

[243] J. Peralta-Ramos and M. S. Nakwacki, arXiv:1010.3672 [hep-ph].

[244] L. D. McLerran, T. Toimela, Phys. Rev. **D31** (1985) 545.

[245] K. Kajantie, M. Kataja, L. D. McLerran *et al.*, Phys. Rev. **D34** (1986) 811.

[246] K. Kajantie, J. I. Kapusta, L. D. McLerran *et al.*, Phys. Rev. **D34** (1986) 2746.

[247] R. Vogt, *Ultrarelativistic Heavy-Ion Collisions*, Elsevier, (2007).

[248] T. Altherr, P. V. Ruuskanen, Nucl. Phys. **B380** (1992) 377-390.

[249] M. H. Thoma, C. T. Traxler, Phys. Rev. **D56** (1997) 198-202. [hep-ph/9701354].

[250] H. van Hees, R. Rapp, arXiv:0706.4443 [hep-ph].

[251] Y. Akiba [PHENIX Collaboration], Nucl. Phys. **A830** (2009) 567C-570C. [arXiv:0907.4794 [nucl-ex]].

[252] K. Dusling and S. Lin, Nucl. Phys. A **809** (2008) 246 [arXiv:0803.1262 [nucl-th]].

[253] G. S. Denicol, T. Kodama, T. Koide and Ph. Mota, Phys. Rev. C **80** (2009) 064901 [arXiv:0903.3595 [hep-ph]].

[254] A. Monnai and T. Hirano, Phys. Rev. C **80** (2009) 054906 [arXiv:0903.4436 [nucl-th]].

[255] A. S. Khvorostukhin, V. D. Toneev and D. N. Voskresensky, Nucl. Phys. A **845** (2010) 106 [arXiv:1003.3531 [nucl-th]].

[256] P. Chakraborty and J. I. Kapusta, Phys. Rev. C **83** (2011) 014906 [arXiv:1006.0257 [nucl-th]].

[257] K. Dusling and D. Teaney, Phys. Rev. C **77** (2008) 034905 [arXiv:0710.5932 [nucl-th]].

[258] M. Gyulassy, T. Matsui, Phys. Rev. **D29** (1984) 419-425.

[259] P. Romatschke, Eur. Phys. J. **C52** (2007) 203-209. [nucl-th/0701032].

[260] H. Song, U. W. Heinz, Phys. Rev. **C78** (2008) 024902. [arXiv:0805.1756 [nucl-th]].

[261] P. F. Kolb, U. W. Heinz, P. Huovinen, K. J. Eskola, K. Tuominen, Nucl. Phys. **A696** (2001) 197-215. [hep-ph/0103234].

[262] A. El, Z. Xu and C. Greiner, Nucl. Phys. A **806** (2008) 287 [arXiv:0712.3734 [hep-ph]].

[263] See for e.g.; http://en.wikipedia.org/wiki/Sonoluminescence